

# Polyamides : hydrogen bonding, the Brill transition, and superheated water

**Citation for published version (APA):**

Dijkstra - Vinken, E. (2008). *Polyamides : hydrogen bonding, the Brill transition, and superheated water*. [Phd Thesis 1 (Research TU/e / Graduation TU/e), Chemical Engineering and Chemistry]. Technische Universiteit Eindhoven. <https://doi.org/10.6100/IR637084>

**DOI:**

[10.6100/IR637084](https://doi.org/10.6100/IR637084)

**Document status and date:**

Published: 01/01/2008

**Document Version:**

Publisher's PDF, also known as Version of Record (includes final page, issue and volume numbers)

**Please check the document version of this publication:**

- A submitted manuscript is the version of the article upon submission and before peer-review. There can be important differences between the submitted version and the official published version of record. People interested in the research are advised to contact the author for the final version of the publication, or visit the DOI to the publisher's website.
- The final author version and the galley proof are versions of the publication after peer review.
- The final published version features the final layout of the paper including the volume, issue and page numbers.

[Link to publication](#)

**General rights**

Copyright and moral rights for the publications made accessible in the public portal are retained by the authors and/or other copyright owners and it is a condition of accessing publications that users recognise and abide by the legal requirements associated with these rights.

- Users may download and print one copy of any publication from the public portal for the purpose of private study or research.
- You may not further distribute the material or use it for any profit-making activity or commercial gain
- You may freely distribute the URL identifying the publication in the public portal.

If the publication is distributed under the terms of Article 25fa of the Dutch Copyright Act, indicated by the "Taverne" license above, please follow below link for the End User Agreement:

[www.tue.nl/taverne](http://www.tue.nl/taverne)

**Take down policy**

If you believe that this document breaches copyright please contact us at:

[openaccess@tue.nl](mailto:openaccess@tue.nl)

providing details and we will investigate your claim.

# **Polyamides:**

**Hydrogen bonding, the Brill transition, and superheated water**

A catalogue record is available from the  
Eindhoven University of Technology Library  
ISBN: 978-90-386-1359-8

Cover-design by CreanzaMedia  
Front cover: WAXD of PA4,6 in water on heating  
Back cover: WAXD of PA4,6 on heating  
Photo pressure vessel: Bram Saeys  
TEM PA4,6 single crystals: Anne Spoelstra

Printed by Universiteitsdrukkerij, Eindhoven University of Technology,  
The Netherlands.

The research described in this thesis was part of the Research Programme of the  
Dutch Polymer Institute (DPI), PO Box 902, 5600 AX Eindhoven, The Netherlands,  
project number #460.

# **Polyamides:**

## **Hydrogen bonding, the Brill transition, and superheated water**

Proefschrift

ter verkrijging van de graad van doctor aan de  
Technische Universiteit Eindhoven, op gezag van de  
Rector Magnificus, prof.dr.ir. C.J. van Duijn, voor een  
commissie aangewezen door het College voor  
Promoties in het openbaar te verdedigen  
op woensdag 17 september 2008 om 16.00 uur

door

ESTHER VINKEN

geboren te Oirsbeek

Dit proefschrift is goedgekeurd door de promotoren:

prof.dr. S. Rastogi  
en  
prof.dr. P.J. Lemstra

Copromotor:  
dr. A.E. Terry

*Now faith is the confidence of things hoped for,  
the evidence of things not seen.*

King James Translation (1611) – Hebrews 11:1



voor mijn moppie



# Contents

<b>Summary</b>	<b>1</b>
<b>1 Introduction</b>	<b>5</b>
1.1 Introduction to synthetic polyamides . . . . .	6
1.2 Crystal structure and hydrogen bonding in polyamides . . . . .	8
1.3 The Brill transition . . . . .	10
1.4 Effect of water on polyamides . . . . .	11
1.5 Superheated water . . . . .	11
1.6 Objectives of this thesis . . . . .	13
1.7 Scope of this thesis . . . . .	13
<b>2 The influence of hydrogen bonding on the conformation changes, the Brill transition, and lamellar thickening in piperazine based (co)polyamides</b>	<b>15</b>
2.1 Introduction . . . . .	16
2.2 Experimental description . . . . .	17
2.3 The Brill transition and lamellar thickening using simultaneous SAXS/WAXD . . . . .	18
2.4 Hydrogen bond density and the Brill transition . . . . .	23
2.5 Conformational changes . . . . .	24
2.6 Conclusions . . . . .	28
<b>3 The influence of stereochemistry on the conformational changes and the Brill transition in 1,4-diaminocyclohexane based (co)polyamides</b>	<b>29</b>
3.1 Introduction . . . . .	30
3.2 Experimental description . . . . .	32
3.3 Results and Discussion . . . . .	32
3.4 Conclusions . . . . .	38

---

<b>4 Crystallization of polyamide 4,6 from superheated water – implications for hydrogen bonding</b>	<b>40</b>
4.1 Introduction . . . . .	41
4.2 Experimental description . . . . .	43
4.2.1 Material . . . . .	43
4.2.2 Preparation of water crystallized PA4,6 crystals . . . . .	43
4.2.3 Simultaneous small and wide angle X-ray diffraction (SAXS/WAXD) . . . . .	43
4.3 Dissolution of PA4,6 in superheated water studied by simultaneous <i>in situ</i> SAXS/WAXD . . . . .	44
4.4 Dissolution of PA4,6 in superheated water with DSC . . . . .	47
4.5 Dissolution or hydrolysis of PA4,6 in superheated water? . . . . .	49
4.6 Single crystals grown from a water solution . . . . .	51
4.7 Sedimented single crystal mats . . . . .	53
4.8 Probing proton mobility by solid state NMR . . . . .	56
4.9 Different mobilities of the amide protons . . . . .	56
4.10 Different mobility of the water molecules in the samples crystallized from acid and water . . . . .	58
4.11 Location of the water molecules in the samples crystallized from acid and water . . . . .	59
4.12 Influence of water on the hydrogen bonding within the crystal . . . . .	62
4.13 Water present in a polymer crystal lattice . . . . .	67
4.14 Removal of water molecules . . . . .	68
4.15 Conclusions . . . . .	72
<b>5 Crystallization of polyamide 6,6 from superheated water – implications for the <math>\alpha</math> and <math>\beta</math> crystal structures</b>	<b>73</b>
5.1 Introduction . . . . .	73
5.2 Experimental description . . . . .	75
5.3 Phase behavior of PA6,6 in superheated water . . . . .	76
5.4 Single crystals grown from superheated water . . . . .	78
5.5 High resolution WAXD . . . . .	79
5.6 Simultaneous SAXS/WAXD . . . . .	81
5.7 Conformational changes . . . . .	85
5.8 DSC on dried water crystallized PA6,6 crystals . . . . .	86
5.9 Influence of superheated water on the PA6,6 $\alpha$ - and $\beta$ -structures . . . . .	87
5.10 Conclusions . . . . .	87

<b>6</b>	<b>Dissolution and crystallization of other even–even polyamides in superheated water</b>	<b>89</b>
6.1	Introduction . . . . .	89
6.2	Experimental description . . . . .	90
6.3	Dissolution of even-even polyamides in superheated water . . . . .	90
6.4	Crystallization of even-even polyamides from superheated water . . . . .	94
6.5	Conclusions . . . . .	95
<b>7</b>	<b>The influence of superheated water on hydrogen bonding in piperazine based (co)polyamides</b>	<b>96</b>
7.1	Introduction . . . . .	97
7.2	Experimental description . . . . .	99
7.3	Dissolution behavior of piperazine based (co)polyamides . . . . .	99
7.4	Influence of superheated water on crystallography of PA2,14 . . . . .	101
7.5	Conformational changes in water crystallized PA2,14 . . . . .	105
7.6	Melting behavior of water crystallized PA2,14 . . . . .	109
7.7	Influence of superheated water on PA2,14 . . . . .	110
7.8	Piperazine copolyamide water grown single crystals . . . . .	111
7.9	Influence of superheated water on crystallography of piperazine copolyamides . . . . .	113
7.10	Conformational changes in water crystallized piperazine copolyamides	113
7.11	Conclusions . . . . .	116
<b>8</b>	<b>Technological assessment and outlook</b>	<b>117</b>
<b>A</b>	<b>Experimental techniques and conditions</b>	<b>119</b>
A.1	In-house designed pressure cell for superheated water . . . . .	119
A.2	X-ray diffraction (XRD) . . . . .	120
A.2.1	High resolution wide-angle X-ray diffraction WAXD . . . . .	120
A.2.2	Simultaneous small and wide-angle X-ray diffraction (SAXS/WAXD) . . . . .	121
A.2.3	WAXD background correction . . . . .	122
A.3	Transmission electron microscopy (TEM) and electron diffraction (ED)	123
A.4	Fourier transform infrared spectroscopy (FTIR) . . . . .	123
A.5	Gel permeation chromatography (GPC) . . . . .	124
A.6	Differential scanning calorimetry (DSC) . . . . .	124
A.7	Solid state nuclear magnetic resonance (NMR) spectroscopy . . . . .	125
A.8	Thermogravimetric analysis and high resolution TGA . . . . .	125
<b>B</b>	<b>Indexing water grown PA2,14 crystals</b>	<b>126</b>

---

<b>Bibliography</b>	<b>128</b>
<b>Samenvatting</b>	<b>138</b>
<b>List of Publications</b>	<b>141</b>
<b>Dankwoord</b>	<b>143</b>
<b>Curriculum vitae</b>	<b>145</b>



# Summary

*Polyamides: Hydrogen bonding, the Brill transition, and superheated water*

Aliphatic polyamide, commonly known as nylon, was the world's first synthetic fiber and has found its largest application range in tires, carpets, stockings, upholstery, and adhesives. All polyamides have a recurring amide group ( $-\text{CONH}-$ ) present in the molecular structure with hydrogen bonds between these recurring amide groups. In comparison to other polymers such as polyethylenes, polyamides have a high melting temperature. Although polyamides have been extensively studied by many research groups, much is still to be learned and achieved regarding these materials.

The first main achievement reached in this thesis concerns a new and improved insight and understanding of the Brill transition seen in many polyamides. The Brill transition is a solid state crystalline transition observed in polyamides on heating. The Brill transition temperature is defined as the temperature at which the characteristic intersheet and interchain reflections observed in wide angle X-ray diffraction (WAXD) merge to a single reflection which is maintained up to the melt. The nature and mechanisms behind the Brill transition has been a matter of debate ever since it was first studied in 1942. The work presented in this thesis creates a better understanding of the mechanisms involved during the Brill transition, and how the Brill transition might be influenced by hydrogen bonding; a major factor influencing many polyamide properties.

It appears plausible that the Brill transition would be influenced by hydrogen bonding, or more specifically, by a weakening of hydrogen bonding. By using a unique set of piperazine based copolyamides specially tailored to study the influence of hydrogen bonding on various (physical) properties, we are able to study how the Brill transition relates to hydrogen bonding. We show that the Brill transition is independent of the piperazine content, and therefore also independent of the hydrogen bond density. The Brill transition is caused by conformational changes in the polyamide main chain which cause the methylene units to twist, whilst hydrogen bonding is retained. When the methylene units next to the amide groups are able to twist sufficiently, the Brill transition is observed. The Brill transition is therefore not a classical first or second order transition, but a solid state crystalline transition driven

by the crankshaft motions in the polyamide main chain.

The work presented on the Brill transition has made a significant contribution towards completely understanding this transition. The use of specially tailored and designed copolyamides together with the use of many high quality analytical techniques proved essential to the successes achieved here. The work presented in this thesis combines the knowledge and expertise from two distinctly different, yet complementary fields in polymer research.

The understanding gained from studying the Brill transition and the chain motions present in polyamides provide the possibility for understanding the influence of water, and more specifically the influence of superheated water, which is water above 100°C, on polyamides in general. The second main achievement described in this thesis involves dissolving polyamide in water. We show that superheated water is a solvent for various (commercial) polyamides, including polyamide 4,6 and polyamide 6,6. The conformational changes in the polyamide during the Brill transition are key in the dissolution process, allowing highly mobile water molecules in the superheated state to penetrate the crystal lattice and break the hydrogen bonds between the amide groups. On crystallization from the water solution, which occurs upon cooling the solution, water molecules associate to the amide group in the crystal lattice, weakening the amide-amide hydrogen bonds. On heating the dried, water crystallized polyamide above the Brill transition, the water molecules are released from the crystal lattice and the hydrogen bonds are restored. The removal of water molecules at the Brill transition is typically observed by an exothermic event in differential scanning calorimetry (DSC) experiments performed on dried sedimented water crystallized polyamide crystals. The influence of water on the crystal lattice is observed very clearly for polyamide 2,14 where the water molecules incorporated in the crystal lattice cause a slip in the hydrogen bonded planes. This slippage results in the coexistence of a triclinic and monoclinic crystal structure observed in WAXD. On heating above the Brill transition temperature, the water molecules exit from the crystal lattice, and the polyamide shows only the triclinic crystal structure.

The work presented in this thesis, especially the work related to the use of superheated water as a polyamide solvent, opens the door for an environmentally friendly processing route. A route in which water instead of organic solvents and acids are used to process polyamides. For the use of (superheated) water in processing applications such as film casting and recycling it is essential that the polyamide crystallization from the superheated water is a controlled process. Currently this is not the case; on cooling the polyamide/water solution the polyamide crystallizes from solution rapidly and uncontrolled when sufficient undercooling is obtained. The growth of large single crystals for example is hampered by this fast crystallization. The next step that needs to be taken is to control the crystallization, for example by adding salts to the solution, thereby preventing or manipulating

---

the crystallization,<sup>33</sup> even at room temperature. Dependent on the choice of ions and the requirements applicable to the applications under consideration, it would be possible to influence or suppress the crystallization. The possibilities for environmentally friendly polyamide processing using water-based technology are a promising prospect for the future.





## Chapter 1

# Introduction

Well known natural polymers are cellulose, starch, chitosan, proteins, and natural rubber. Nature produces these proteins and polypeptides from 20 amino acid building blocks with a high precision and, if so required, in large amounts.<sup>64</sup> The precise combination of amino acids and the order in which they are arranged along the chain ultimately controls the mechanical properties of the material which they form.<sup>104</sup> Scientists have invested great effort into understanding and mimicking the natural processing and properties of these materials. Amongst the most studied proteins is silk.<sup>31,97</sup> Spiders and silkworms produce several kinds of silk,<sup>107</sup> but the dragline silk of the *Nephila clavipes* spider, commonly known as the golden orb weaver, is considered as nature's high performance fiber with a remarkable combination of strength and toughness.

The properties of silk are due to the molecular structure and arrangement of the proteins. Silk contains crystalline and amorphous domains. The crystalline domains are responsible for the strength of the material whereas the amorphous matrix allows the crystalline domains to orient under strain to increase the strength of the material and introduces flexibility to increase the energy to break.<sup>97</sup> Unfortunately, the properties of silk are highly dependent on moisture content and relative humidity. Water present in silk acts as a plasticizer, lowering the glass transition temperature significantly.<sup>43</sup>

It is highly desirable to produce artificial high performance fibers from materials such as silk and other biopolymers from natural, renewable feedstocks. However, despite considerable effort, this goal is proving elusive, in part through an inability to control the protein conformation and morphology during artificial or biomimetic spinning.<sup>80</sup> For this reason, polyamides with a crystalline structure rather similar to proteins such as silk should be investigated in an attempt to shed light on how to control hydrogen bonding, and thus conformation.

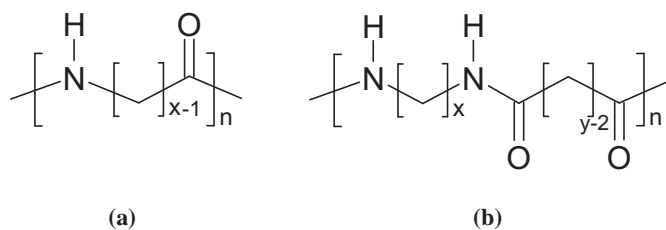


**Figure 1.1:** General structure of linear aliphatic polyamides, also known as nylon. (a) polyamide x and (b) polyamide x,y.

## 1.1 Introduction to synthetic polyamides

Polyamides, also known as nylons, are essentially man-made polypeptides. Aliphatic polyamide, commonly known as nylon, was invented by Wallace Carothers in 1935 whilst working at the Du Pont Company and was the world's first synthetic fiber.<sup>16</sup> Nylons have found their largest application range in tires, carpets, stockings, upholstery, and adhesives<sup>8</sup> and have become indispensable in today's society. All polyamides have a recurring amide group ( $-\text{CONH}-$ ) present in the molecular structure,<sup>12</sup> and can be split into two main categories, namely aliphatic and aromatic polyamides. The aliphatic polyamides form the focus of this thesis.

The general structure of linear aliphatic polyamide is depicted schematically in Figure 1.1. The aliphatic polyamides are identified by means of a numerical system according to the number of carbon atoms present in the monomer structure.<sup>8</sup>

A single number (Figure 1.1(a)) indicates that the particular polyamide was prepared from a single monomeric substance, whereas the number itself represents the number of carbon atoms in the recurring unit. An example of such a polymer is polyamide 2, which is in essence a protein; polyamide 2 has the same backbone chemistry as the polypeptide polyglycine. This feature is an illustration of how the hydrogen bonding mechanisms of protein chains and synthetic polyamides bear a relation to each other.

Another example of a polymer prepared from a single monomeric substance is polyamide 6 which is synthesized by a step-growth mechanism following the ring-opening polymerization of  $\epsilon$ -caprolactam as shown in Figure 1.2. This bulk polymerization process of polyamides is said to be a step-growth polymerization because each bond in the polymer is formed independent of the others. Step-growth polymerization commonly proceeds by a condensation reaction, in which a small molecule (typically water or an alcohol) is eliminated in each step.<sup>5</sup> In the synthesis of polyamide 6,  $\epsilon$ -caprolactam is allowed to react with water, hydrolyzing a few percent of the  $\epsilon$ -caprolactam to  $\epsilon$ -aminocaproic acid. Ring-opening polymerization

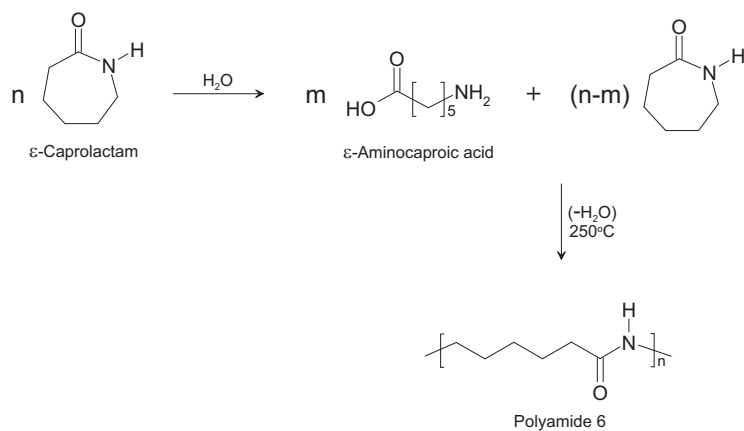


**Figure 1.2:** Synthesis of polyamide 6 (PA6) from  $\epsilon$ -caprolactam.

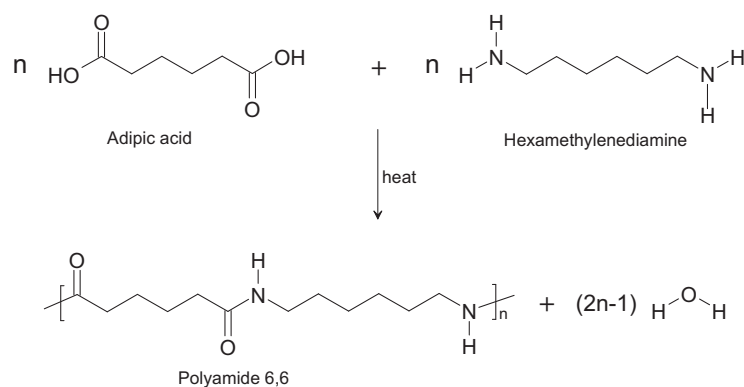


**Figure 1.3:** Synthesis of polyamide 6,6 (PA6,6) from adipic acid and hexamethylenediamine.

of the  $\epsilon$ -caprolactam is initiated by the  $\text{NH}_2$  groups of the  $\epsilon$ -aminocaproic acid, and is followed by a polycondensation reaction of the  $\text{NH}_2$  and  $\text{COOH}$  endgroups of the low molecular weight product of the ring-opening polymerization reaction, resulting in a high molecular weight product. During the final step water is eliminated.<sup>90</sup>

When two numbers are given, as shown in Figure 1.1(b), separated by a comma, a dash, or a space, the polyamide was prepared using two reactants, namely a diamine and a diacid.<sup>73</sup> The first number refers to the number of carbon atoms in the diamine, and the second number refers to the number of carbon atoms in the diacid. Polyamides are grouped together based on this nomenclature. For instance, even-even polyamides are polyamides in which both the number of carbon atoms in the diamine and the diacid are even, for example polyamide 6,y, where  $y = 6,8,10$  etc. Polyamide 6,6 is prepared by the reaction of the six-carbon adipic acid with the six-

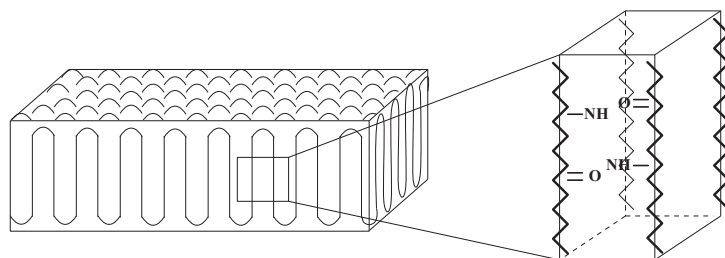


**Figure 1.4:** Folded chains in a crystalline structure (left-hand side), and a schematic unit cell for nylon (right-hand side).

carbon hexamethylenediamine at 280°C as shown in Figure 1.3. In commercial processes these two compounds are allowed to react in equimolar proportions to produce a 1:1 salt.<sup>90</sup> Heating the salt in a first reaction step in water under high pressure to a temperature of 280°C causes an oligomerization reaction to take place. Water molecules are lost as a condensation reaction occurs between the  $\text{-COO}^-$  and  $\text{-NH}_3^+$  groups of the salt to give the prepolymer. In the final polycondensation step occurring in the melt at 1 bar, high molar mass polyamide 6,6 is generated.

## 1.2 Crystal structure and hydrogen bonding in polyamides

Important concepts in the field of polyamides are crystal structure and hydrogen bonding. An ideal polymer crystal is made from an ordered, infinite repetition of identical structural units in space, referred to as the crystalline state.<sup>57</sup> When no order is present, the polymer is in the so-called amorphous state. In general, polymers do not have an ideal crystal structure due to the great length and irregularity of polymer molecules.<sup>1</sup> Certain polymers do not crystallize at all and remain in the amorphous state. Most polymers, including polyamides, are semicrystalline, which means that these polymers contain crystalline and amorphous regions.

Polymer crystals are thin and lamellar in nature.<sup>1</sup> The polymer's molecular chains are folded back and forth between the two principal faces of each lamella. A sketch of this chain folding in a crystal is given in Figure 1.4 together with a schematic unit cell for polyamide. Crystals grown from dilute solution typically have lamellar dimensions<sup>3</sup> in the order of  $1000 \text{ nm}^2 \times 6 \text{ nm}$ .

Many polymers, such as polyamides, exhibit a form of cross-linking in the polymer crystal through hydrogen bonding. Hydrogen bonding is a special case of the dispersional forces which are present between molecules in the absence of

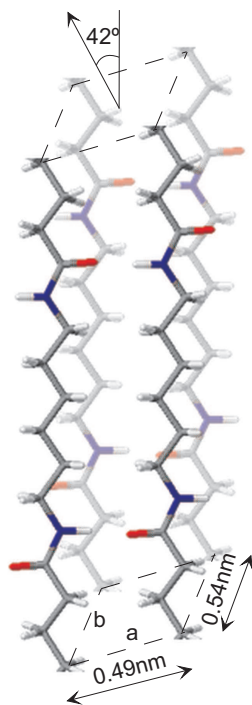


**Figure 1.5:** The unit cell of polyamide 6,6 after Bunn and Garner.<sup>13</sup> Here blue is nitrogen (N), red is oxygen (O), grey is carbon (C), and white is hydrogen (H). The cell is triclinic with  $a = 0.49\text{nm}$ ,  $b = 0.54\text{nm}$ ,  $c = 1.72\text{nm}$ ,  $\alpha = 48.5^\circ$ ,  $\beta = 77^\circ$ ,  $\gamma = 63.5^\circ$ . The hydrogen bonds between the amide groups form a hydrogen bonded sheet in the  $ac$ -plane, with an interchain distance of  $0.44\text{nm}$ . Van der Waals forces are present between the sheets, with an intersheet distance of  $0.37\text{nm}$ .

strong permanent dipoles.<sup>12</sup> Under regular circumstances, a neutral hydrogen should form a covalent bond with only one other atom. It is known, however, that under the right conditions a hydrogen atom is attracted by rather strong forces to two atoms, thus forming a hydrogen bond between these two atoms. In the extreme event, the hydrogen atom loses its electron to another atom and the bare proton forms the hydrogen bond.<sup>57</sup> Thus, in general for polyamides, a hydrogen bond is formed between a proton donor (e.g. the NH in the amide group) and a proton-acceptor (e.g. the carbonyl-oxygen in the amide group).<sup>12</sup>

All even-even polyamide crystals have the same principal structure; chain folded, hydrogen bonded sheets held together by van der Waals forces.<sup>52</sup> Figure 1.5 shows the unit cell, the repeating crystalline unit in a polymer, for polyamide 6,6. Here the hydrogen bonds are formed in the sheets, and the van der Waals forces are present between the sheets. The hydrogen bonding patterns of various polyamides differ. The cause of these differences are twofold: the stereochemistry of a particular nylon determines how the hydrogen bonds align between adjacent chains, and the hydrogen bonded sheets do not always stack in the same manner; in some cases the sheets stack with a triclinic unit cell (progressive shear), and in others with a monoclinic unit cell (alternating up and down shear).

### 1.3 The Brill transition

On heating certain polyamides show a solid state crystalline transition known as the Brill transition. When a polyamide is heated, the room temperature triclinic crystal structure changes into a high temperature so-called “pseudo-hexagonal” crystal structure at the Brill transition temperature.<sup>11</sup> The term pseudo-hexagonal is often misleading; in hexagonal systems one of the unit cell angles needs to be 60° or 120° and the other two angles need to be 90° each. The original powder diffraction patterns used by Brill<sup>11</sup> only showed a *projected* angle of 60°. There was no proof of a true hexagonal phase. Unfortunately the term “pseudo-hexagonal” has led to dilemmas and mis-interpretations in the past. Nonetheless, the Brill transition temperature is defined as the lowest temperature for which the interchain distance within a hydrogen bonded sheet and the intersheet distance between hydrogen bonded sheets are equal. This implies that at the Brill transition, the projection along the *c*-axis shows that

$$a \sin \beta = b \sin \alpha = 0.42\text{nm},$$

and implies that the chains in this projection, looking along the chain direction, pack in a two-dimensional lattice.

Brill transitions have been observed for many polyamides,<sup>50,113</sup> but the true nature of the transition is unclear. The Brill transition shows hysteresis upon heating and cooling typical of a first order process.<sup>79</sup> However, an exothermic peak in DSC traces at the Brill transition temperature is usually not observed. Additionally the temperature at which the Brill transition occurs is strongly dependent on molecular structure and crystallization conditions.<sup>79</sup>

The role of hydrogen bonding in the Brill transition is also uncertain. Many groups<sup>15,21,38,45</sup> believe that the integrity of the hydrogen bonded sheet structure, present in the room temperature structure, is maintained throughout the Brill transition, and up to the melting point. Supporting evidence for this theory is a deuterated polyamide 6,6 (PA6,6) NMR study where it is shown that the motion of the ND groups can only be modelled by assuming a restricted motion of these groups below the melt temperature.<sup>38</sup> Also an X-ray diffraction study on PA6,6 shows that the intersheet distances between the amide groups are too large to allow hydrogen bond formation.<sup>21</sup> Furthermore, a polarized  $\mu$ -FTIR study on PA6,6 model systems show that the Brill transition proceeds without significant hydrogen bond rearrangement.<sup>22</sup> Other groups however do see evidence for the pseudo-hexagonal phase being the cause of a (partial) rearrangement of hydrogen bonds into intersheet directions, similar to that first postulated by Brill. It has even been proposed that the amide groups flip out of the hydrogen bonded plane, by 60° or even 120°, to form intersheet hydrogen bonds.<sup>53</sup> The rearrangement of hydrogen bonds does however provide a simple explanation for the interchain distances remaining virtually constant

between the Brill transition temperature and the melting temperature. Recently, it has been proposed that conformational disorder in the main polymer chain is the driving force behind the Brill transition. During the conformational disordering of the methylene sequences the intermolecular hydrogen bonds between the amide groups are maintained.<sup>95</sup>

## 1.4 Effect of water on polyamides

Next to the interactions between polyamide chains leading to hydrogen bonding and crystallization as discussed above, there are also external interactions between the polyamide chain and its surroundings. One such interaction is between the amide group and water molecules. Water molecules which are readily present in the air adsorb onto the amide groups in the amorphous phase. The amount of water present is dependent on the relative humidity of the air with which the polyamide is in equilibrium. The amount of water adsorbed at a given temperature and relative humidity is proportional to the amorphous fraction.<sup>92</sup> The sorption of water by polyamides has a major effect on the polyamide's mechanical properties,<sup>93</sup> similar to the effect water has on the mechanical properties of silk. The modulus and yield stress decreases, and the elongation and energy to break increases with an increase in water content. Water present in the amorphous phase exerts a plasticizing effect on all aliphatic polyamides that is quantitatively the same.<sup>83</sup> Therefore the reported properties of polyamides are usually those of a mixture of polyamide and water.

Polyamides are also sensitive to hydrolysis by water molecules due to the amide group present in the polymer main chain.<sup>17</sup> During hydrolysis, water present in the amorphous phase can, at elevated temperatures, cause a reversal of the reactions shown in Figures 1.2 and 1.3 leading to a decrease in the degree of polymerization. In water at high temperatures the decomposition of polyamides proceeds very rapidly because at these conditions water possesses acid-like properties which favor hydrolysis. For example, 30 minutes at 380°C and 280bar completely decomposes PA6,6 to monomer units.<sup>74</sup> At lower temperatures, particularly below 374°C, the decomposition rate is relatively low.

## 1.5 Superheated water

As discussed above, water is a significant variable that can greatly influence a polyamide's properties. Water is a clear, colorless, odorless, tasteless liquid with a unique set of properties.<sup>75</sup> Without water, life on earth as we know it would simply not be possible. Water is found in various states; the most common are solid (ice),



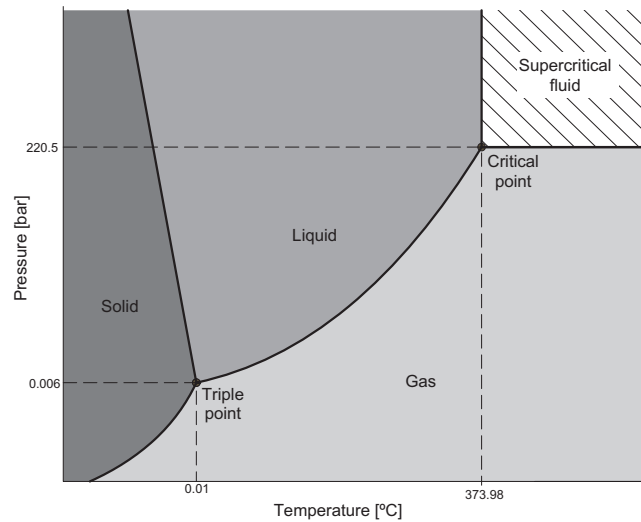


**Figure 1.6:** Temperature/pressure phase diagram for water (not to scale). Above 100°C and sufficient pressure to maintain the liquid state, water is in the superheated state.

liquid (potable water), and gas (steam). However, water can also be in the superheated or the supercritical state.

Superheated water, also known as subcritical water, is water in the liquid state between 100 and 373.98°C. At the critical temperature (373.98°C), water goes from the superheated state to the supercritical state.<sup>19</sup> Superheated water is found in nature in the form of geysers and hydrothermal vents.<sup>75</sup> Water inside cave-like reservoirs is heated by the earth's magma and becomes superheated. Boiling does not occur because of pressure on the water. The higher the pressure on the surface of the water, the higher its boiling point. At some point even this superheated water may be hot enough to start boiling, even at the elevated pressures within the reservoir. As it does, the steam that forms creates a bubble that expands very rapidly, pushing the superheated water around it out the geyser/vent. The eruption carries steam, superheated water, and dissolved gases into the surrounding environment.

The superheated temperature region is characterized by an increase in pressure with temperature. Figure 1.6 shows the phase diagram of water. Above 100°C, and provided the pressure is sufficiently high to maintain the liquid state, water is in the superheated state. At temperatures below 300°C liquid water is fairly incompressible, which means that pressure has little effect on the physical properties of water. Above 300°C, water starts to behave as a near-critical liquid, and the physical properties, such as density, start to change more significantly with pressure. Water changes more dramatically when it becomes a supercritical fluid because of the breakdown of its structure as the temperature rises.<sup>19</sup> As temperature increases, the thermal

motion of the molecules disrupt the hydrogen bonding network. Superheated water has an expanded structure due to weak intermolecular hydrogen bonding,<sup>25</sup> but in the supercritical state its nature approaches that of a collection of light mobile molecules.<sup>19</sup>

Superheated water is finding an ever increasing application field, especially in the field of compound extraction. Extraction using superheated water tends to be fast because diffusion rates increase with temperature. Organic materials tend to increase in solubility with temperature, for example, the extraction of essential oils from rosemary<sup>6</sup> and coriander<sup>28</sup> are performed using superheated water. Superheated water is being used commercially to extract starch material from marsh mallow root for skincare applications and to remove low levels of metals from high-temperature resistant polymers.<sup>18</sup>

In a ‘Gedankenexperiment’, of which the outcome is discussed in Chapter 4, it seems plausible that (superheated) water will have a significant influence on the hydrogen bonding in polyamides. In the superheated state, water molecules are highly mobile and due to the elevated temperatures the hydrogen bonding in polyamides weakens. Although the interactions between the highly active water molecules and the weakening polyamide hydrogen bonds is unknown at the beginning of this thesis, it will become apparent that these interactions are substantial and that the superheated water molecules have sufficient energy to break the already weakened hydrogen bonds completely, leading to a polyamide/water solution.

## 1.6 Objectives of this thesis

The goals of this thesis are twofold: one is to investigate the influence of hydrogen bonding and the Brill transition on the crystallographic properties of polyamides. The objective of a part of this research is to obtain a better understanding of the mechanisms involved during the Brill transition, and how the Brill transition is influenced by hydrogen bonding. Secondly, we will show that polyamides can be dissolved in superheated water. The knowledge gained in the first part of this thesis is used to further understand how the Brill transition and hydrogen bonding in polyamides are influenced by superheated water.

## 1.7 Scope of this thesis

**Chapter 2** addresses the cause of the Brill transition. This chapter shows by means of a unique set of piperazine based copolyamides that the Brill transition is integrally linked to conformational changes in the main polymer chain. The piperazine based

copolyamides allow for variations in the hydrogen bond density without affecting the crystallographic properties of the polyamide. The influence of hydrogen bonding on the Brill transition is also investigated. In **Chapter 3** a different set of copolyamides is investigated in which a peculiar Brill transition is observed. The peculiarity of the transition discussed in Chapter 3 is that instead of a merger of the interchain and intersheet reflections, a crossover of the two reflections is observed. **Chapter 4** discusses the influence of superheated water on polyamide 4,6, which is a polyamide with a high hydrogen bond density. Therefore the influence of superheated water on the hydrogen bonds should be the greatest on this polyamide in comparison to other polyamides. **Chapter 5** compares polyamide 6,6 to polyamide 4,6. Experiments similar to those performed on polyamide 4,6 are performed on polyamide 6,6 which has a tilted unit cell compared to polyamide 4,6. **Chapter 6** shows the generality of the principles discussed in the previous chapters by studying various (commercially available) synthetic polyamides in the presence of superheated water. **Chapter 7** combines the knowledge obtained in Chapters 2 and 4 by describing how superheated water influences the hydrogen bonding in the piperazine based copolyamides first presented in Chapter 2. The effect of hydrogen bonding together with superheated water on polyamides is also studied in this chapter. Finally this thesis concludes with a discussion of the technological significance and applications of this work, together with an outlook of what still remains to be achieved.

## Chapter 2

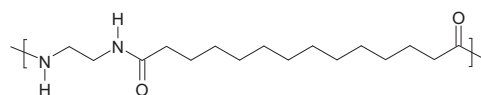
# The influence of hydrogen bonding on the conformation changes, the Brill transition, and lamellar thickening in piperazine based (co)polyamides\*

Copolyamides, based on 1,12-dodecanedicarboxylic acid and different ratios of 1,2-ethylenediamine and piperazine, i.e. PA2,14-*co*-pip,14, as well as the homopolymers PA2,14 and PApip,14 are studied. Incorporation of the piperazine component in the homopolymer PA2,14 reduces the number of hydrogen bonds. This provides a unique opportunity to investigate the influence of hydrogen bonding on the origin of the Brill transition and chain mobility within polymer crystals. Time resolved conformational, structural, and morphological changes during heating are followed by FTIR spectroscopy, WAXD, and SAXS. For a piperazine content between zero and 62mol% the Brill transition occurs at approximately the same temperature. The transformation is triggered by conformational changes in the methylene sequences of the main chain, followed by twisting in the methylene sequences next to the amide group. This results in enhanced chain mobility along the *c*-axis causing lamellar thickening. For a piperazine content of 80mol% and higher, no Brill transition is observed. However, conformational changes in the methylene sequences of the main chain trigger lamellar thickening.

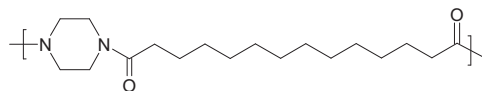
---

\*This chapter is largely based on:

E. Vinken, A.E. Terry, S. Hoffmann, B. Vanhaecht, C.E. Koning, and S. Rastogi, *Macromolecules* **2006**, 39, 2546–2552.



(a) PA2,14



(b) PApip,14

**Figure 2.1:** Chemical structure of (a) 1,2-ethylenediamine-based and (b) piperazine-based repeat units.

## 2.1 Introduction

Polyamides have a relatively high melting point in comparison to other polymers due to the hydrogen bonds that form between the recurring amide groups. By varying the density of these hydrogen bonds, it is possible to greatly influence the polyamide's physical properties.<sup>27</sup> One route to change the hydrogen bond density is to change the length of the aliphatic portions in the linear polyamide chains, which results in a change in the spatial separation between the amide groups, and hence an overall change in the hydrogen bond density.<sup>12</sup> However, this approach leads to different polyamides, such as polyamide 4,6, polyamide 6,6, etc. which inevitably leads to different crystal structures, lamellar thicknesses, etc. All of these variables inevitably complicate the study of the hydrogen bond density in polyamides. Therefore a second route to change the hydrogen bond density becomes more attractive; replace the amide group with a different chemical unit that reduces the possibility of hydrogen bond formation, but has similar structural features and size as the amide group. These similarities in structure enables the different chemical units to co-crystallize with the amide units. A suitable co-monomer is piperazine, shown schematically in Figure 2.1. Since a piperazine residue does not contain an amide hydrogen it is unable to act as a hydrogen bond donor, thus hydrogen bonding is reduced. However, piperazine can act as a hydrogen bond acceptor.<sup>39,98</sup>

In a previous study a range of random copolyamides of polyamide 2,14 (PA2,14) and polyamide piperazine,14 (PApip,14)<sup>39,98</sup> were synthesized with varying piperazine content from 30mol% to 90mol%. The homopolymers PA2,14 and PApip,14 were also prepared. The copolymers exhibit a decrease in melting

and crystallization temperature with increasing piperazine content. Although the introduction of a rigid cyclic monomer usually leads to an increase in the melting temperature with respect to the homopolymer, the reduced ability of the piperazine units to form hydrogen bonds overrules this effect. It was also shown that up to a piperazine content of 62mol%, the PA<sub>2,14</sub> and PA<sub>pip,14</sub> units co-crystallize into a common crystal lattice, which differs only slightly from the PA<sub>2,14</sub> crystal lattice.<sup>39</sup> For a piperazine content of 90mol% and higher, the crystal structure was distorted from that of PA<sub>pip,14</sub>. For an intermediate piperazine content of 70mol% and 82mol%, the studies indicated a co-existence of the PA<sub>2,14</sub> and PA<sub>pip,14</sub> crystal structures. It was further concluded that the piperazine rings incorporated into the copolyamides were oriented parallel to the hydrogen bonded sheets, the sheets being shifted parallel to one another.

In the studies mentioned above<sup>39,98</sup> the crystal structure of the homopolymers and the copolymers were only investigated at room temperature. It is known, however, that many polyamides show a Brill transition<sup>11,22,50,79,95,103</sup> upon heating. The Brill transition entails a solid state crystalline transformation from a low temperature triclinic to a high temperature pseudo-hexagonal phase, as shown by the fact that the 100 reflection related to the interchain distance and the 010 reflection related to the intersheet distance merge into a single reflection. As discussed in Section 1.3, the true nature of the Brill transition is still a matter of debate. The Brill transition is strongly dependent on molecular structure and crystallization conditions.<sup>79</sup> Therefore the Brill transition should be affected by the incorporation of a second diamine residue such as piperazine into the polyamide chain, both due to the possible influence on the crystal structure and, more importantly, due to the decrease in the hydrogen bond density. This chapter investigates the behavior upon heating of the homopolymers PA<sub>2,14</sub> and PA<sub>pip,14</sub>, and the copolymers PA<sub>2,14-co-pip,14</sub> by simultaneous SAXS/WAXD and Fourier transform infrared (FTIR) spectroscopy. With these experiments we aim to understand the origin of the Brill transition in polyamides in general.

## 2.2 Experimental description

The homopolymers PA<sub>2,14</sub> and PA<sub>pip,14</sub> as well as the copolymers PA<sub>2,14-co-pip,14</sub> are synthesized via a polycondensation reaction of 1,12-dodecanedicarbonyl dichloride and varying amounts of 1,2-ethylenediamine and piperazine as described elsewhere.<sup>98</sup> Thermal and molecular characterization is also described elsewhere.<sup>39,98</sup> The piperazine-based copolyamides used in this study have a piperazine molar fraction of 0.30, 0.46, 0.54, 0.62, 0.82, and 0.90. These copolymers are referred to as coPA 0.30 through to coPA 0.90, respectively.

Simultaneous small and wide angle X-ray diffraction experiments are

performed on the High Brilliance beamline (ID02),<sup>96</sup> at the ESRF in Grenoble (France). The experiments are performed as described in Appendix A.2.2 using a Linkam TMS94 hotstage and controller. Sample preparation is done by sealing each of the (co)polyamides in aluminium DSC pans and heating them in a TA Instruments Q1000 DSC to temperatures well above (at least 15°C) their respective melting temperatures and cooling to room temperature at 10°C/min. This is performed twice for each sample. The samples are subsequently allowed to relax at room temperature for more than a week. This is because of changes in the lamellar spacings at room temperature previously observed for these materials.<sup>39</sup> After this pre-treatment, the samples are removed from the DSC pans and placed in 2mm diameter Lindemann capillaries used to perform the X-ray diffraction experiments. All diffraction patterns are corrected for absolute intensity and integrated to give intensity against  $q$ . The SAXS results are Lotentz corrected, i.e. the intensity data are multiplied by  $q^2$ . The position and intensity of the crystalline peaks in the WAXD patterns are fitted using a pseudo-voigt function for each crystalline peak. Additionally, the fitting function contains a linear term to account for residual scattering arising from the background and the Lindemann tube. The melting end point and the crystallization onset temperatures observed during the DSC measurements are used to calibrate the temperatures at which the sample is completely amorphous and when crystallization has just begun, respectively, as detected by WAXD.

FTIR experiments on melt crystallized (co)polyamides are performed as described in Appendix A.4.

### 2.3 The Brill transition and lamellar thickening using simultaneous SAXS/WAXD

Figure 2.2 shows the data obtained from simultaneous WAXD and SAXS patterns collected on the High Brilliance beamline ID02 at the ESRF. The integrated WAXD patterns of intensity against  $q$  are fitted using a number of pseudo-voigt functions and a linear background. The  $d$ -spacings are obtained from the fitted peak positions via the relation  $d = 2\pi/q$ . The WAXD pattern, Figure 2.2(a), for the homopolymer PA2,14 at 50°C corresponds well to other data reported for this homopolymer at room temperature.<sup>39,68</sup> On heating, the interchain 100 ( $d = 0.42\text{nm}$ ) and intersheet 010 ( $d = 0.39\text{nm}$ ) reflections merge to an extent that no further deconvolution is feasible. The merger of the interchain 100 and intersheet 010 reflections is shown in Figure 2.2(a). This behavior is typically called the Brill transition<sup>11</sup> in polyamides, and the temperature at which it occurs corresponds to the Brill transition temperature. PA2,14 shows a melt temperature of 236°C which compares well with other results.<sup>39,98</sup> On cooling from the melt the reverse behavior is seen,

albeit at some undercooling. At  $\sim 25^\circ\text{C}$  below the melting point, the homopolymer crystallizes, resulting in a single reflection which splits into two reflections on further cooling. The WAXD patterns for coPA 0.30 up to coPA 0.62 also show a Brill transition at  $\sim 150^\circ\text{C}$  and a melt temperature in the order of  $200^\circ\text{C}$ . Upon undercooling, crystallization occurs in the vicinity of  $190^\circ\text{C}$  and the Brill transition occurs in the vicinity of  $140^\circ\text{C}$ . In a previous study<sup>105</sup> reminiscence of the low temperature phase was seen at high temperatures for coPA 0.54. In the data shown in Figure 2.2 this is not seen. The differences could be due to inhomogeneities in the starting sample, thermal history, (a lack of good) thermal contact with the heating device, or other experimental error in the previous study. Hence more care is taken in the current experiments shown in Figure 2.2 to avoid such experimental artefacts. CoPA 0.82 and coPA 0.90 show behavior similar to homopolymer PApip,14 where the intersheet 010 and interchain 100 reflections do not merge into a single reflection prior to melting.

In Figure 2.2 the position of the SAXS patterns at  $50^\circ\text{C}$  shows an increase with increasing piperazine content, which is also noted in a previous study.<sup>39</sup> On heating, all the (co)polyamides show a gradual increase in lamellar thickness just before melting to double (or more) their initial value at  $50^\circ\text{C}$ . Note that while the lamellar thickness increases to twice the initial value, no considerable changes in crystallinity are observed. For the homopolymer PA2,14 and the copolyamides up to a piperazine content of 62mol% the lamellar thickness changes more rapidly with increasing temperature above  $165^\circ\text{C}$  (above the Brill transition temperature), see Figures 2.2(b) to 2.2(j). For the coPA 0.82, coPA 0.90, and the homopolymer PApip,14 the SAXS peak position changes more rapidly above  $110^\circ\text{C}$ , i.e.  $\sim 40^\circ\text{C}$  below the melt temperature. A remarkable observation is that polymers with high piperazine content do not show the Brill transition, although lamellar thickening occurs similarly to the copolymers that do show the Brill transition. The corresponding WAXD patterns for the high piperazine content (co)polymers do not suggest any changes in crystallinity or a phase transition around  $110^\circ\text{C}$ .

After cooling from the melt the lamellae spacing at  $50^\circ\text{C}$  is slightly higher than before heating. Due to problems with the detector, no SAXS patterns could be collected on cooling coPA 0.82 and coPA 0.90 from the melt. Based on the WAXD patterns, shown in Figure 2.2, it is expected that the SAXS cooling runs of coPA 0.82 and coPA 0.90 will follow a similar behavior as the SAXS cooling run of PApip,14. A previous study<sup>39</sup> showed that the crystal structure in the recrystallized (co)polyamides still relaxes at room temperature and that this relaxation is only observed in the large repeat distance of the lamellar stacking and not in the interchain 100 and intersheet 010 distances. This could explain why the lamellar spacing at  $50^\circ\text{C}$  in the copolyamides is larger directly after crystallization from the melt than before heating to the melt. Indeed, following sample preparation for these experiments, the



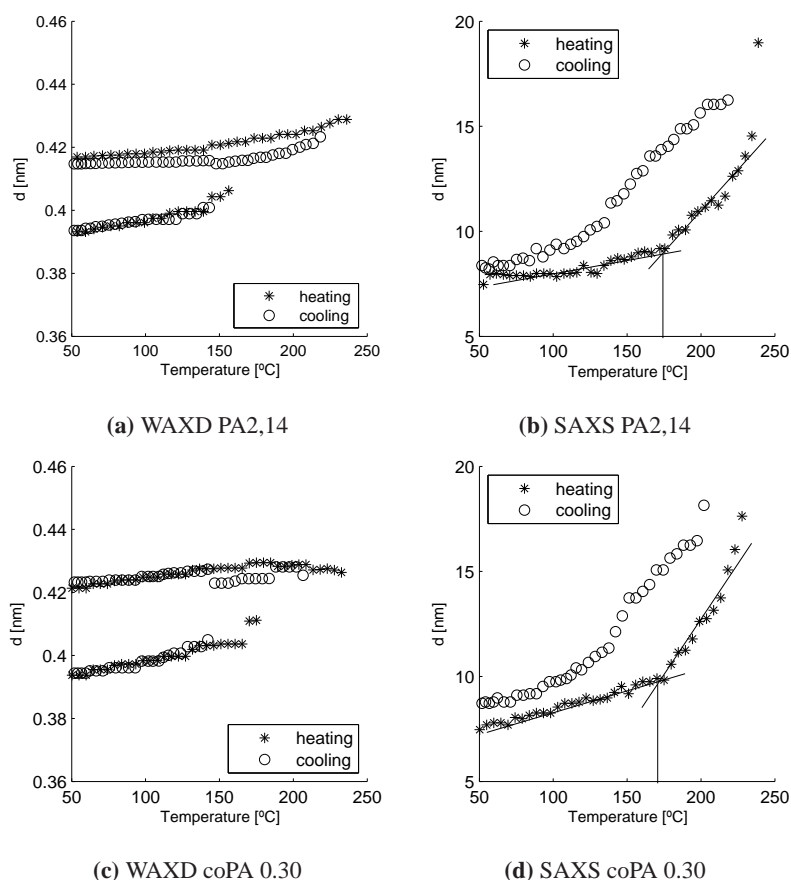
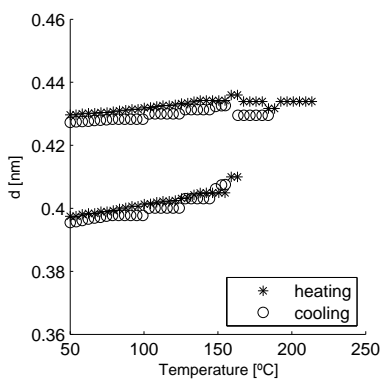


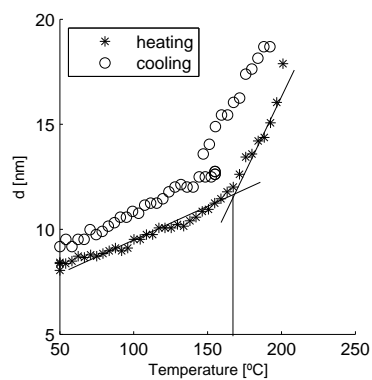
**Figure 2.2:** Simultaneous WAXD (a,c,e,g,i,k,m,o) and SAXS (b,d,f,h,j,l,n,p) of the homopolymers PA2,14 and PApip,14, and the copolymers coPA 0.30; 0.46; 0.54; 0.62; 0.82; and 0.90 during heating from 50°C to the melt and cooling from the melt to 50°C at 10°C/min. The Brill transition is observed up to a piperazine content of 62mol%. The Brill transition temperature has been taken as the last data point where deconvolution of the interchain 100 and the intersheet 010 reflections can be made. The lines over the SAXS heating runs serve as a guide to the eye. Due to problems with the detector no SAXS patterns are available for the cooling runs of coPA 0.82 and coPA 0.90. The WAXD peak positions are  $\pm 0.01$ nm and the SAXS peak positions are  $\pm 0.2$ nm.

samples were allowed to relax at room temperature for nearly a week prior to making any measurements.

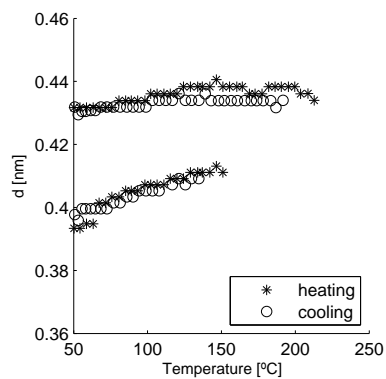
The sudden shift in the temperature required for lamellar thickening from 165°C to 110°C with an increase in the piperazine content from 62mol% to 82mol% correlates well with the sudden changes in the interchain and intersheet distances observed with an increasing amount of piperazine content from 62mol% to 82mol%,



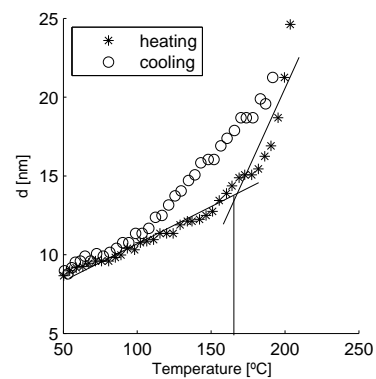
(e) WAXD coPA 0.46



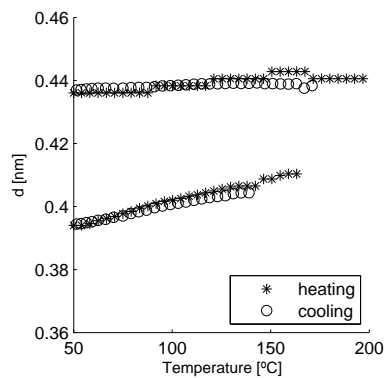
(f) SAXS coPA 0.46



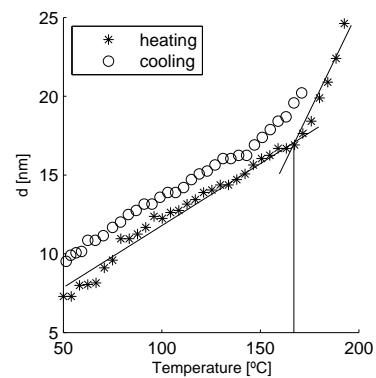
(g) WAXD coPA 0.54



(h) SAXS coPA 0.54

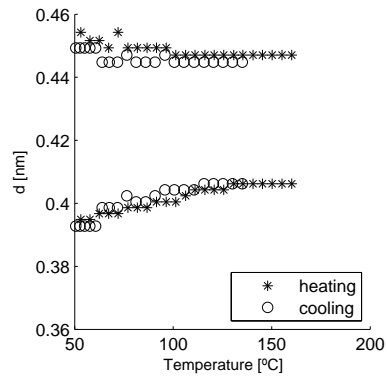


(i) WAXD coPA 0.62

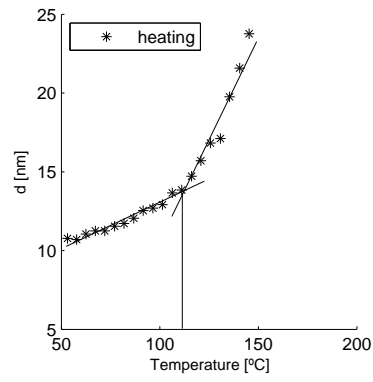


(j) SAXS coPA 0.62

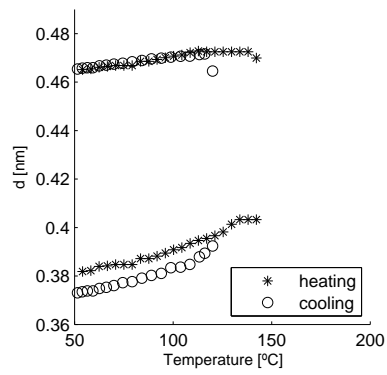
Figure 2.2: (continued)



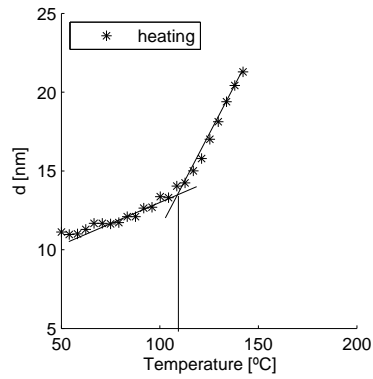
(k) WAXD coPA 0.82



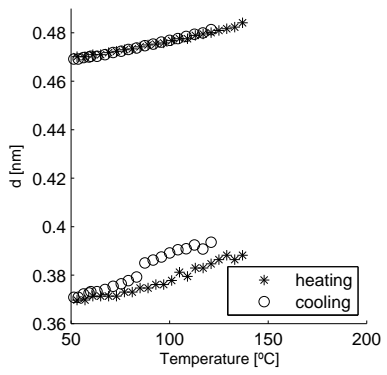
(l) SAXS coPA 0.82



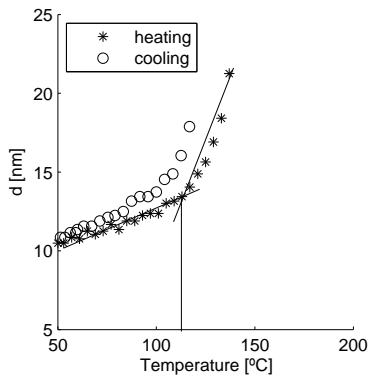
(m) WAXD coPA 0.90



(n) SAXS coPA 0.90



(o) WAXD PApip,14



(p) SAXS PApip,14

Figure 2.2: (continued)

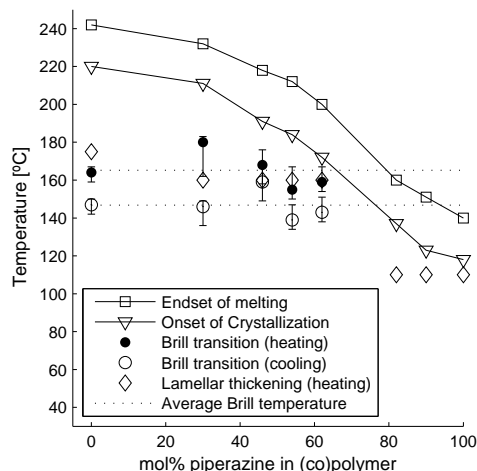


**Figure 2.3:** The Brill transition temperature on heating and cooling over the molar piperazine fraction. The Brill transition is observed up to a piperazine content of 62mol% and is taken as the last data point where deconvolution of the interchain 100 and the intersheet 010 reflections is still feasible. The onset of lamellar thickening on heating is taken from Figure 2.2. The endpoint of melting and the onset of crystallization temperatures<sup>98</sup> are given as a reference. All lines serve as a guide to the eye.

and in the  $d$ -values observed at 50°C in the WAXD patterns shown in Figure 2.2 and Figure 3 of Hoffmann *et al.*<sup>39</sup>

## 2.4 Hydrogen bond density and the Brill transition

Figure 2.3 summarizes the Brill transition temperatures on heating and cooling for the various (co)polyamides investigated. The Brill transition temperature reported in Figure 2.3 has been determined from the data reported in Figure 2.2. The last data point where deconvolution of the interchain 100 and the intersheet 010 reflections can be made is taken as the Brill transition temperature. As a reference, the temperatures of the end of melting endotherm ( $T_m$ ) from DSC measurements and the detection of the onset of crystallization ( $T_c$ ) for the (co)polyamides<sup>98</sup> are also given. The Brill transition temperature remains approximately constant, both on heating and cooling, up to a piperazine content of 62mol%. On heating the average Brill transition temperature is 165°C, and on cooling 147°C. It is to be noted that the average Brill transition temperature on heating and cooling for these lower piperazine content copolymers is higher than  $T_m$  (or  $T_c$ ) for coPA 0.82, coPA 0.90, and the homopolymer

PApip,14. This suggests that the reason that the Brill transition is not observed in coPA 0.82, 0.90, and PApip,14 is because on extrapolation the Brill transition occurs at a temperature higher than  $T_m$ .

The invariance in the Brill transition temperature for the copolyamides up to 62mol% of piperazine is unique. This has not been seen previously for other polyamide systems. When the Brill transition temperature for many different polyamides are compared,<sup>50</sup> no apparent trend is observed as a function of alkane chain length, and therefore also hydrogen bond density. Instead the different chain length polyamides crystallize into different crystalline structures.<sup>50</sup> For the copolyamides investigated here the piperazine units co-crystallize with the polyamide units yielding the same crystalline structure up to a piperazine concentration of 62mol%. Having established that the Brill transition can only be a function of the hydrogen bond density, and not of the crystal structure, it is important to examine any conformational changes occurring within these materials upon heating. For this reason FTIR spectra are collected.

## 2.5 Conformational changes

Figure 2.4 shows the FTIR spectra collected for the polymers used in this study at 30°C. All spectra are normalized relative to the area under the methylene bands between 3000 and 2800cm<sup>-1</sup> which are invariant in this range of copolymers. Figure 2.4(a) shows the frequency range from 3600 to 2800cm<sup>-1</sup>. With increasing piperazine content, the bands at 3303, 3215, and 3085cm<sup>-1</sup> show a strong decrease, whereas the band at 3005cm<sup>-1</sup> appears at higher piperazine content. The bands at 3303, 3215, and 3085cm<sup>-1</sup> are associated with NH stretch vibrations, and those at 3215 and 3085cm<sup>-1</sup> are also associated with Amide I and II overtones.<sup>47</sup> The reduction in the NH stretch vibrational bands is in line with the decreasing amount of NH groups present in the copolymers with increasing piperazine content. The band appearing at 3005cm<sup>-1</sup>, which becomes more apparent with increasing piperazine content, is most likely due to the methylene groups in the piperazine rings.

Figure 2.4(b) shows the frequency range from 1350 to 850cm<sup>-1</sup>. Close inspection of the spectral bands present in this region leads to the observation that there are several bands that can be specifically assigned to the homopolymers PA2,14 and PApip,14, respectively. Additionally, there are bands that are common to both homopolymers. Specific bands that are associated with the homopolymer PA2,14 are 946, 977, 1230, 1242, 1263, and 1320cm<sup>-1</sup>. The bands associated with the homopolymer PApip,14 are 985, 1010, 1024, 1172, 1226, 1253, and 1283cm<sup>-1</sup>. Bands common to the both homopolymers are 1054, 1188, and 1305cm<sup>-1</sup>. As expected, depending on the piperazine content, the copolyamides show either the

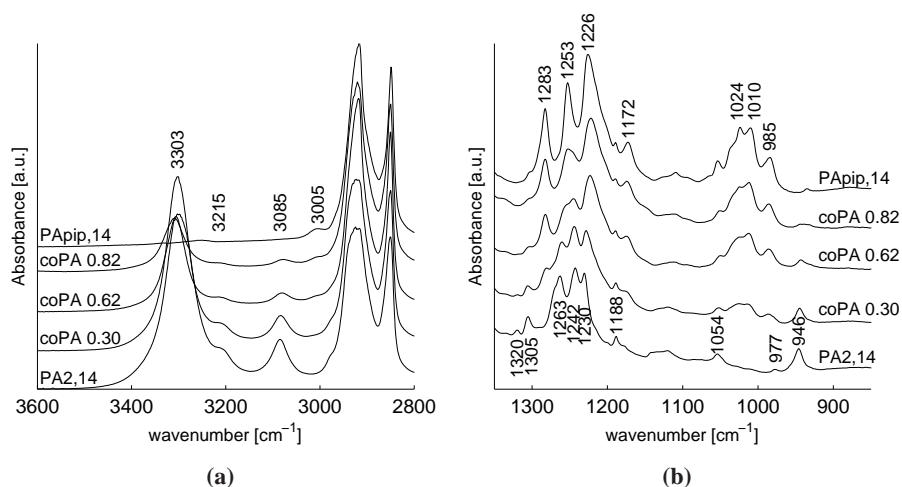


**Figure 2.4:** FTIR spectra of homopolymers PA2,14 and PApip,14 and copolyamides coPA 0.30, coPA 0.62, and coPA 0.82 recorded at 30°C. (a) shows the frequency range 3600 to 2800 $\text{cm}^{-1}$  and (b) 1350 to 850 $\text{cm}^{-1}$ .

bands associated with the homopolymer PA2,14 (see coPA 0.30 in Figure 2.4(b)), the homopolymer PApip,14 (see coPA 0.82 in Figure 2.4(b)), or both (see coPA 0.62 in Figure 2.4(b)).

Figure 2.5 shows the FTIR spectra obtained in the frequency range 1350 to 850 $\text{cm}^{-1}$  while heating the homopolymers PA2,14 and PApip,14, and the copolyamides coPA 0.30 and coPA 0.82 from 30°C to the melt. Figure 2.5(a) shows the FTIR spectra for the homopolymer PA2,14 at different temperatures. On heating, the bands at 977, 1054, 1188, 1230, 1305, and 1320 $\text{cm}^{-1}$  arising from the bending, wagging and rocking vibrations of the methylene segments<sup>23,103</sup> disappear between 150 and 180°C. This is the same temperature region where the Brill transition is anticipated, for comparison see Figure 2.2(a). For simplicity, these bands are therefore referred to as Brill bands. However, the lamellar thickening observed in the SAXS pattern for PA2,14 also occurs in this temperature region. Therefore, it is possible that some of the Brill bands seen here may be associated with the lamellar thickening and not with the Brill transition, but it is not possible to distinguish between these two effects from these FTIR spectra alone. On further heating, the bands at 946, 1243, and 1263 $\text{cm}^{-1}$  broaden considerably or disappear altogether on melting and are therefore associated with the crystalline phase. The crystalline bands at 1243 and 1263 $\text{cm}^{-1}$  are Amide III bands coupled with out-of-plane methylene motions, whereas the band at 946 $\text{cm}^{-1}$  is the Amide IV vibration.<sup>23,24,113</sup>

Figure 2.5(d) shows the FTIR spectra for the homopolymer PApip,14 on heating from 30°C to the melt. On heating from 30°C, the bands at 1188 and 1305 $\text{cm}^{-1}$

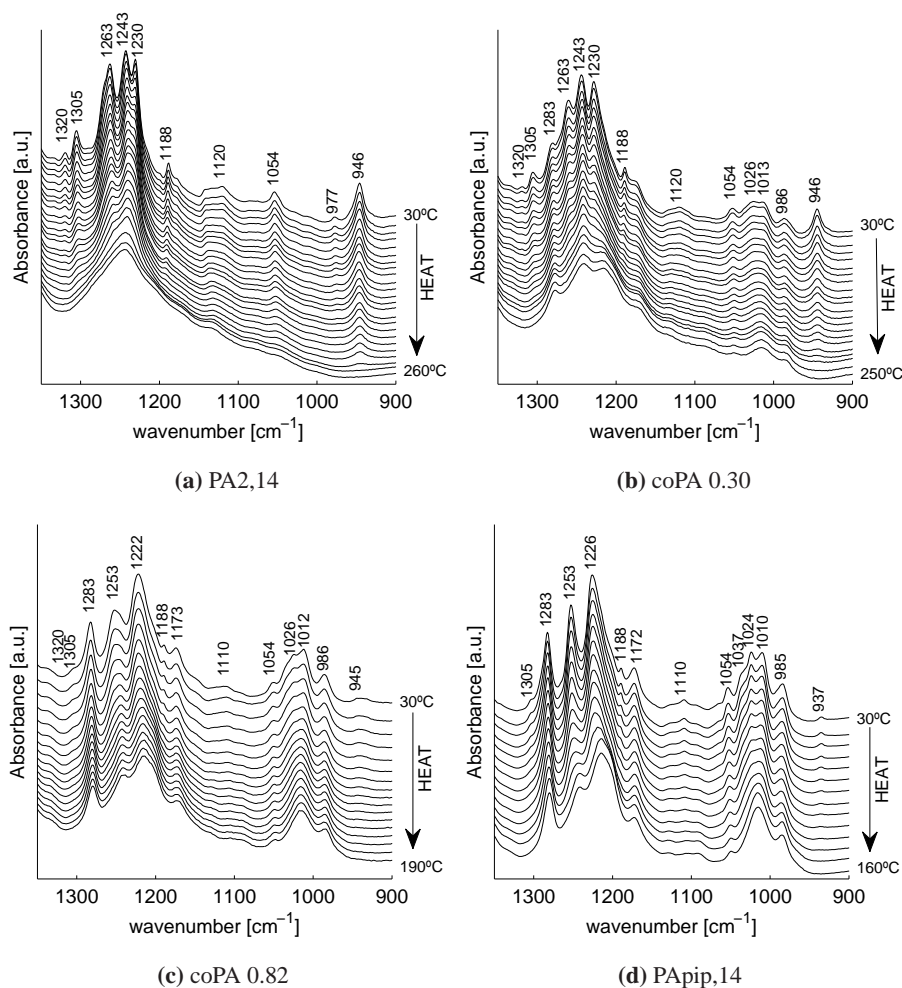


**Figure 2.5:** FTIR measurements of homopolymers PA2,14 and PApip,14, and copolyamides coPA 0.30 and coPA 0.82 on heating from 30°C to the melt at 10°C/min at regular 10°C intervals.

disappear between 100 and 110°C, i.e. in the temperature region where the change in the lamellae thickness is observed in the SAXS patterns, see Figure 2.2(p). On heating to the melt the bands at 985, 1010, 1024, 1037, 1054, 1172, 1226, 1253, and 1283 $\text{cm}^{-1}$  broaden. The bands that disappear at the Brill transition in the homopolymer PA2,14 (see Figure 2.5(a)) are also present, albeit with some changes in the homopolymer PApip,14 (see Figure 2.5(d)). The methylene band at 977 $\text{cm}^{-1}$  in PA2,14 is now present at 985 $\text{cm}^{-1}$  in PApip,14, the band at 1230 $\text{cm}^{-1}$  is at 1226 $\text{cm}^{-1}$ , and the band at 1320 $\text{cm}^{-1}$  is absent in PApip,14. These changes are

due to the differences in chemical structure and an increased rigidity of the main chain in the homopolymer PApip,14 when compared to the homopolymer PA2,14.

In previous studies<sup>95,113</sup> performed on several polyamides (PA6,10; PA6,12; PA10,10), it was found that during the Brill transition, conformational disorder occurs in the methylene sequences. With increasing temperature the intermolecular hydrogen bonding between the amide groups weaken, although it is retained up to the melt. The methylene sequences between the NH groups are found to become more disordered than the methylene sequences between the CO groups. In order to model the changes in the FTIR spectra close to the Brill transition, the methylene units adjacent to the amide groups needed to be decoupled from the remaining methylene segments. It was concluded that even after the Brill transition hydrogen bonding is retained, thus making chain rotation along the *c*-axis in the pseudo-hexagonal phase impossible. Structural changes in the methylene parts of the molecular chains were observed. Similar observations are reported by others.<sup>22,38</sup>

For the homopolymer PA2,14 shown in Figure 2.5(a), the vibrational bands associated to the methylene sequences next to the CO groups are 977 and 1054cm<sup>-1</sup> and the bands associated to the methylene sequences next to the NH groups are 1230 and 1320cm<sup>-1</sup>.<sup>24,113</sup> On heating, all these bands decrease in intensity and ultimately disappear above the Brill transition temperature but below the melting point. However, the methylene bands next to the NH group decrease faster than the methylene bands next to the CO groups. These observations are in agreement with the results reported by Yoshioka *et al.*<sup>113</sup> and Tashiro *et al.*<sup>95</sup>

Unlike in PA2,14, in PApip,14 the vibrational bands of the methylene groups next to the N (1226cm<sup>-1</sup>) and the CO (985 and 1054cm<sup>-1</sup>) groups remain even after melting. These observations suggest that in PApip,14 the rigidity along the main chain inhibits the complete disappearance of these bands, although close to the melting point broadening and a slight shifting to higher frequencies of these bands is noticed. However, similar to PA2,14, in PApip14 the bands at 1188 and 1305cm<sup>-1</sup> disappear but at lower temperatures, i.e. between 100 and 110°C, see Figure 2.5(d). These bands are related to the main chain methylene stretching and wagging motions.<sup>24</sup> Considering the absence of the Brill transition in PApip,14 these bands are not immediately related to the Brill transition. The disappearance of these two bands coincides with the change in the lamellar thickness observed in the SAXS patterns for all the polymers investigated. Conformational changes in the main chain combined with the lamellar thickening suggest the presence of enhanced chain mobility along the *c*-axis. Increased chain mobility would lead to the disappearance of the trans conformers, i.e. the methylene main chain bands at 1188 and 1305cm<sup>-1</sup>. Similar chain mobility is seen in linear polyethylenes<sup>81</sup> above room temperature as is seen in polyamides above the Brill transition temperature.<sup>26</sup>

Figure 2.5(b) shows the FTIR spectra for coPA 0.30 and Figure 2.5(c) for



coPA 0.82 on heating from 30°C to the melt. The FTIR spectra for coPA 0.30 follow the same behavior as PA<sub>2,14</sub> and the spectra of coPA 0.82 follow the same behavior as PApip<sub>14</sub>.

## 2.6 Conclusions

The thermal behavior of homopolymers PA<sub>2,14</sub> and PApip<sub>14</sub> and their copolyamides, varying from 30mol% up to 90mol% piperazine, are investigated using simultaneous SAXS/WAXD and FTIR spectroscopy. These studies provide an insight into the effect of incorporating a secondary diamide that reduces the number of hydrogen bonds within the crystal lattice; thus likely to influence the Brill transition temperature.

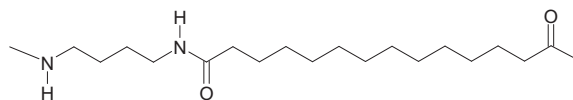
The observations are that the Brill transition temperature remains independent of the piperazine content up to a piperazine content of 62mol%. FTIR measurements suggest disorder in the trans planar zigzag conformations of the methylene segments of the main chain at the Brill transition temperature. In PA<sub>2,14</sub> this conformational disorder occurs at a higher temperature (150 to 180°C) than for PApip<sub>14</sub> (100 to 110°C). The higher temperature required for the disorder in PA<sub>2,14</sub> compared to PApip<sub>14</sub> is a consequence of the presence of hydrogen bonding in PA<sub>2,14</sub>. With the disappearance of conformational bands in the FTIR spectra, enhanced chain mobility along the *c*-axis is seen, which leads to lamellar thickening to twice the lamellae's initial, room temperature value. The striking observation is that this increase in lamellar thickening is independent of piperazine content up to 62mol%. The disappearance of the trans conformers suggests that with increasing piperazine content, i.e. as the number of hydrogen bonds decrease, changes in the intensity of these methylene bands occur at lower temperatures.

Combining the FTIR and X-ray diffraction data it can be stated that with the disappearance of the trans conformers of the methylene chain segments in PA<sub>2,14</sub> and the piperazine copolymers, chain mobility along the *c*-axis arises once the methylene unit next to the carbonyl group is able to twist, although hydrogen bonding is likely to be retained. These observations are in agreement with previous studies.<sup>22, 38, 95, 113</sup> In PApip<sub>14</sub>, where hydrogen bonding is absent, the chain mobility occurs earlier and twisting is not observed due to the piperazine rings that are oriented parallel to the hydrogen bonded sheets.<sup>39</sup>

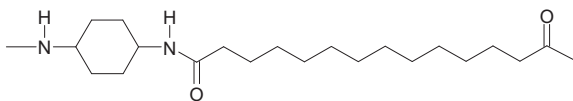
## Chapter 3

# The influence of stereochemistry on the conformational changes and the Brill transition in 1,4-diaminocyclohexane based (co)polyamides

Copolyamides based on 1,4-diaminobutane and 1,4-diaminocyclohexane (1,4-DACH) are studied. The copolyamides seem to exhibit a peculiar Brill transition; an apparent crossing instead of a merging of the intersheet and interchain reflections during the Brill transition is observed. At the temperature at which the crossover is seen in the X-ray diffraction patterns, no anomalous behavior is observed in the vibrational bands associated with the Brill transition in FTIR spectroscopy. However, other vibrational bands at elevated temperatures do provide an insight into the possible nature of this crossover. The studies suggest that the crossover is not a true Brill transition but involves an amorphous component arising due to the non-hydrogen bonded amide groups becoming more mobile above the Brill transition temperature. The trans 1,4-DACH units co-crystallize with the PA4,14 units where the cyclic units align and stack onto one another influencing the alignment of other amide units, and ultimately the hydrogen bond formation in the polymer crystal. The cyclic 1,4-DACH entities appear to cause more non-hydrogen bonded amides to occur in the amide crystal lattice. On heating above the Brill transition temperature the non-hydrogen bonded amide groups present in the copolyamide become increasingly mobile, resulting in a partial melting seen as an amorphous phase in WAXD and an exothermic event in DSC in the vicinity of the Brill transition. It is this partial melting which gives the impression of a crossover at the Brill transition.



(a) PA4,14



(b) PA1,4-DACH,14

**Figure 3.1:** Chemical structure of (a) 1,4-diaminobutane based and (b) 1,4-diaminocyclohexane (1,4-DACH) based repeat units.

### 3.1 Introduction

Polyamides form part of the engineering plastics and have found a wide application range in many products because they are strong and durable materials. On crystallization the polyamide chains fold into sheets with hydrogen bonds between the recurring amide groups; the hydrogen bonded sheets stack to form a three-dimensional structure with van der Waals forces between the sheets.

Many aliphatic polyamides show a solid state crystal transition on heating known as the Brill transition.<sup>11</sup> This transition involves the transformation from a low temperature triclinic/monoclinic crystal structure to a high temperature pseudo-hexagonal structure.<sup>3</sup> The Brill transition temperature is defined as the lowest temperature for which the interchain distance within a hydrogen bonded sheet and the intersheet distance between the hydrogen bonded sheets are equal. The most common method for determining the Brill transition is temperature dependent wide angle X-ray diffraction (WAXD). The Brill transition is observed by a merger of the interchain and intersheet reflections into a single reflection which is maintained up to the melt.

Recently Vanhaecht *et al.*<sup>99</sup> observed a peculiar Brill transition for copolyamides of polyamide 4,14 (PA4,14). In these copolyamides the diamine segment of the polyamide chain is replaced by trans isomers of 1,4-diaminocyclohexane (1,4-DACH), shown schematically in Figure 3.1. The randomly distributed trans 1,4-DACH moieties co-crystallize with the PA4,14 units and are built into the crystal structure with the cycloaliphatic rings oriented perpendicular to the hydrogen bonded sheets.<sup>99</sup> On heating these copolyamides, an apparent Brill transition occurs as is

seen by a merging of the interchain and intersheet reflections into a single reflection. However, on further heating the merged single pseudo-hexagonal reflection seems to split again into two reflections. This crossing in the Brill transition was also reported for a set of copolyamides based on 1,4-cyclohexanedicarboxylic acid (1,4-CHDA).<sup>102</sup>

In both cases the authors<sup>99,102</sup> argue that the cycloaliphatic residues prevent the formation of a pseudo-hexagonal phase during heating prior to melting. In their argumentation the authors<sup>99,102</sup> assume that during the Brill transition the alkane segments in the polymer chain exert a torsional force on the amide groups, causing them to break and flip by 60° (or even 120°) to form a three-dimensional network of intersheet and intrasheet hydrogen bonds, as proposed by Jones *et al.*<sup>53</sup> The intrachain hydrogen bonds would prevent the chains from moving further apart, causing the interchain and intersheet distances to become equal; resulting in the single reflection observed for the pseudo-hexagonal phase.<sup>53</sup> The cycloaliphatic residues incorporated in the polyamide chain could reduce the rotational mobility of the amide bonds and hence prevent the flipping of the hydrogen bonds and thus also the formation of intrasheet hydrogen bonds.<sup>99,102</sup> The authors<sup>99,102</sup> appropriately note that NMR<sup>38</sup> and infrared<sup>110,112,113</sup> studies on linear polyamide systems clearly show that the hydrogen bonds are maintained up to the melt. Therefore the hypothesis whereby the cycloaliphatic units would prevent the flipping of the hydrogen bonds and thus cause a crossing in the Brill transition, is unlikely.

Alternatively the authors<sup>99,102</sup> postulate that the presence of cyclic residues lowers the symmetry needed for a pseudo-hexagonal phase. However, in a study involving cyclic piperazine units<sup>105</sup> (see Chapter 2), which were incorporated in polyamide chains, no changes in the observed Brill transition with increasing piperazine content is observed.<sup>105</sup> It is to be noted here that the piperazine moieties are incorporated parallel to the hydrogen bonded sheets whereas the 1,4-CHDA and 1,4-DACH moieties are perpendicular to the sheets.

It is likely that the trans 1,4-DACH and 1,4-CHDA residues influence the mobility in the polyamide chain, and hence also the Brill transition. However, the exact nature of the relation between these cyclic residues and the Brill transition is still unknown. Here we investigate this unusual phenomenon, a crossing Brill transition, using the 1,4-DACH copolyamides. In this study we also use synchrotron radiation to perform WAXD experiments, but in contrast to the previously discussed publications<sup>99,102</sup> we have expanded the thermal region from room temperature up to the melt for each of the (co)polyamides. By doing so the transitions studied in this chapter become more apparent. Additionally, this is the first time that these copolyamides are investigated using infrared spectroscopy. The use of high brilliance X-ray diffraction and infrared spectroscopy should provide more insight into the cause of this crossing. This phenomenon provides a unique opportunity to further study and understand the mechanisms behind the Brill transition.

## 3.2 Experimental description

The homopolymer PA4,14 and the copolymers PA4,14-*co*-1,4-DACH,14 are synthesized via a polycondensation reaction of 1,12-dodecanedicarbonyl dichloride and varying amounts of 1,4-diaminobutane and 1,4-diaminocyclohexane (1,4-DACH) as described elsewhere.<sup>100</sup> The 1,4-DACH-based copolyamides used in this study have an all-trans conformation with 1,4-DACH molar fractions of 0.07, 0.14, and 0.20. These copolymers are referred to as coPA 0.07, coPA 0.14, and coPA 0.20 respectively. The molecular weights for the copolyamides are comparable.<sup>99</sup>

Melt crystallized samples are placed in 1mm diameter Lindemann capillaries and heated using a Linkam TMS94 hotstage and controller. Time resolved WAXD measurements are performed at the High Brilliance beamline ID02<sup>96</sup> at the European Synchrotron Radiation Facility (ESRF), Grenoble, France as described in Appendix A.2.2. FTIR and DSC measurements are performed on the melt crystallized (co)polyamides as described in Appendix A.4 and A.6.

## 3.3 Results and Discussion

Vanhaecht *et al.*<sup>99</sup> first observed what they believed to be a crossing instead of the traditional merger of the intersheet and interchain reflections during the Brill transition. The data originally collected by Vanhaecht *et al.*<sup>99</sup> was performed on the Dutch-Belgium beamline DUBBLE (BM26)<sup>10</sup> at the ESRF in Grenoble, France. We have repeated the original experiments on the High Brilliance beamline (ID02), the results of which are shown in Figure 3.2, where we used a larger thermal regime in comparison to the original data, i.e. we have studied the copolyamides from room temperature up to the melt. This is done specifically to make the observed transitions more apparent and clear. The WAXD patterns for PA4,14 (Figure 3.2(a)) shows a regular Brill transition occurring at  $\sim 210^{\circ}\text{C}$ , followed by melting at  $228^{\circ}\text{C}$ . CoPA 0.07 shows an apparent Brill transition by a merger of the intersheet and interchain reflections at  $170^{\circ}\text{C}$ , lower than the Brill transition temperature for PA4,14. On further heating there seems to appear a broad reflection in the vicinity of  $0.5\text{nm}$  at  $180^{\circ}\text{C}$ . This reflection remains up to the melt, increasing slowly in intensity. This appearance of a new reflection above the Brill transition is unusual. CoPA 0.14 and coPA 0.20 show similar behavior, albeit that the Brill transition occurs at progressively lower temperatures. This is because, although the position of the interchain reflection remains approximately constant for the copolyamides at  $0.45\text{nm}$ , the intersheet distance becomes progressively larger, changing from  $0.37\text{nm}$  for PA4,14 to  $0.41\text{nm}$  for coPA 0.20. It is likely that a further increase in 1,4-DACH content will result in an apparent single reflection at room temperature because the

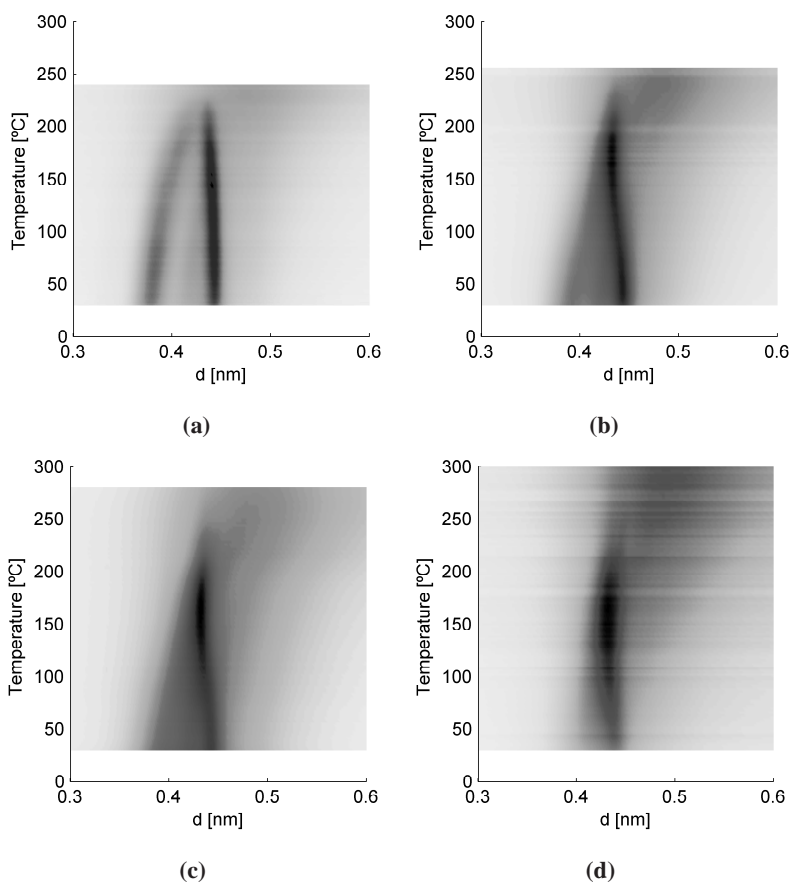


**Figure 3.2:** WAXD patterns collected on heating melt crystallized samples from 30°C to the melt at 10°C/min for (a) PA4,14, (b) coPA 0.07, (c) coPA 0.14, and (d) coPA 0.20.

interchain and intersheet reflections will become indistinguishable. The increase in the intersheet distance is a direct result of the *trans* 1,4-DACH moieties, which are incorporated in the crystalline phase.<sup>99</sup> The 1,4-DACH moieties are aligned perpendicular to the hydrogen bonded sheets, causing an increase in the average intersheet distance measured with increased 1,4-DACH content. The temperatures at which the apparent crossover occurs together with the melt and Brill transition temperatures are shown in Figure 3.3. The melt temperature increases with increasing copolymer content because of the increased rigidity along the polymer chain caused by the introduction of a cyclic entity in the polymer crystal lattice.

The Brill transition as shown in Figure 3.2 is clearly an unusual transition which requires a deeper look at and understanding of the Brill transition. The behavior and origin of the Brill transition is related to conformational changes in the polymer

main chain<sup>105, 113</sup>. In FTIR spectroscopy the Brill transition is characterized by the disappearance of the methylene bands next to the amide groups; these are the bands at 977 and 1054cm<sup>-1</sup> for the methylene units next to the CO groups, and 1230 and 1320cm<sup>-1</sup> for the methylene units next to the NH groups. If this crossover is related to the Brill transition, the FTIR vibrational bands characterizing the Brill transition should be influenced. Also, the introduction of the 1,4-DACH units in the polymer chain could also affect the Brill transition bands.

The FTIR spectra for PA4,14 and the 1,4-DACH copolyamides are, however, surprisingly similar, as shown in Figure 3.4. Minor differences between the samples include the appearance of bands at 1240 and 902cm<sup>-1</sup> for the 1,4-DACH copolyamides together with a decrease and broadening of the bands at 692, 742, 948, 1036, 1419, and 1478cm<sup>-1</sup>. The bands at 1240 and 902cm<sup>-1</sup> are most likely related to the methylene bending and rocking vibrations in the DACH cyclic ring. The band at 902cm<sup>-1</sup> is also a so-called amorphous band; the vibration remains virtually unchanged even after melting. The band at 692cm<sup>-1</sup> is the Amide V NH-out-of-plane scissoring vibration,<sup>24</sup> 742cm<sup>-1</sup> is a CH<sub>2</sub> rocking mode,<sup>24, 113</sup> 948cm<sup>-1</sup> is the Amide IV C-CO stretch vibration,<sup>47, 111</sup> 1036cm<sup>-1</sup> is a CH<sub>2</sub> wagging/twisting mode together with an Amide III vibration,<sup>22, 103</sup> 1419cm<sup>-1</sup> is the CH<sub>2</sub> scissoring vibration next to the CO group in the trans conformation,<sup>22</sup> and 1478cm<sup>-1</sup> is the CH<sub>2</sub> scissoring vibration next to the NH group in the trans conformation.<sup>22</sup> The decrease and broadening of these bands can be attributed to the cyclic ring which is incorporated in the polymer main chain, reducing the mobilities of especially the amide groups and the adjacent methylene units.

The Brill transition temperature for PA4,14 is observed at ~210°C by WAXD where the intersheet and interchain reflections merge into a single reflection without showing any crossover behavior, i.e. a classical Brill transition. Indeed, the FTIR vibrational bands associated to the Brill transition in the FTIR data all show the same behavior for both the homopolymer and the copolyamides: a gradual decrease in intensity to finally disappear completely at ~200°C. The FTIR results suggest that the copolyamides also show a Brill transition at ~200°C with the Brill bands all disappearing and not re-appearing (or remaining) above this temperature. Therefore the WAXD observations for the copolyamides must be that there is a Brill transition occurring, which is the merging of the intersheet and interchain reflections, but that the crossover is due to some other underlying mechanism which becomes noticed only after the Brill transition.

Further inspection of the FTIR spectra is required to provide a possible answer to this peculiar crossover. At room temperature a band at 1712cm<sup>-1</sup> which originates from non-hydrogen bonded CO groups<sup>69</sup> is present for all the (co)polyamides. On heating this band broadens considerably for all the (co)polyamides investigated. Simultaneously, at 3445cm<sup>-1</sup> a band originating from non-hydrogen bonded NH

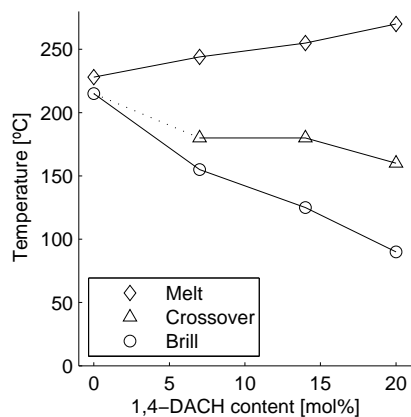


**Figure 3.3:** The melt,<sup>99</sup> Brill, and apparent crossover temperatures for PA4,14 and the 1,4-DACH copolyamides. The Brill transition temperature is taken as the lowest temperature for which the intersheet and interchain reflections can no longer be distinguished.

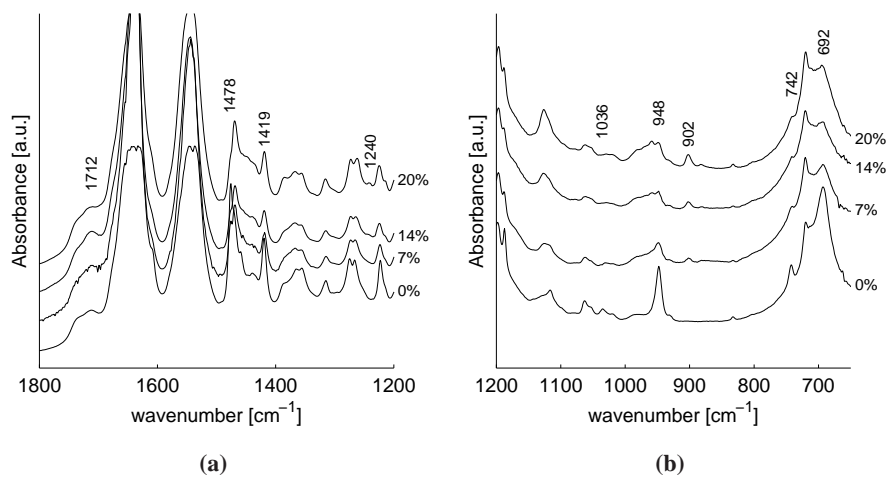


**Figure 3.4:** FTIR spectra obtained for the (co)polyamides containing 0% DACH (PA4,14), 7% DACH (coPA 0.07), 14% DACH (coPA 0.14), and 20% DACH (coPA 0.20) at 30°C between 1800 and 650 $\text{cm}^{-1}$ .



**Table 3.1:** The table shows the melt temperatures ( $T_m$ ), the temperature at which the vibrational band at  $3445\text{cm}^{-1}$  appears and  $1712\text{cm}^{-1}$  broadens in the FTIR spectra ( $T_{ir}$ ), the Brill transition temperature ( $T_B$ ), and the crossover temperature ( $T_{xo}$ ), i.e. the temperature at which the single, high temperature WAXD reflection seems to separate into two reflections, for the (co)polyamides investigated.

	DSC <sup>99</sup>	FTIR	WAXD	
	$T_m$	$T_{ir}$	$T_B$	$T_{xo}$
PA4,14	228°C	200°C	210°C	–
coPA 0.07	244°C	180°C	–	180°C
coPA 0.14	255°C	170°C	–	180°C
coPA 0.20	270°C	160°C	–	160°C

stretch vibrations<sup>69</sup> appears at higher temperatures. Table 3.1 shows the temperatures at which the vibrational bands at  $3445\text{cm}^{-1}$  appears and  $1712\text{cm}^{-1}$  broadens together with the so-called crossover temperature for the copolyamides, i.e. the temperature at which the new reflection seems to appear in the WAXD patterns, and the classic Brill transition temperature for the homopolymer. The similarity between these temperatures is striking. This correlation in temperatures strongly suggests a relation between these two observations.

Non-hydrogen bonded NH and CO groups, especially at elevated temperatures, are usually present in the amorphous phase. It seems plausible therefore that the reflection observed in the WAXD patterns is not a crystalline reflection, but a broad underlying amorphous halo resulting from a partial melting occurring in the copolyamides. Indeed, the position of this crossover halo is similar to the position of the melt amorphous halo, as shown in Figure 3.5 for coPA 0.07 and coPA 0.14; coPA 0.20 shows a similar behavior.

If the crossover halo observed in the copolyamides arises from a partial melting occurring in the sample, an exothermic peak should be visible in the vicinity of the Brill transition temperature when performing DSC experiments on the samples. Figure 3.6 shows the DSC traces obtained on heating melt crystallized 1,4-DACH based copolyamides to the melt at  $10^\circ\text{C}/\text{min}$ . Evident from these traces is that all the spectra show two distinct exothermic events; one event at  $\sim 200^\circ\text{C}$  in the vicinity of the Brill transition temperature, and one event at the expected melt temperatures for the respective (co)polyamides. The observation of an exothermic event in the vicinity of the Brill transition temperature confirms that the crossover halo observed in the WAXD patterns is indeed related to a partial melting.

We envisage the following happening; on heating the incoming gauche

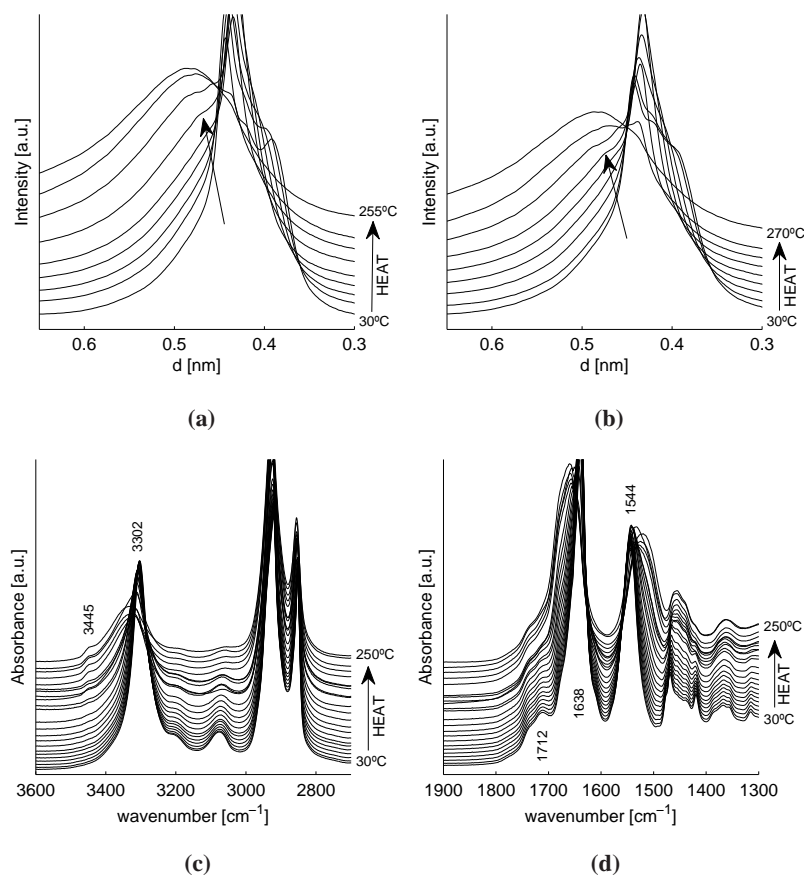


**Figure 3.5:** (a) and (b) show WAXD patterns of coPA 0.07 and coPA 0.14 at 30°C intervals from 30°C to 255°C and 270°C respectively. Note how the broad crossover reflection (indicated by the arrow) at  $\sim 0.5$  nm correlates with the position of the amorphous halo on melting. (c) and (d) shows FTIR spectra of coPA 0.14 from 30°C to the melt. Note the band at  $3445\text{cm}^{-1}$  appearing on heating and the band at  $1712\text{cm}^{-1}$  broadening.

conformers allow for more mobility along the polymer chain. The placement of the amide groups along the polymer chain in PA4,14 and the copolyamides is not ideal; there are many amide groups in the crystalline phase that are not hydrogen bonded. The 1,4-DACH units co-crystallize with the PA4,14 units where the cyclic units, which are in the stretched all-trans (fully extended) conformation, are likely to align and stack onto one another. This influences the alignment of other amide units, and ultimately the hydrogen bond formation in the polymer crystal. Possibly these cyclic entities cause more non-hydrogen bonded amides to occur in the amide crystal lattice. This is supported by a slight increase in the non-hydrogen bonded

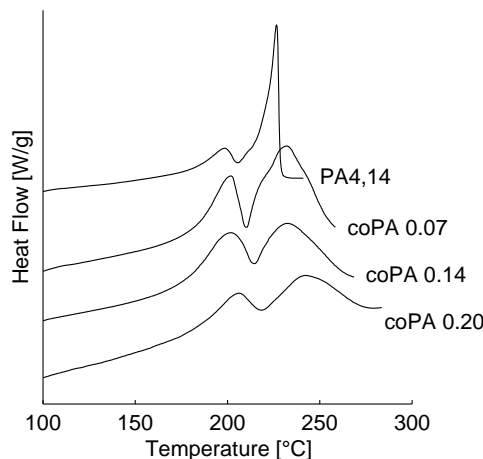


**Figure 3.6:** DSC traces of melt crystallized 1,4-DACH based (co)polyamides.

CO groups observed at room temperature at  $1712\text{cm}^{-1}$  with increasing copolymer content as shown in Figure 3.4(a). When reaching/approaching the Brill transition temperature the gauche conformers allow for the non-hydrogen bonded amide groups in the crystalline phase, together with the non-hydrogen bonded amide groups in the amorphous phase to become increasingly mobile, as seen by the incoming band at  $3445\text{cm}^{-1}$  in the FTIR spectra, resulting in an increase of the amorphous phase. In PA4,14 this increase in the amorphous phase is not observed because the Brill transition temperature is too close to the melt temperature. For the copolyamides the Brill transition temperature is sufficiently far removed from the melt temperature to allow for the observation of the partial melt amorphous phase. This also explains why the crossover is more readily observed for higher copolymer content as the melt temperature increases with increasing copolymer content but the crossover temperature is approximately constant.

### 3.4 Conclusions

Here we investigated a crossing instead of a merger of the intersheet and interchain reflections during the Brill transition for a series of 1,4-DACH based copolyamides. The observed crossover in the WAXD patterns is not the result of a crystalline reflection, but a broad underlying amorphous halo resulting from non-hydrogen bonded amide groups. On heating above the Brill transition temperature more conformational disorder is introduced in the polymer main chain due to the incoming

of gauche conformers at elevated temperatures. In PA4,14 and the 1,4-DACH copolymers many amide groups are non-hydrogen bonded due to the poor alignment of the amide groups between adjacent re-entrant chains in the crystal lattice. The presence of these amide groups is already observed in FTIR spectra at room temperature. On heating above the Brill transition the conformational changes allow for these amide groups to become more mobile, resulting in the partial melting observed as an amorphous phase in the WAXD pattern which is at approximately the same position as the amorphous phase obtained on melting. DSC traces of the (co)polyamides on heating show an exothermic event at the Brill transition temperature, confirming the partial melt behavior seen in the WAXD and FTIR data.

The work presented in this chapter, as well as Chapter 2, illustrates how smart chemistry and tailor made materials can be employed to study a particular phenomena. In this thesis smart chemistry is used to study the Brill transition and how it is influenced by hydrogen bonding and stereochemistry. Controlled chemistry together with detailed analytical techniques provide a unique opportunity to study and understand phenomena which would be impossible to study using commercial materials.

## Chapter 4

# Crystallization of polyamide 4,6 from superheated water – implications for hydrogen bonding\*

Here we demonstrate that water, in the superheated state, is a solvent for polyamide 4,6 (PA4,6) and that the water molecules strongly influence hydrogen bonding. Dissolution of PA4,6 in superheated water occurs at nearly 100°C below the melting point of the polymer. Almost no chain scission or reduction in molecular weight occurs upon dissolution, unless the polymer is retained in solution above the dissolution temperature for more than 10 minutes. Thus the dissolution of the aliphatic polymer in superheated water is mainly a physical process as opposed to a chemical process. Time resolved X-ray studies show that the dissolution occurs prior to the Brill transition temperature.

Single crystals grown upon cooling the dilute PA4,6/water solution show a lath-like morphology with “ideal” interchain/intrasheet and intersheet distances similar to the distances obtained for crystals grown from other known solvents.<sup>3,65</sup> Diffraction studies show that the chains in these single crystals are perpendicular to the *ab*-plane with a lamellar thickness of 6nm, which is also in accordance with other reported studies,<sup>3</sup> confirming that the single crystals incorporate four repeat units between re-entrant folds with an amide group incorporated in the tight fold. Solid state NMR studies performed on mats of these single crystals show two different mobilities of the proton associated to the amide

---

\*This chapter is largely based on:

S. Rastogi, A.E. Terry, and E. Vinken, *Macromolecules* **2004**, 37, 8828–8828.

E. Vinken, A.E. Terry, O. van Asselen, A.B. Spoelstra, R. Graf, and S. Rastogi, *Langmuir* **2008**, 24, 6313– 6326.

groups: a higher mobility linked to the amide protons in the fold and a reduced mobility of the hydrogen bonded amide protons within the crystal. Additionally, the solid state NMR and infrared studies on the dried water crystallized single crystals show the presence of water molecules in the vicinity of the amide groups within the crystalline lattice.

Upon heating above 200°C the water incorporated in the lattice is released and upon subsequent cooling the polyamide returns to conventional melt behavior. TGA confirms weight reduction upon losing water. It is therefore plausible that water molecules are indeed incorporated with the polyamide crystalline lattice without altering the lattice parameters.

## 4.1 Introduction

In comparison with the more common polyamide 6 (PA6) and polyamide 6,6 (PA6,6), polyamide 4,6 (PA4,6) is a high performance material with a high melting point and enhanced mechanical properties.<sup>30</sup> The unique properties of PA4,6 are a result of the equally spaced successive amide groups that lead to a high hydrogen bond density in the crystal.

At room temperature and ambient pressure, the chains in the crystals of most polyamides, including PA4,6, are folded with hydrogen bonds between the folded chains. The thus formed hydrogen bonded sheets are linked by van der Waals interactions. Previous studies<sup>3,37,50,54</sup> on PA4,6 using wide-angle X-ray diffraction (WAXD) show two strong and characteristic diffraction signals at 0.37nm and 0.44nm. These Bragg spacings correspond to the triclinic/monoclinic structure and refer to the intersheet 010 and interchain/intrasheet 100 reflections, respectively. The monoclinic intersheet and interchain distances are strongly affected by crystal perfection, whereby the conventional spacings of 0.37nm and 0.44nm are only achievable after annealing at elevated temperature or upon solution crystallization.<sup>78</sup>

A detailed study<sup>3</sup> performed on the single crystals of PA4,6 and PA6,6 shows a clear distinction in the nature of the chain folding and chain packing within the crystals of these two polyamides. Unlike PA6,6, in PA4,6 an amide group resides in the fold where the adjacent re-entrant chains exist perpendicular to the *ab*-plane and have a similarity with the  $\beta$ -bends in proteins. Detailed computer calculations involving space filling modelling suggest that the outermost thickness of a lamella will be approximately 6nm, which is in accordance with the experimental observations by the authors.<sup>3</sup>

Upon heating PA4,6 single crystal mats,<sup>37</sup> an expansion of the intersheet 010

reflection and a contraction of the interchain 100 reflection occurs, the former due to lattice expansion and the latter due to the propagation of gauche conformers along the methylene units.<sup>95,105,113</sup> The two reflections tend to merge at the so-called Brill transition.<sup>11</sup> The temperature at which the Brill transition occurs for PA4,6 varies between 180 and 250°C<sup>50,78</sup> and is dependent on the crystallization conditions<sup>79</sup> and the degree of crystallinity. For solution crystallized PA4,6 single crystals the Brill transition occurs at 245°C,<sup>37,54</sup> much below the melting temperature of ~295°C.<sup>8</sup>

PA4,6 has a high hydrogen bond density due to the regularity in the spacings of the amide groups along the polyamide chains. Therefore PA4,6 shows a high tendency to interact with water molecules in the amorphous phase upon immersing PA4,6 in water. The water content of PA4,6 can be up to 13wt% for samples with a low crystallinity in a 100% relative humidity environment.<sup>30</sup> The tendency for PA4,6 to absorb water molecules from the air at room temperature is known.<sup>93</sup> However little is known about the interactions between water molecules and the hydrogen bonds in polyamides if the polyamide is placed in water in a sealed vessel and heated to above the ambient boiling point and below the supercritical point, where water is in the superheated state. In the superheated state, the hydrogen bonding between water molecules weakens considerably and the water molecules are highly mobile.<sup>25</sup> Thus, in a polymer where hydrogen bonding exists, for example PA4,6, the presence of water in its superheated state, and thus with enhanced diffusion permeability, should have a significant influence on the hydrogen bonds and the polyamide in general.

In this chapter we explore the structural and conformational changes which occur during the interactions between PA4,6 and superheated water and its implications on the hydrogen bonding strength of PA4,6. It is shown that PA4,6 dissolves in superheated water at ~200°C. Time-resolved WAXD illustrates the dissolution process. High pressure differential scanning calorimetry (DSC) is performed for a range of polyamide concentrations in water in order to investigate the influence of polymer concentration on the dissolution process. Any possible hydrolysis resulting in a decrease in molecular weight, is investigated by gel permeation chromatography (GPC) performed before and after the dissolution experiments. GPC analysis is also performed on PA4,6 dissolved in water to investigate the influence the length of time the material remains in solution has on the molecular weight. Single crystals grown from dilute PA4,6/water solutions upon cooling are investigated by transmission electron microscopy (TEM). Single crystal mats obtained after the removal of the excess water are studied by small and wide angle X-ray diffraction (SAXS/WAXD). To locate and determine the influence of water molecules in the single crystal mats, solid state nuclear magnetic resonance (NMR) studies are performed. These results are further supported by Fourier transform infrared (FTIR) spectroscopy and high resolution thermogravimetric analysis (TGA).

## 4.2 Experimental description

### 4.2.1 Material

The polymer used in this study is a commercially available DSM produced PA4,6, commonly known as Stanyl<sup>®</sup>. A PA4,6 film is prepared by dissolving the polymer in formic acid (5g/l) and subsequently solvent casting the polymer onto a glass plate after which the solvent is allowed to evaporate.<sup>30</sup> The melt crystallized material is obtained by heating PA4,6 crystallized from formic acid to the melt and cooling to room temperature at 10°C/min using a Linkam TMS94 hotstage.

### 4.2.2 Preparation of water crystallized PA4,6 crystals

Solvent cast PA4,6 film with distilled water is added to a glass capillary to make an ~1wt% polymer concentration and sealed. When preparing single crystals for further analysis, the following protocol is always used; the capillary is heated from room temperature to 200°C at 10°C/min, held for 1 min and cooled to room temperature at 10°C/min using the in-house designed and built pressure cell shown in Section A.1. Above 100°C, the water in the capillary goes into the superheated state. At ~200°C, the polyamide dissolves in the superheated water, and recrystallizes upon cooling, forming a white suspension of PA4,6 crystals in water. The thus obtained single crystals are investigated using DSC, FTIR spectroscopy, NMR spectroscopy, TEM, GPC, and TGA as described in Appendix A.

### 4.2.3 Simultaneous small and wide angle X-ray diffraction (SAXS/WAXD)

Simultaneous small and wide angle X-ray diffraction (SAXS/WAXD) are performed on dried solvent cast PA4,6 film and water (30wt% polymer concentration) using the pressure cell described in Appendix A.1. The changes occurring are followed *in situ* by means of simultaneous SAXS/WAXD at the High Brilliance beamline<sup>96</sup> (ID02) at the European Synchrotron Radiation Facility (ESRF), Grenoble, France as described in Appendix A.2.2. Background corrections for the WAXD data are performed as described in Appendix A.2.3. In a separate SAXS/WAXD experiment, a mat of PA4,6 water crystallized single crystals is prepared by filtering, at room temperature, the suspension of single crystals through a Büchner funnel lined with filter paper. The excess water still present in the mats after filtering is allowed to evaporate overnight under ambient conditions. The dried single crystal mats are placed in a 2mm Lindemann glass capillary and heated on a Linkam TMS94 hotstage.



### 4.3 Dissolution of PA4,6 in superheated water studied by simultaneous *in situ* SAXS/WAXD

To follow structural and morphological changes, detailed simultaneous SAXS/WAXD studies are performed under controlled conditions on the High Brilliance beamline (ID02) at the ESRF. Figure 4.1 shows the simultaneously recorded SAXS/WAXD data obtained on heating 30wt% of PA4,6 crystallized from formic acid, in water in a sealed vessel from 50 to 200°C at 10°C/min. As shown in Figure 4.1(a), on heating, prior to the merging of the 100 interchain and 010 intersheet reflections, the polymer becomes amorphous, i.e. the interchain and intersheet reflections disappear or merge into a halo around 180°C. As the normal melting point for PA4,6 is expected to be at  $\sim 295^\circ\text{C}$ ,<sup>8</sup> the behavior shown in Figure 4.1 shows the dissolution of PA4,6 in superheated water  $\sim 100^\circ\text{C}$  below the melting point. With the onset of dissolution, i.e. the last few frames at about 8°C prior to dissolution, the interchain and intersheet reflections deviate from each other and decrease in intensity. This is most likely due to the water molecules, which are highly mobile due to the elevated temperatures, penetrating the crystal lattice and breaking the hydrogen bonds between the amide groups. This causes the interchain distance to increase, and consequently the intersheet distance to decrease. The simultaneously recorded SAXS data shown in Figure 4.1(b) show a well defined halo corresponding to a *d*-spacing of 9.5nm at 50°C. On heating, up to 150°C, the lamellar thickness hardly changes. Above 150°C the lamellar thickness increases with a broadening of the halo and finally disappears completely at 180°C. On cooling the polymer/water solution from 200°C as shown in Figure 4.1(c), crystallization occurs directly in the triclinic phase with the appearance of two reflections corresponding to the 100 interchain/intrasheet and 010 intersheet reflections respectively. The simultaneously recorded SAXS data shown in Figure 4.1(d) show the appearance of a sharp halo on crystallization at much lower angles than before dissolution corresponding to a lamellar thickness of  $\sim 13\text{nm}$ , i.e. considerably larger than the value of 9.5nm prior to dissolution. The considerable increase in lamellar thickness suggests that a considerable amount of water resides within the amorphous and/or crystalline component of the lamellae. As we have already commented, water easily adheres to the amorphous component of polyamides;<sup>93</sup> PA4,6 can contain up to 13wt% water in the amorphous phase at low crystallinity. We return to this point later in this chapter. The increase in lamellar thickness may also be due to a change in crystallinity. However, the WAXD data does not suggest that a large change in crystallinity has occurred. On cooling to 50°C, almost no shift in the lamellar thickness is observed.

We have demonstrated that PA4,6 can be dissolved in superheated water at  $\sim 200^\circ\text{C}$  by encapsulating the polymer with water in a closed vessel and heating the vessel to 200°C, which is well below the melting point of PA4,6 ( $\sim 295^\circ\text{C}$ <sup>8</sup>). The

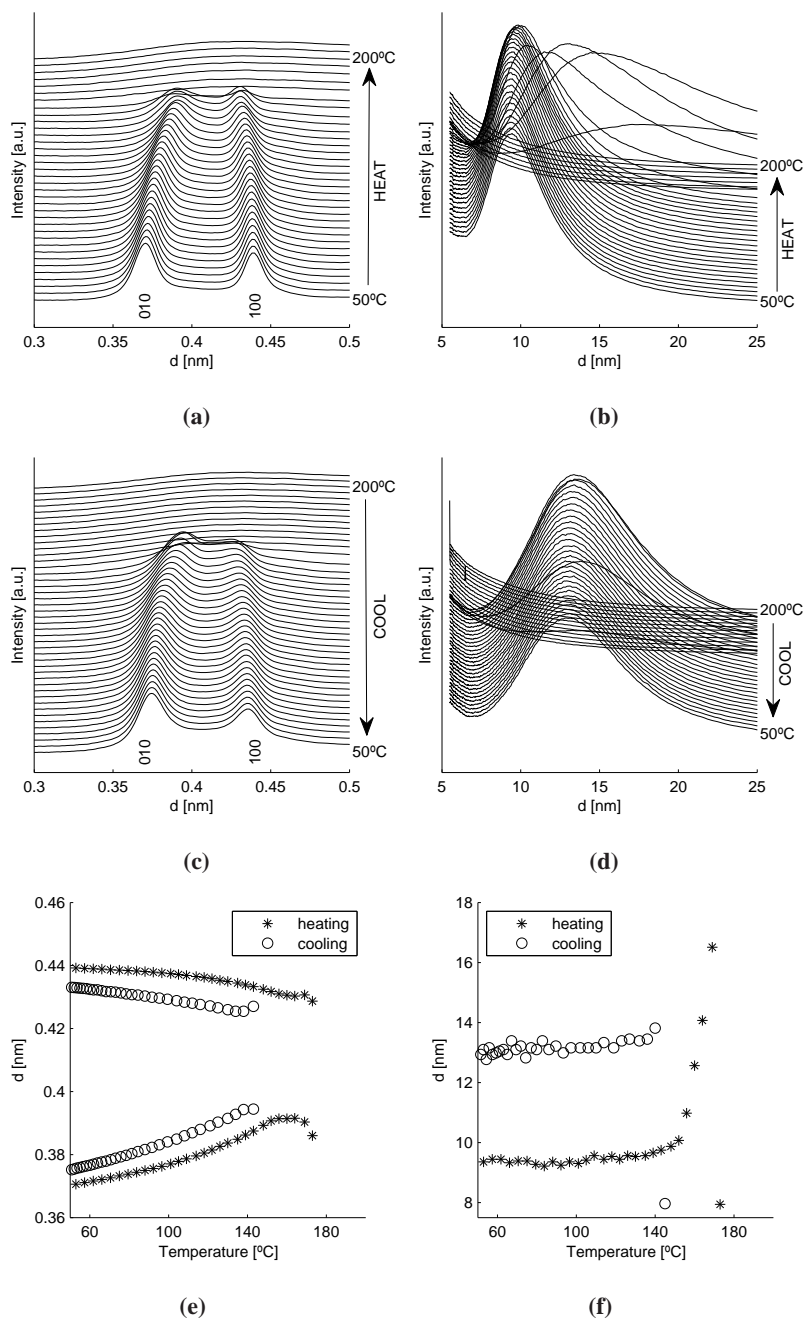


**Figure 4.1:** Simultaneous SAXS/WAXD collected on heating/cooling 30wt% PA4,6 in water between 50°C and 200°C at 10°C/min. The contribution from the glass capillary, water, and amorphous component have been subtracted from each diffraction pattern. Every second data file is plotted for clarity.

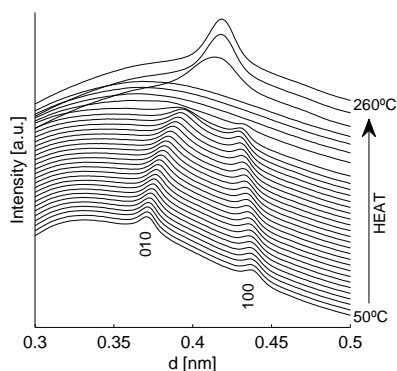


**Figure 4.2:** WAXD patterns of PA4,6 and water in a sealed glass capillary (heating/cooling rates used are 20°C/min) for heating from 50 to 260°C during which the capillary breaks at  $\sim 245^\circ\text{C}$ . An exposure is taken every 5°C; no background correction is performed for this experiment. The data are collected at ID11<sup>63</sup> as described in Appendix A.2.1.

dissolution of polyamide in water is also reported in a patent in which polyamide nanocomposites are obtained by mixing a polyamide in the melt phase with anisotropic particles dispersed in water by means of an extruder.<sup>60,61</sup> The buildup of temperature and pressure in the extruder leads to the formation of superheated water, and thus to the dissolution of the polyamide in water. In a separate study, PA6 and montmorillonite nanocomposites were prepared using superheated water.<sup>114</sup>

The process shown in Figure 4.1 proceeds under pressure, i.e. as water enters the superheated state, pressure increases. In an interesting experiment the sample was sealed with water in a glass capillary such that the pressure is released just after dissolution whilst still at elevated temperatures, but below the melting point of PA4,6. Figure 4.2 shows WAXD patterns recorded during the dissolution of water crystallized PA4,6 crystals in the presence of excess water. Here no background correction is performed. As anticipated, the intersheet and interchain reflections move closer to each other on heating. At  $\sim 205^\circ\text{C}$ , the two crystalline reflections disappear as dissolution of the PA4,6 in superheated water occurs, leaving a broad amorphous halo. The capillary with a solution of PA4,6 and water is heated further. Vapor pressure increases with increasing temperature and at  $\sim 245^\circ\text{C}$ , when the vapor pressure is anticipated to be approximately 36.5bar,<sup>32</sup> the glass capillary can no longer withstand the pressure and breaks. Water at these high temperatures and now at atmospheric pressure evaporates from the capillary almost instantaneously. The water-free PA4,6 at  $245^\circ\text{C}$ , much below its melting temperature ( $\sim 295^\circ\text{C}$ <sup>8</sup>), crystallizes directly into the pseudo-hexagonal phase. Therefore, the Brill transition for the water solution crystallized sample must be between 205 and  $245^\circ\text{C}$ . The last

three frames, heating to a maximum temperature of 260°C in Figure 4.2, shows the crystallization of PA4,6 in the pseudo-hexagonal phase. The single broad reflection at 0.42nm of the pseudo-hexagonal phase just after the Brill transition typically increases in intensity and becomes sharper with time.

The effect of (over) pressure on the dissolution process is investigated by applying an external pressurized nitrogen gas in the lid sealing the glass sample capillary. Up to a external gas pressure of 25bar no deviation from the data presented above is observed. From these experiments we can conclude that not pressure, but temperature and thus mobility of the water molecules is determinant in the dissolution process.

During the dissolution process described in Figure 4.1 superheated water molecules, which are highly mobile,<sup>25</sup> enter the crystal lattice and break the hydrogen bonds between the amide groups. However, it is important to determine if this dissolution is governed by a physical or a chemical process. For this reason, the phase behavior of PA4,6 in superheated water is investigated using DSC.

#### 4.4 Dissolution of PA4,6 in superheated water with DSC

In the previous section it is shown that PA4,6 can be dissolved in superheated water. DSC is used to follow the phase behavior of PA4,6 in water. Figure 4.3(a) shows an example of the second heating run, from room temperature to 310°C for pure PA4,6, and from room temperature to 220°C for 27wt% PA4,6 in water. For pure PA4,6 a single melting endotherm is observed at 290°C. As anticipated, no peak is observed at the expected Brill transition temperature of ~245°C.<sup>54</sup> In contrast, PA4,6 in water shows a single asymmetric, broad peak on a high background. The background may arise due to the pressure of the solvent water.<sup>108</sup> The single peak at 200°C corresponds to the temperature at which dissolution is observed by *in situ* X-ray diffraction.

A substantial difference (~90°C) is seen between the melt and dissolution temperatures. Figure 4.3(b) shows the end dissolution temperature measured from DSC endotherms representing the temperature at which the PA4,6 dissolves completely in water for different concentrations. Figure 4.3(b) also shows the onset point of the exotherm on cooling, i.e. the onset temperature at which crystallization of the PA4,6 from water occurs, at different polymer concentrations as determined by WAXD. With a decrease in polymer concentration, the dissolution temperature decreases for the first heating run, until a plateau is reached at 180°C for 60wt% of polymer. At the plateau, the polymer dissolution temperature is invariant of the polymer concentration. The dissolution behavior shown in Figure 4.3 implies that superheated water is a solvent for PA4,6. The crystallization behavior follows the same trend as the dissolution behavior with the phase diagram levelling off at a

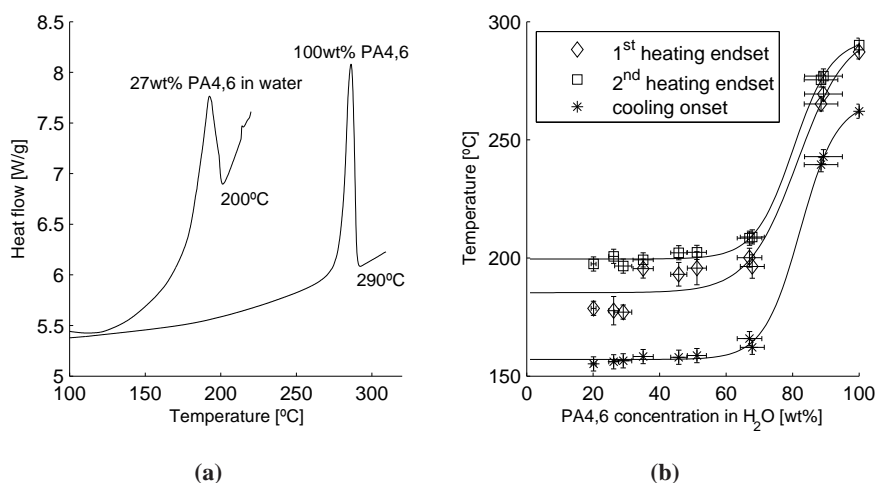


**Figure 4.3:** Influence of polymer concentration on the dissolution of polyamide 4,6 in water. (a) shows DSC traces of the second heating cycle of PA4,6 and PA4,6 in water, and (b) shows the phase diagram constructed from the measured temperature of the end of the dissolution endotherm and onset of recrystallization exotherm, for various concentrations of PA4,6 in water. All lines serve as a guide to the eye.

plateau of 154°C for ~60wt% of polymer. On heating the PA4,6 crystallized from a water solution (second heating run), the dissolution occurs at a higher temperature (199°C) than the first heating run. Once again the plateau value is reached at ~60wt% PA4,6. Some variation in the data points in the plateau region during the first heating run can be attributed to poor thermal contact of the water and polymer within the DSC pan.

By DSC at a heating/cooling rate of 10°C/min, 106J/g is required to both dissolve in superheated water or to melt an acid crystallized sample, in comparison to 84J/g to melt the melt crystallized sample, Tables 4.1 and 4.2. In a second heating run of the dissolution of PA4,6 in superheated water, only 84J/g is now measured within the dissolution endotherm, i.e. for water crystallized PA4,6. However, if the same water crystallized samples are extracted from the pressure vessel and sedimented and dried, 106J/g will again be needed to melt the sample. The causes of this change in enthalpy will become apparent in the discussion on the structural properties of PA4,6 later in this chapter. We also perform GPC analysis on PA4,6 before and after the dissolution process to verify whether hydrolysis has occurred, as discussed in the following section.

**Table 4.1:** Melt temperatures and heats of fusion of PA4,6 crystallized from water, formic acid, and the melt.

	1st heating run			2nd heating run	
	Melting temperature		$\Delta H$	Melting temperature	$\Delta H$
	Peak 1	Peak 2	Peak 1+2		
PA4,6 from formic acid	285°C	289°C	106J/g	287°C	86J/g
PA4,6 from melt	–	286°C	84J/g	286°C	83J/g
PA4,6 from water	273°C	290°C	106J/g	287°C	84J/g

**Table 4.2:** Dissolution temperatures and heats of fusion in superheated water of PA4,6 crystallized from water and formic acid.

	Dissolution temperature	$\Delta H$
PA4,6 from formic acid	185°C	106J/g
PA4,6 from water	192°C	79J/g

## 4.5 Dissolution or hydrolysis of PA4,6 in superheated water?

Considering the synthesis of nylons, where water is released during polymerization, it is important to investigate if the polymer dissolves, or if dissolution proceeds via hydrolysis in superheated water, therefore the molecular weight of the polymer is determined after the first and second heating runs for the polymer retrieved from the DSC pans. Figure 4.4(a) shows a broad molecular weight distribution of PA4,6 as received from DSM, with a peak at 70,000g/mol and a long higher molecular weight tail up to 400,000g/mol. The molecular weights of the PA4,6 crystallized from water after the first and second heating runs are comparable within experimental errors although minor reduction in molecular weight does occur. The values obtained from the GPC traces are shown in Table 4.3. These observations suggest that, within the experimental conditions of our studies, PA4,6 does not undergo any substantial hydrolysis.

However, if the polymer is left in the presence of superheated water after

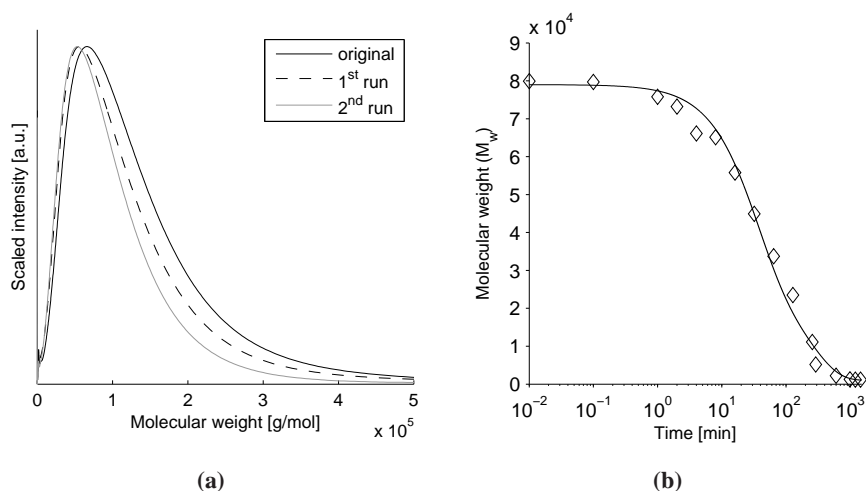


**Figure 4.4:** Determination of the degree of hydrolysis by changes in the molecular weight distribution of PA4,6 by GPC analysis. (a) shows the molecular weight distribution of the original PA4,6 in comparison to the molecular weight distribution of PA4,6 in the presence of water (27% polymer in water) after the first heating/cooling and second heating/cooling cycle in the DSC. (b) shows  $\bar{M}_w$  as a function of time in minutes, where time is given on a logarithmic scale. The line serves as a guide to the eye.

dissolution has occurred for sufficiently long time, hydrolysis would be expected to occur and therefore it is essential to know how long the sample can be left in solution at high temperatures. To determine these experimental boundary conditions, GPC analysis of crystallized samples from 15wt% PA4,6 in a water solution held at 200°C, i.e. in the superheated state and well above the dissolution temperature, for various lengths of time is performed, the result of which is shown in Figure 4.4(b) where time is given on a logarithmic scale for clarity. The first point in the GPC diagram,  $t = 10^{-2} \simeq 0$  min, refers to the molecular weight of the PA4,6 film prior to dissolution. A considerable decrease in the molecular weight occurs if the sample is left for more than 10 minutes at 200°C and would suggest that the polymer in solution should not be left at these high temperatures for more than 10 minutes. However, the time required for the dissolution process of PA4,6 in water ranges between 2–3 minutes, i.e. the time taken to raise the temperature from 150°C to the dissolution temperature of  $\sim 175^\circ\text{C}$  at a heating rate of 10°C/min. Given that this time is quite short and that these temperatures do not exceed the temperature of 200°C at which the hydrolysis was determined as a function of time, it is thought that the dissolution protocol adopted as described in Section 4.2.2 has little influence on the molecular weight of PA4,6. It is also apparent therefore that the dissolution of polyamides occurs via a physical process and not via a chemical process, i.e. not

**Table 4.3:** Molecular weight of PA4,6 as received from DSM (original), after the first DSC heating run (1<sup>st</sup> run), and after the second DSC heating run (2<sup>nd</sup> run). Here PDI is the polydispersity index.

	$M_w$ (Daltons)	$M_n$ (Daltons)	PDI
Original	79600	24800	3.2
1 <sup>st</sup> run	72600	33000	2.2
2 <sup>nd</sup> run	62800	31700	2.0

by hydrolysis altering the molecular weight of the polyamide. These results are in agreement with the heat of fusion involved in the dissolution process of polyamides (see the previous section) and the findings are further strengthened by the FTIR studies later in this chapter.

## 4.6 Single crystals grown from a water solution

For the TEM studies, a drop of the turbid suspension of PA4,6 water crystallized crystals dispersed in water is left to dry on a carbon coated copper grid. Figure 4.5(a) shows a micrograph of the crystals obtained after evaporation of the excess water. The crystals appear lath-like with lengths ranging from 5 to 15  $\mu\text{m}$ , and a width of  $\sim 1 \mu\text{m}$ , similar to PA4,6 crystals grown from other known solvents such as 1,4-butanediol<sup>3</sup> and glycerine.<sup>65</sup>

Electron diffraction on the individual laths gives rise to the diffraction patterns as shown in Figure 4.5(b) and 4.5(c), which are characterized by a six-arc pattern. Although the arcs are relatively long, they serve to show the single crystal nature of the lath-like crystals. The three Bragg reflections have characteristic spacings of  $0.448 \pm 0.009 \text{ nm}$ ,  $0.366 \pm 0.007$ , and  $0.378 \pm 0.005$  for very strong, strong and medium intensities respectively and are similar to the diffraction pattern reported by Atkins *et al.*<sup>3</sup> for PA4,6 single crystals grown from 1,4-butanediol who considered a monoclinic unit cell for PA4,6. The reflections can thus be indexed as 100, 010, and  $1\bar{1}0$  with a similar angle of  $65^\circ$  between the two strongest reflections. The presence of the third reflection arises due to twinning of the crystals, which is likely to arise due to stress relaxation, an argument made previously for the six point pattern for the 1,4-butanediol grown single crystals of PA4,6.<sup>3</sup>

In their studies Atkins *et al.*<sup>3</sup> also concluded that in the single crystals of



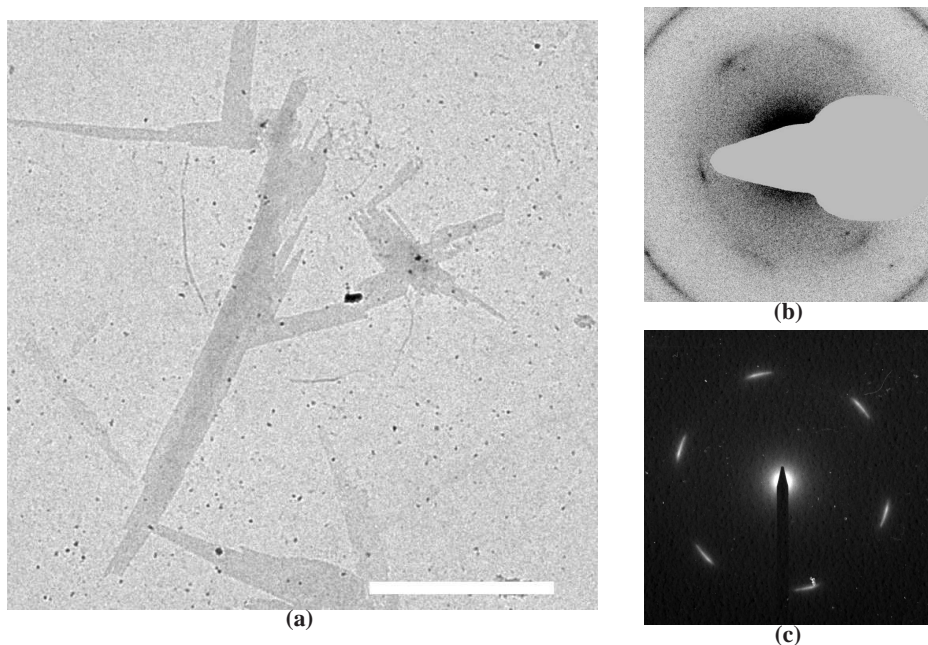


**Figure 4.5:** (a) shows lath-like single crystals obtained on crystallizing PA4,6 from water where the scale bar represents  $5\mu\text{m}$ , (b) and (c) show electron diffraction patterns obtained from these single crystals ((b) is shown in reverse gray scale for clarity). The outermost reflection in (b) originates from a gold coating used for calibration purposes.

PA4,6 the chains are normal to the basal plane of the lamellae and that the chain folds run parallel to the hydrogen bonded sheets along the long axis of the crystal. Therefore, from the orientation of the electron diffraction pattern, PA4,6 crystallizes from superheated water to form single crystals which have the same crystallographic basis as that previously observed, i.e. the hydrogen bonded sheets are parallel to the long axis of the crystals.

Atkins *et al.*<sup>3</sup> also stated that the optimum crystal thickness along the *c*-axis is approximately 6nm, corresponding to the stacking of four unit cells ( $4 \times 1.47\text{nm}$ ), where the chains within the crystal are packed perpendicular to the basal plane having adjacent re-entry with an amide group in the fold. To probe this stacking in the water grown single crystals, simultaneous time resolved SAXS/WAXD studies during heating and cooling are performed on a dried sedimented single crystal mat.

## 4.7 Sedimented single crystal mats

The single crystals are sedimented from the water solution through a Büchner funnel to form a mat. This single crystal mat is allowed to dry under ambient conditions before performing simultaneous SAXS/WAXD on the samples.

Figure 4.6 elucidates the heating/cooling run of the dried sedimented crystal mats on a Linkam hotstage. X-ray diffraction patterns are recorded while heating/cooling the crystal mats between 50 and 250°C at a rate of 10°C/min. Figure 4.6(a) shows the WAXD patterns of the solution grown crystals. The starting values for the interchain and intersheet distances at 0.44 and 0.37nm respectively are comparable to the crystals grown from other solvents.<sup>54</sup> The Brill transition from the monoclinic to the pseudo-hexagonal phase is observed around 205°C. On cooling from 250°C, i.e. below the published melting temperature of 295°C,<sup>8</sup> the crystals in the pseudo-hexagonal phase transform into the monoclinic phase around 120°C (see Figure 4.6(c)). At 50°C, upon comparison with the starting material, a considerable change in the interchain and intersheet distances is observed, indicating a change in the molecular packing within the lattice. Quantitative changes in the interchain and intersheet distances on heating and cooling are summarized in Figure 4.6(e).

On heating, the expected increase in the 010 intersheet distance of the single crystal mats can be explained by the thermal expansion of the lattice, whereas the decrease in the 100 interchain distance is due to the motion of the methylene units between the amide groups. The motion in the methylene unit next to the amide group will weaken the hydrogen bonding and will cause some translational motion along the *c*-axis. If the intermolecular chains on the hydrogen bonded plane are adjacently re-entrant, the translational motion between the adjacent chains is likely to be in the opposite direction, thus maintaining the lamellar thickness although perturbing the interchain and intersheet packing. On cooling from a temperature below the melting temperature, the expected contraction in the intersheet distance decreases. The strength of the hydrogen bonding between the interchain amide groups increases due to a decrease in the motion of the methylene units. This causes an increase in the intersheet distance with respect to the original distance. A complete recovery of the unit cell to the dimensions prior to heating will not be feasible since on cooling the strengthening of the hydrogen bonds between the chains prevent their translation back to their original positions. The Brill transition temperature will depend on the extent to which the interchain and intersheet distances are recovered on cooling. The large interchain and small intersheet distance and the corresponding high Brill transition temperature of the water crystallized sample suggests that the solution crystallized sample is the thermodynamically stable crystal.

Figure 4.6(b) shows the simultaneously recorded SAXS patterns. Note that the lamellar thickness of 6nm hardly changes on heating/cooling the sample to/from

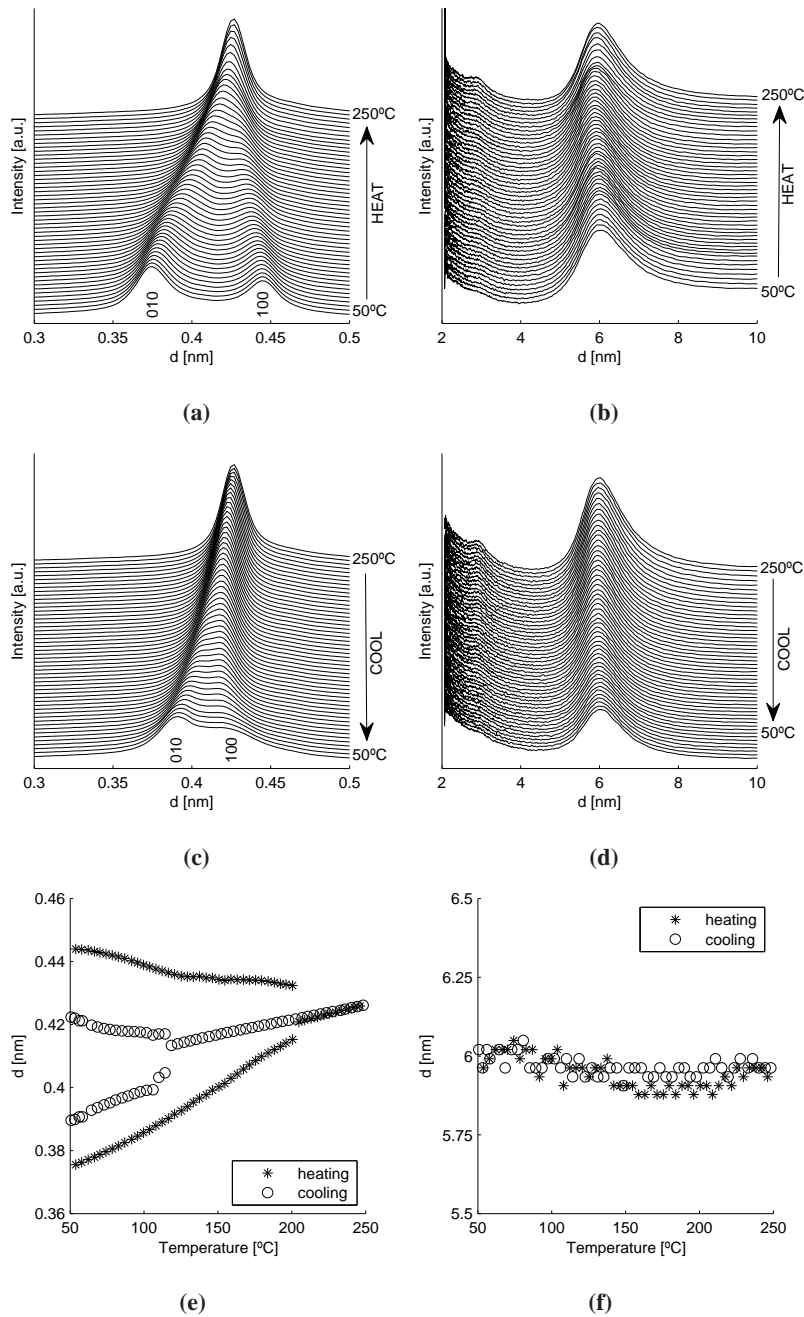


**Figure 4.6:** Simultaneous SAXS/WAXD patterns collected on heating a PA4,6 single crystal mat (PA4,6 was crystallized from water and sedimented to form a mat) from 50°C to 250°C and cooling from 250°C to 50°C; both at 10°C/min. Data treatment as described in Appendix A.2.3 has removed any contribution from the amorphous glass and water components in the WAXD data.

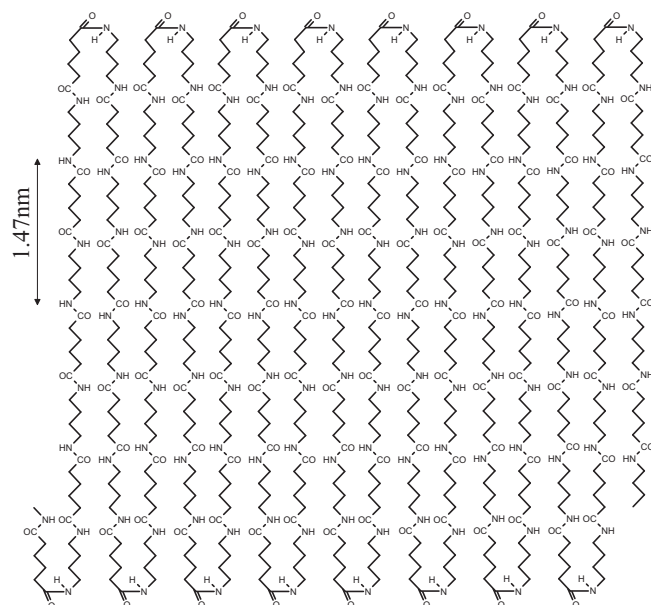


**Figure 4.7:** A representation of a PA4,6 chain-folded sheet where the amide group is incorporated in the fold, adapted from Atkins *et al.*,<sup>3</sup> Figure 11.

250°C, see Figures 4.6(b), 4.6(d), and 4.6(f), despite the changes in the interchain and intersheet distances. This thickness of 6nm corresponds well with the lamellar thickness reported by Atkins *et al.*<sup>3</sup> where the long period consists of four chemical repeat units along the chain, i.e.  $4 \times 1.47\text{nm} = 5.88\text{nm}$ . These findings, together with those of Atkins *et al.*,<sup>3</sup> strongly suggest that the PA4,6 crystals grown from water are made up of tight folds and adjacently entrant chains similar to the  $\beta$ -bends in proteins. This is only feasible if an amide group is incorporated in the fold, rather than an alkane segment, as shown in Figure 4.7 (adapted from Atkins *et al.*,<sup>3</sup> Figure 11). Considering the correlation between the lamellar thickness of 6nm and the anticipated theoretical value of 5.88nm, the possibility of loose folding can be overruled. Having an amide group on the surface of the crystal has implications for the adsorption of water on the crystal surface and the mobility of the amide protons.

The model in Figure 4.7 should exhibit two different proton mobilities associated to the amide groups; a free amide group residing in the fold surface and the amorphous component, and the hydrogen bonded amide group within the crystal. We explore the different mobilities of these two protons by solid state NMR.

## 4.8 Probing proton mobility by solid state NMR

Prior to discussing the different mobilities of the amide protons it is essential to assign the signals of the  $^1\text{H}$  MAS spectra obtained from the single crystals of PA4,6. The room temperature  $^1\text{H}$  MAS NMR spectrum of the dried water crystallized mats together with the spectra of a melt crystallized and a formic acid crystallized sample, all recorded under the same conditions, are shown in Figure 4.8. Even at 30kHz MAS spinning frequency, the  $^1\text{H}$  MAS NMR spectrum of the melt crystallized sample is featureless and shows only broad signals. The asymmetric line shape of the signal at lower ppm values suggests the presence of several overlapping signals. Additionally, a relatively sharp signal is present at 4.1ppm. The sample crystallized from formic acid shows several well resolved signals in the lower ppm region, indicating a more regular packing of the PA4,6 chains in comparison with the melt crystallized sample as would be expected. These peaks are labelled as shown in the scheme in Figure 4.8. The signal at 4.1ppm is also present in the acid crystallized sample. However, this signal is now much better resolved and much stronger. In the region of higher ppm values, the signal at 8.0ppm is very broad and asymmetric. The spectrum of the dried water crystallized sample shows similarities to the acid crystallized sample, also indicating a regular packing of the PA4,6 chains. The most significant difference, in comparison to the acid crystallized sample, is that the signal at 4.1ppm has moved to 5.0ppm in the water crystallized sample and is now significantly broader. A  $^1\text{H}$  double-quantum filtered NMR spectrum, where all highly mobile or non dipolar coupled sites are suppressed, has been used to identify that the signals at 4.1ppm and 5.0ppm are due to water. The shaded areas around 4.5 and 8.0ppm shown in Figure 4.8 indicate a broadening in the site due to a non-uniform formation of hydrogen bonds and the possible incorporation of water in the crystals.

## 4.9 Different mobilities of the amide protons

A closer look at the signal present in the 8.0ppm region, assigned to the amide proton, shows differences between the melt and solution crystallized samples. The signal in the solution crystallized samples (acid and water crystallized) is asymmetric, suggesting the presence of two overlapping signals. On heating, the two signals become well resolved into a broad signal at 8.1ppm and a sharp signal at 7.6ppm, see Figure 4.9. The presence of two signals in this region is indicative of amide protons in two different (chemical) environments. A sharp signal is suggestive of a higher mobility, which is likely to arise due to the presence of free amide protons incorporated in the fold, whereas the broad signal originates from amide protons within the hydrogen bonded sheets which have a restricted mobility, see Figure 4.7.

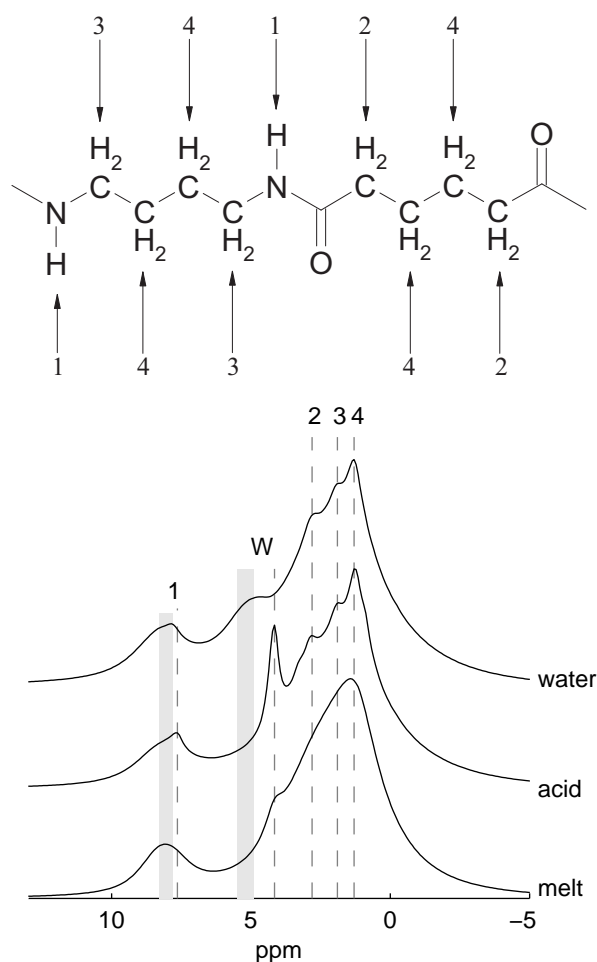


**Figure 4.8:**  $^1\text{H}$  MAS spectra of PA4,6 crystallized from the melt, from formic acid, and from water, all at  $27^\circ\text{C}$ .

It should be emphasized that the NMR studies are performed on single crystal mats prepared from dilute solution and thus possessing a high degree of crystallinity which to a great extent rules out the possibility of a mobile component originating from non-crystalline regions. On heating from  $27^\circ\text{C}$  to  $117^\circ\text{C}$ , the broad signal at 8.1 ppm hardly shifts or sharpens, while the signal at 7.6 ppm sharpens and shifts to lower ppm values (7.0 ppm at  $117^\circ\text{C}$ ). These changes are observed for the amide protons of both solution crystallized samples, independent of the solvent, acid or water. With the sharpening of the amide proton signals, the signals associated to the methylene protons also sharpen.

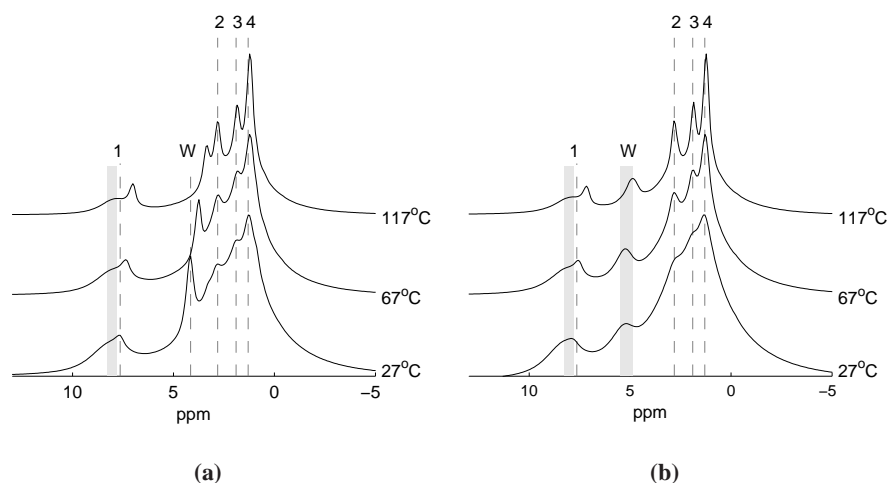


**Figure 4.9:**  $^1\text{H}$  MAS spectra of (a) PA4,6 crystallized from formic acid and (b) PA4,6 crystallized from water at 27°C, 67°C, and 117°C.

#### 4.10 Different mobility of the water molecules in the samples crystallized from acid and water

It is expected that water molecules will be present in the polyamide merely by adsorption from the air. As stated before a  $^1\text{H}$  double-quantum filtered NMR spectrum has been used to identify that the signals at 4.1ppm and 5.0ppm are due to water. It should be noted that the mobility of the associated water is highly reduced compared to that of free bulk water, which exhibits a line width of 0.007ppm at 27°C. At 27°C, Figure 4.9(a) shows a sharp signal at 4.1ppm and Figure 4.9(b) shows a broader signal around 5.0ppm, both originating from the water protons. This shows that independent of the crystallization conditions, water molecules are present in the solution crystallized PA4,6. It is important to note that the water molecules present in the melt and acid crystallized samples have a different chemical shift compared to the water molecules in the water crystallized sample (see Figure 4.8). This indicates that the environment of the water molecules in the two solution crystallized samples is notably different.

In the sample crystallized from formic acid, the sharp water signal shown in Figure 4.9(a) shifts on heating to 67°C to lower ppm values (3.7ppm) and decreases in intensity. On further heating to 117°C a further decrease in signal intensity occurs combined with a simultaneous shift to lower ppm values. Within the defined temperature range, both effects are indicative of the weakening in the binding strength of the water molecules. Unlike the water protons from the acid grown crystals,

the water signals in the water grown crystals observed at 5.0ppm hardly shifts on heating, i.e. no decrease in intensity and only a slight sharpening of the signal is observed. Thus the coordination of the water in the water grown crystals is considerably different to that of the water present in the acid grown crystals.

#### **4.11 Location of the water molecules in the samples crystallized from acid and water**

As already mentioned,  $^1\text{H}$  double quantum filtration suppresses the water signal due to the fast local reorientations of the water molecules. Therefore the spatial proximity between the water molecules and other proton sites of the polymer cannot be probed by double-quantum NMR methods but rather by Nuclear Overhauser Enhancement Spectroscopy (NOESY) techniques. A two-dimensional NOESY correlation spectrum of the PA4,6 crystallized from formic acid recorded with 10ms NOE transfer time at 67°C and 30kHz MAS is given in Figure 4.10(a). As expected, NOE contacts are found between all the proton sites along the polymer, including the amide proton. In order to quantify the NOESY intensities of the water proton with other sites in the sample, a slice taken from the two dimensional NOESY data set at the water signal (3.7ppm, under the experimental conditions), as indicated by the red line in Figures 4.10(a) and 4.10(b) is compared with the  $^1\text{H}$  MAS spectrum of the sample under the same experimental conditions, given by the black line in Figure 4.10(b). The NOESY data and the MAS spectrum of the acid crystallized sample show similar relative intensities and line widths for all the different  $^1\text{H}$  sites of the sample, keeping in mind that the water signal in the NOESY data cannot be interpreted, since it results from untransferred  $^1\text{H}$  polarization of the water molecules. Thus, it depends strongly on the NOE contact time rather than the individual NOE transfer efficiency of the other proton sites with the water. On close inspection of the NOESY intensities, the sharp amide signal at 7.6ppm is slightly reduced with respect to the other signals, whereas the broad amide signal at 8.1ppm is more pronounced.

The two dimensional NOESY NMR spectrum recorded under the same experimental conditions on the water crystallized sample, shown in Figure 4.11(a), exhibits broader NOE signals than the sample crystallized from formic acid. Comparing the NOESY signals taken from the two-dimensional data set at the position of the water signal (indicated by the red line in Figures 4.11(a) and 4.11(b)) with the  $^1\text{H}$  MAS spectrum recorded under the same experimental conditions (see black line in Figure 4.11(b)), the line broadening of the NOE signals becomes evident. Moreover, the intensity of the aliphatic signals are significantly reduced, whereas the broad signal at 8.1ppm of the amide protons gains in intensity. Note that the intensity of the sharp amide signal at 7.6ppm is strongly reduced so that it appears



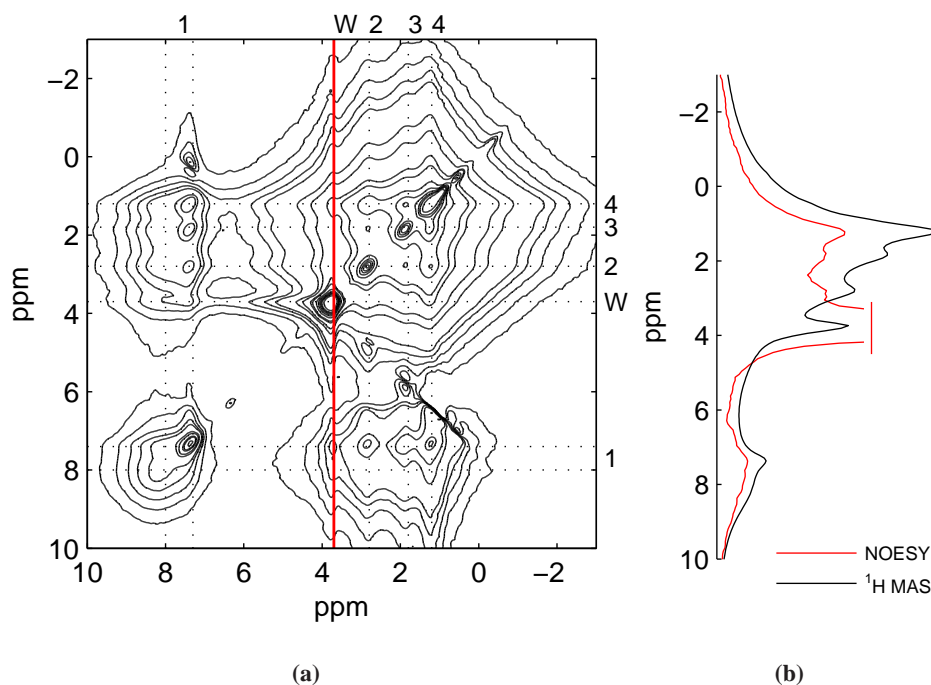


**Figure 4.10:** (a) 2D and (b) 1D  $^1\text{H}$  NOESY spectrum at 30kHz MAS of PA46 crystallized from formic acid at 67°C using a mixing time of 10ms. (b) also shows the  $^1\text{H}$  MAS spectra (black) recorded under the same experimental conditions.

only as a small shoulder on the broad amide signal.

To summarize, two different chemical environments for the amide proton within the solution crystallized samples exist; by comparison with the published crystallographic representation<sup>3</sup> one can assume that one amide resides on the crystal surface and the other within the crystal in the hydrogen bonded sheets. These two chemical environments give rise to the two amide proton signals in the acid and water crystallized samples; a broad, almost temperature independent signal at 8.1ppm and a sharp signal at 7.6ppm, which sharpens and shifts towards lower ppm values upon heating. The sharp proton signal at 7.6ppm is assigned to the more mobile amide proton on the crystal surface, whereas the broad proton signal at 8.1ppm originates from the amide proton in the hydrogen bonded sheets. In Figures 4.11(a) and 4.11(b) the signal at 5.0ppm, assigned to the immobilized water molecules in the water crystallized sample, exhibits a high NOE transfer rate to the rigid amide positions in the hydrogen bonded sheets, whereas the NOE transfer to the more mobile amide positions in the folds is strongly reduced. In the acid crystallized sample, the NOE transfer signals of the water protons are basically unselective. Only the NOE transfer

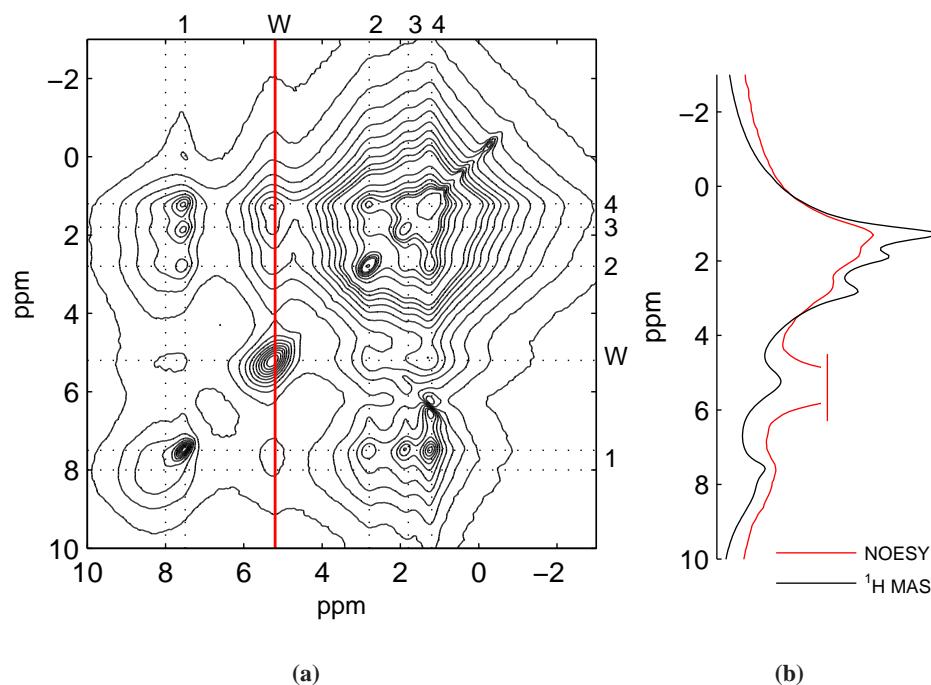


**Figure 4.11:** (a) 2D and (b) 1D  $^1\text{H}$  NOESY spectrum at 30kHz MAS of dried water grown PA46 single crystal mats at 67°C using a mixing time of 10ms. (b) also shows the  $^1\text{H}$  MAS spectra (black) recorded under the same experimental conditions.

rate to the mobile amide site in the chain folds is lower due to their higher mobility.

The water present on the crystal surface evaporates at around 100°C (this will be discussed in more detail in Section 4.14), whereas the water bound within the hydrogen bonded sheets is retained even at 127°C. The latter is the case even when the sample is left at 127°C for 20hrs at a rotor speed of 30kHz. From these findings it can be conclusively stated that water bound to the crystal exists in two different chemical environments – on the crystal surface as seen in the PA4,6 crystallized under normal circumstances, i.e. from formic acid, or within the hydrogen bonded sheets if the sample is crystallized from superheated water. To further investigate the influence of water on hydrogen bonding, FTIR studies are performed.

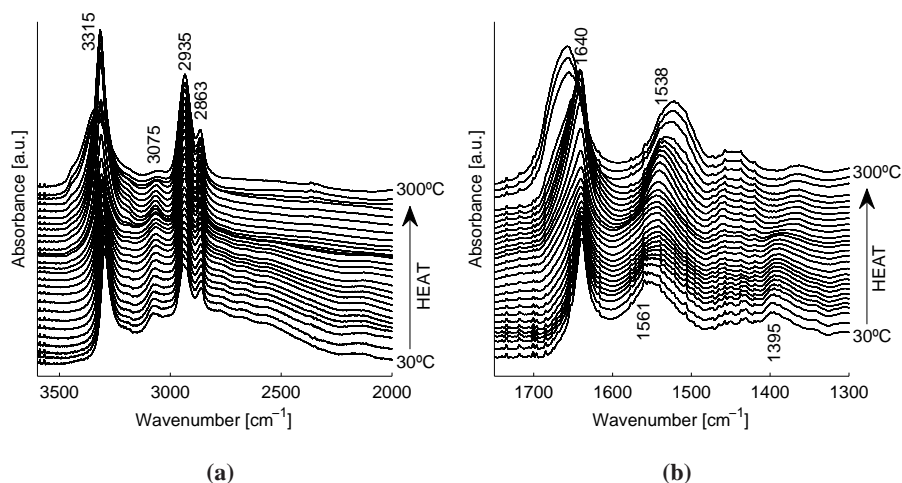


**Figure 4.12:** FTIR spectra obtained when heating dried water crystallized PA4,6 from 30 to 300°C at 10°C/min. The spectra are recorded at regular intervals of 10°C.

## 4.12 Influence of water on the hydrogen bonding within the crystal

Solid state NMR studies performed on the water and acid crystallized samples conclusively demonstrate the presence of water molecules in the vicinity of the amide groups within the lattice and at the crystal surface. In this section we investigate the influence of water molecules on the vibrational bands of the amide groups. For the FTIR studies, PA4,6 crystallized from water is compared to PA4,6 crystallized from formic acid and from the melt.

Figure 4.12 shows the FTIR spectra obtained on heating the dried water grown crystals of PA4,6 on a ZnSe disc at 10°C/min from 30 to 300°C. Each spectra is recorded whilst holding at a constant temperature in regular intervals of 10°C. Figures 4.12(a) and 4.12(b) show spectra in the frequency range of 3600 to 2000 $\text{cm}^{-1}$  and 1700 to 1300 $\text{cm}^{-1}$ , respectively. All spectra are normalized relative to the methylene bands between 3000 and 2800 $\text{cm}^{-1}$ .<sup>47</sup> The prominent bands in Figure 4.12(a) are the NH stretch vibration at 3315 $\text{cm}^{-1}$ , the Amide II overtone at 3075 $\text{cm}^{-1}$ , and the methylene bands between 3000 and 2800 $\text{cm}^{-1}$ . At 30°C all bands are superimposed on an underlying broad band ranging from 3200 to 2300 $\text{cm}^{-1}$ . The underlying broad band disappears at higher temperatures.

On heating the dried water grown PA4,6 crystals, the NH stretch band at 3315 $\text{cm}^{-1}$  shows a remarkable behavior; initially from 30°C to 180°C the band intensity remains approximately constant, but from 180°C the band intensity increases, reaching a maximum at 250°C. On heating the sample further, the band

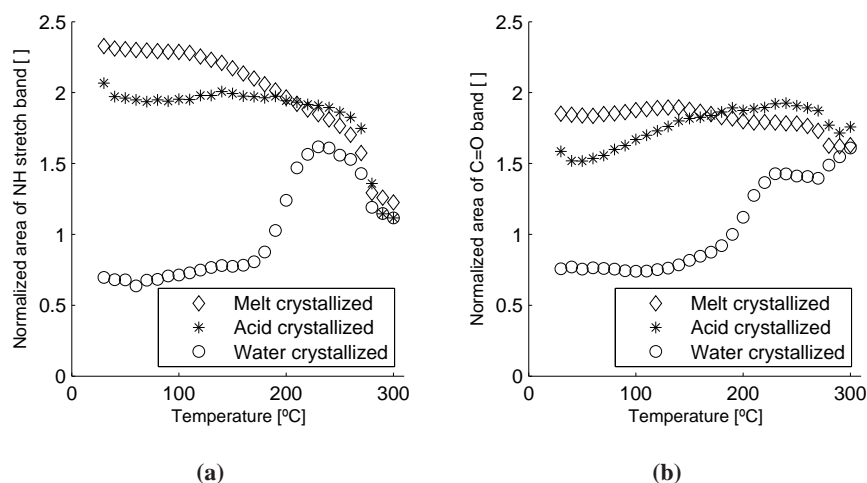


**Figure 4.13:** Normalized area of the (a) NH and (b) C=O vibrational bands of PA4,6 crystallized from water, formic acid, and the melt. The normalization has been done relative to the methylene bands between  $3000$  and  $2800\text{cm}^{-1}$ .

intensity decreases with the onset of the melt at  $\sim 295^\circ\text{C}$ .<sup>8</sup> This behavior is shown more clearly in Figure 4.13(a) where the area of the NH stretch band at  $3315\text{cm}^{-1}$  is plotted against temperature for the dried PA4,6 crystals grown from water showing the increase in area of this band on heating from 180 to  $250^\circ\text{C}$ . An increase in the intensity of this band would occur if the mobility of the NH group is being reduced, for example as would happen if the hydrogen bond strength is increased.

For comparison, the area of the NH stretch vibration of PA4,6 crystallized from formic acid and PA4,6 crystallized from the melt are also plotted, see Figure 4.13(a). The area of the NH stretch band of the PA4,6 crystallized from formic acid remains approximately constant prior to the melt, whereas the NH stretch vibration of melt crystallized PA4,6 shows a steady decrease before melting. From 250 to  $300^\circ\text{C}$ , the area of the NH band of the three differently crystallized samples approach each other as melting occurs. Therefore, if one assumes that at  $30^\circ\text{C}$  water resides within the lattice for water grown PA4,6 crystals as suggested by the NMR data, the lower area of the normalized NH stretch band for the dried water grown crystals compared to the melt and acid crystallized samples, suggests that the presence of water molecules within the lattice are influencing the NH stretch vibration. The NMR data shown in Figure 4.11 shows an association of water molecules in the crystal lattice with the NH group; preventing/shielding of the hydrogen bond formation between adjacent polyamide chains occurs, leading to a greater mobility of the NH group. For further insight into the assumption that the presence of water molecules influences the hydrogen bonding in polyamides crystallized from superheated water,

the spectroscopic changes in the Amide I band, which is the C=O stretch vibration, are investigated.

Figure 4.12(b) shows the Amide I vibration<sup>47</sup> at  $1640\text{cm}^{-1}$  for PA4,6 crystallized from water. On heating, the intensity of the Amide I band remains approximately constant up to  $180^\circ\text{C}$  after which the band intensity increases, reaching a plateau at  $250^\circ\text{C}$ . The area of the Amide I vibrational band depicted in Figure 4.13(b) shows a trend similar to the NH band area shown in Figure 4.13(a). Figure 4.13(b) also depicts the areas of the Amide I band of PA4,6 crystallized from formic acid and from the melt. Unlike the dried PA4,6 crystals grown from water, the area of the Amide I band of the PA4,6 crystallized from formic acid and from the melt remain nearly constant. Once melting occurs, the areas of the Amide I band of the three differently crystallized samples approach each other. Similarly to the area for the NH stretch band, the area of the Amide I band of the PA4,6 crystallized from water also shows an increase between 180 and  $250^\circ\text{C}$ . Considering the previous suggestion for the influence of water upon the NH groups, it is logical that water molecules must also reside in the vicinity of the amide groups, in agreement with the NMR studies reported earlier in this chapter. On heating, around  $180^\circ\text{C}$ , as the tendency of the water molecules to be associated to the amide group becomes less, the shielding of the hydrogen bonds weaken, leading to the recovery of the intensity of the Amide I band. This further strengthens the suggestion that the presence of water molecules within the crystalline lattice weaken the hydrogen bonding between polymer chains. A possibility for the positioning of these water molecules is depicted in Figure 4.14(a). The positioning of these water molecules within the folded hydrogen bonded sheets is shown in Figure 4.14(b). If this projection for the position of the water molecules is true, the emergence of new vibrational bands originating from  $\text{NH}_3^+$  and  $\text{COO}^-$  interactions are anticipated.

On heating from room temperature onwards, the other noticeable changes in the temperature region of 180 to  $250^\circ\text{C}$ , see Figure 4.12, are the disappearance of the weak vibrational bands at  $1561$  and  $1395\text{cm}^{-1}$  together with the broad underlying band between  $3200$  to  $2300\text{cm}^{-1}$ . These changes become more evident on subtraction of the vibrational spectra at  $250^\circ\text{C}$  from the spectra at  $30^\circ\text{C}$ , see Figure 4.15(a). In contrast to the water crystallized sample, the melt crystallized sample does not show the existence of two vibrational bands at  $1561$  and  $1395\text{cm}^{-1}$ , even upon spectral subtraction as shown in Figure 4.15(b).

The band at  $1561\text{cm}^{-1}$  is assigned to an asymmetric  $\text{COO}^-$  vibration whereas the band at  $1395\text{cm}^{-1}$  can be assigned to a symmetric  $\text{COO}^-$  vibration.<sup>69</sup> The very broad vibration between  $3200$  and  $2300\text{cm}^{-1}$  originates from a primary amine  $\text{NH}_3^+$  ion.<sup>69</sup> The appearance of these vibrations at  $30^\circ\text{C}$  indicates that an intermediate structure exists in the dried crystals grown from water which is absent in the crystals grown from acid or from the melt. On heating above  $180^\circ\text{C}$ , the intermediate

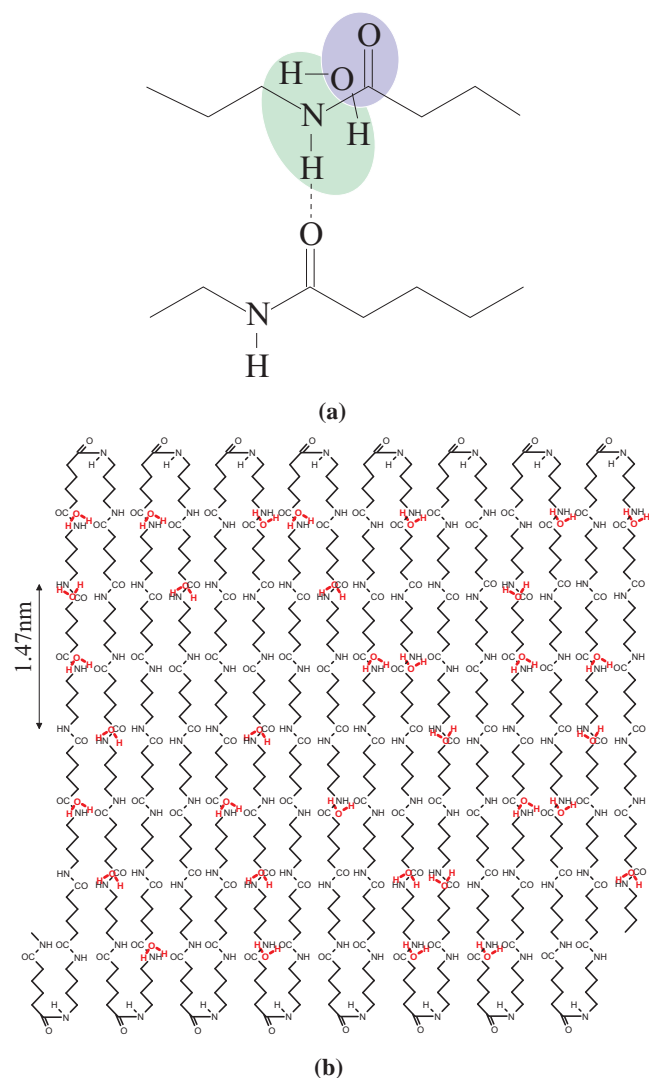


**Figure 4.14:** Possible positioning of the water molecules in the proximity of the amide groups in the crystal lattice of PA4,6. (a) shows the water molecules in close proximity of the amide groups, (b) shows the water molecules as incorporated in the hydrogen bonded sheets; the water molecules are shown in red for clarity. Note that the water molecules are highly mobile, and therefore not limited to one amide position, but most likely shared between various amide groups.

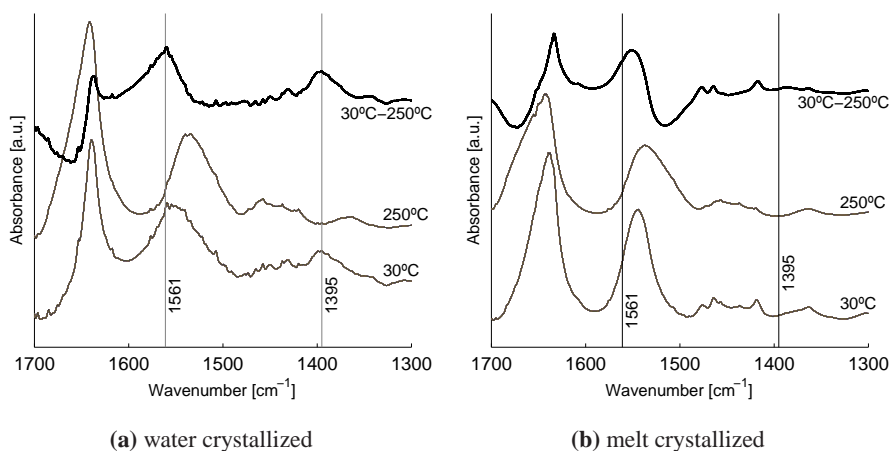


**Figure 4.15:** FTIR spectra of (a) dried water grown PA4,6 single crystals and (b) PA4,6 crystallized from the melt. Both figures show the spectra at 30 and 250°C as well as the spectral subtraction of these two spectra.

structure present in the crystals grown from water gets disrupted resulting in the gradual disappearance of these bands. Thus it can be concluded that water molecules encapsulated in the crystal lattice are responsible for the origin of the bands at 1561 and 1395cm<sup>-1</sup> and the broad underlying band between 3200 and 2300cm<sup>-1</sup>. The suggested position of water in the polyamide lattice, Figure 4.14(a), could indeed give rise to the new vibrations seen in Figure 4.12, as the coupling of the oxygen in the water molecule with the carbonyl group gives rise to the appearance of the symmetric and asymmetric COO<sup>-</sup> vibrations whereas the hydrogens in the water molecule couples with the NH in the amide group to form an NH<sub>3</sub><sup>+</sup> group.

On heating, once the water molecules become sufficiently mobile to move out of the vicinity of the amide groups, the hydrogen bonding between the NH and carbonyl groups of the neighboring chains is restored. This phenomenon results in the recovery of the band intensity and the disappearance of the symmetric and asymmetric COO<sup>-</sup> vibrations and the NH<sub>3</sub><sup>+</sup> vibration. Normally free water molecules leave a polymer around 100°C, however the bound single water molecules incorporated within the PA4,6 crystal lattice can only leave the polymer above 180°C, well above the boiling point of water. This is because a boiling point is a bulk property; hence single water molecules do not show a boiling point. The driving force for the removal of the water molecules from the crystal lattice is likely to be the crank-shaft motion that the CH<sub>2</sub> groups in the main chain will acquire with increasing temperature.<sup>105</sup>

The FTIR spectra shown in Figure 4.12 further confirm that little or no hydrolysis of the PA4,6 has occurred during sample preparation. If hydrolysis of the amide groups had taken place, an ester-carbonyl band at 1740cm<sup>-1</sup> and an amine band

at  $3400\text{cm}^{-1}$  should have been present. The absence of these bands confirms and further strengthens the conclusions already drawn previously in this chapter; the dissolution of PA4,6 in superheated water is a physical process and not merely a chemical hydrolysis of PA4,6.

### 4.13 Water present in a polymer crystal lattice

The NMR results presented above strongly suggest the presence of water at two distinctly different positions of the crystal lattice. Water molecules present near the amide group on the crystal surface are shown to be highly mobile. The presence of water on a crystal surface is a well-known occurrence. In proteins for example, there is a layer of water molecules close to the surface of the protein molecule.<sup>48</sup>

The incorporation of water molecules as part of the crystal lattice is however a lesser known anomaly. Srikrishnan and Parthasarathy<sup>91</sup> showed for the first time how water molecules are “sandwiched” between pyrimidine bases. In their study the most remarkable feature is the location of the water molecules which are positioned between successive, parallel pyrimidine bases. The water molecules are held in position by a strong hydrogen bond from the carbonyl group. Indeed, carbonyl groups often accept hydrogen bonds simultaneously from main-chain NH and water molecules in  $\alpha$ -helices,  $\beta$ -turns, and  $\beta$ -sheets.<sup>49</sup> Bluhm *et al.*<sup>9</sup> also showed the presence of a water sandwich between layers of a polysaccharide where the water molecules are intercalated in the unit cell. The incorporation of water molecules in other macromolecules has also been explored by Maréchal<sup>71,72</sup> who showed the incorporation of water molecules in polysaccharides by following the hydration mechanism.

In a separate study Parthasarathy *et al.*<sup>76</sup> showed that tripeptides are stabilized by two water molecules which enable the peptides to complete a turn of the helix and extend the helical structure throughout the crystal by linking peptides by hydrogen bonds. The extension of the helix through the crystal takes place by connecting translationally related molecules along a cell edge by using one or two water molecules. The water molecules provide the type of hydrogen bond typical of the  $\alpha$ -helix. Hence the tripeptide molecules not only assume a helical conformation in the solid state, but are also able to extend the helix with just a few water molecules.

Water molecules are also frequently observed inserted between NH and C=O groups in  $\alpha$ -helices.<sup>48</sup> Evidence of water molecules between the NH and C=O groups is also seen in the FTIR data shown above. Iizuka<sup>44</sup> showed an interesting molecular model for spider silk where neighboring segments of each subunit are hydrogen bonded between the peptide groups through water molecules. Here water molecules form an integral part of the crystal’s hydrogen bonded network.



Bella *et al.*<sup>7</sup> showed that water molecules are organized in a semi-clathrate like structure that surrounds and interconnects triple helices in the crystal lattice of collagen peptide. Harlow<sup>36</sup> showed how water molecules co-crystallize with a RGD peptide, where the water molecules are positioned in the voids/channels of the peptide crystals to form a clathrate-like structure. Savage<sup>86,87</sup> also showed water molecules present in the crystal structure of vitamin B<sub>12</sub> co-enzymes.

All the above works and our observations do therefore point to the highly likely scenario that, upon crystallization from dilute PA4,6 solution, water is indeed incorporated into the polyamide lattice in the vicinity of the amide groups in the crystalline lattice acting as a bridge between successive hydrogen bonded sheets and screening hydrogen bonding interactions. Upon heating these crystals, it should be possible to “drive off” the water at elevated temperatures.

#### 4.14 Removal of water molecules

We now return to our previous discussion on the heats of fusion presented earlier in Section 4.4. If water molecules are indeed bound to the amide groups in the crystal, these water molecules should exit the polymer well above 100°C and should also be readily measurable with thermogravimetric analysis (TGA). High resolution TGA is used to improve the resolution of any possible weight loss. Figure 4.16 shows the derivative weight loss with respect to time on heating PA4,6 crystallized from formic acid and from water from 30 to 500°C. The weight loss of the two samples generally follow the same trend with the exception that the water crystallized sample shows an event between 180 and 250°C. This event suggest the possible exit of water molecules from the polymer.

Tables 4.1 and 4.2 summarize the melt and dissolution temperatures as well as the heats of fusion obtained for DSC runs on PA4,6 crystallized in various ways as shown in Figures 4.3 and 4.17. When acid crystallized PA4,6 is heated the polymer shows two peaks at 285°C and 289°C with a total heat of fusion  $\Delta H = 106\text{J/g}$  (see Figure 4.17(c)). When melt crystallized PA4,6 is heated the polymer melts at a similar temperature of 286°C, but now has a much lower  $\Delta H = 84\text{J/g}$ . This reduction in the heat of fusion in the melt crystallized sample in comparison to the acid crystallized sample can be attributed to a lower crystallinity and a less perfect crystal packing in the melt crystallized sample.

When acid crystallized PA4,6 is heated in the presence of water, dissolution of the polymer in the superheated water occurs at 185°C with a  $\Delta H = 106\text{J/g}$  (see Table 4.2). The heat of fusion involved during the dissolution of the acid crystallized PA4,6 is similar to the heat of fusion involved in melting the acid crystallized PA4,6.

The PA4,6 that is dissolved in superheated water is crystallized and all excess

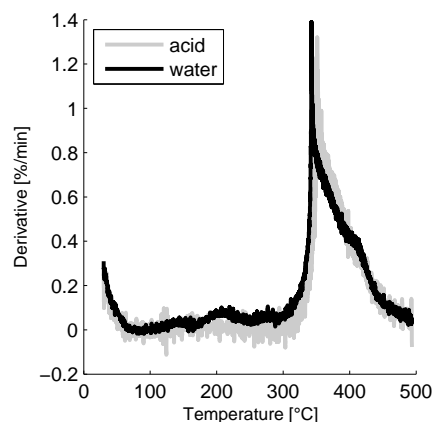


**Figure 4.16:** High resolution TGA for PA4,6 crystallized from formic acid and from water. Considering the changes in the FTIR spectra, the weight loss above 180°C in the water crystallized sample is associated to the removal of water molecules from the crystal lattice.

water is allowed to evaporate under ambient conditions. On heating the dried water crystallized PA4,6 three thermic events occur as shown in Figure 4.17(a). A broad exotherm is observed between 200 and 230°C (see Figure 4.17(b) for more detail) with a  $\Delta H = 14\text{J/g}$  and a melting endotherm is observed at 290°C (with a shoulder at 273°C) with a total  $\Delta H = 106\text{J/g}$ . The exotherm between 180 and 230°C is remarkable and does not return on a second heating, i.e. when the same sample is crystallized from the melt, nor does the shoulder at 273°C. In the second heating run an endotherm is observed having a peak temperature at 287°C with a  $\Delta H = 84\text{J/g}$ . Clearly the polymer did not succumb to degradation because of the comparable heats of fusion between the second melting endotherm of the water crystallized PA4,6 and the melt crystallized PA4,6. We propose that the exothermic event seen results from water molecules, which are located in the vicinity of the amide groups, exiting the polymer, resulting in a strengthening and reorganization of the hydrogen bonds as shown in the FTIR data in Figure 4.13.

Finally, when the water crystallized sample is redissolved in superheated water a dissolution temperature of 195°C is obtained with a  $\Delta H = 79\text{J/g}$ . The heat of fusion is now much lower than when dissolving the acid crystallized PA4,6 in water. This is most likely due to weakening of the hydrogen bond strength due to the presence of water molecules within the crystal lattice.

The DSC trace of the first heating run of the water crystallized PA4,6 shown in Figure 4.17(a) shows a reorganization/crystallization in the same temperature region where the weight loss occurs in the TGA data (Figure 4.16). In this temperature region the strengthening of the hydrogen bonds is seen in the FTIR data

(Figure 4.13). This experimental evidence strongly suggests that water molecules are present in close proximity to the amide groups and disturb the hydrogen bonds between the recurring amide groups. On heating above the Brill transition the water molecules exit the polymer. These events shown in the TGA and DSC data between 180 and 230°C are in agreement with the disappearance of the symmetric and asymmetric COO<sup>-</sup> vibrations and the NH<sub>3</sub><sup>+</sup> band observed in the FTIR spectra. The water molecules are most likely shared between different amide groups in a three-dimensional structure causing substantial changes in the NMR and FTIR spectra. The water molecules present in the unit cells are likely to be highly mobile, more mobile than the time resolution of the spectral techniques used in this study. Therefore only average spectral data can be collected.

Although only a small number of water molecules are present in the polymer (evident from the low response in the TGA), their presence is nonetheless sufficient to account for the disappearance of certain bands in the FTIR data and the notable shift observed in NMR spectra of the water crystallized PA4,6 at the temperature where the water molecules are expelled from the crystal lattice. The findings reported here strongly suggest that this small amount of the water molecules is sufficient to influence the hydrogen bonding. It is most likely that the water molecules within the sheets are highly mobile, rather than bound to a specific amide position. Compared to the reported findings on hydrate crystals of M5, where the alternating layers of water molecules present in the lattice causes modifications in the X-ray diffraction pattern, more specifically the 200 reflection increases by 17% when water molecules are present in the M5 crystal lattice,<sup>58</sup> in the dried PA4,6 crystallized from water no changes in the X-ray diffraction pattern is observed. Furthermore, water molecules present in rigid polymers have a tendency to form mobile clusters. Only at extremely low concentrations are water molecules expected to be present separately, without hydrogen bonds forming between them. We have found no evidence of water clusters in the FTIR data where one would expect an OH-vibration if such clusters were indeed present. The absence of these clusters and of any modifications in the X-ray diffraction pattern arises due to the small amount of water molecules present within the lattice and their freedom to move. This hypothesis has been addressed in a model hydrogen bonded system which is based on an ester amide N,N'-1,2-ethanediyl-bis(6-hydroxyhexanamide) (EDHA) where no chain folding and/or amorphous regions are present which indeed supports our finding.<sup>34,35</sup>

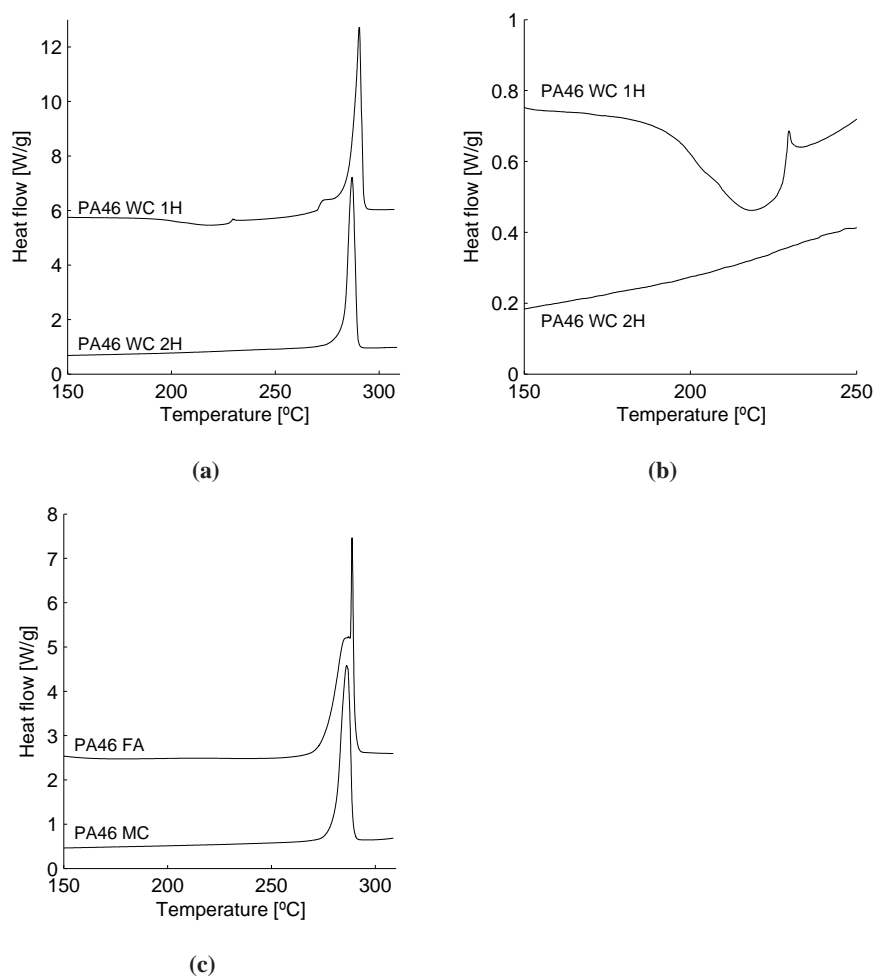


**Figure 4.17:** (a) shows DSC traces of PA4,6 crystallized from water (PA46 WC) during the first and second heating runs (1H and 2H) respectively. (b) is a magnification of the temperature region 150 to 250°C shown in (a). Remarkable is the exothermic event which occurs in the first heating run of water crystallized PA4,6 between 180 and 230°C. This event is not repeated in the second heating run. (c) shows the DSC traces of PA4,6 crystallized from formic acid (PA46 FA) and from the melt (PA46 MC).

## 4.15 Conclusions

From the experiments performed here it is evident that superheated water is a good solvent for polyamide 4,6. In the presence of superheated water the melting temperature of the polymer is suppressed. Within the given experimental time scale for the DSC, FTIR and X-ray studies reported in this chapter, the molar mass of the polymer after dissolution can be considered to be constant; strengthening the concept that the dissolution of nylon is a physical process. However, hydrolysis occurs if the polymer is retained in the water solution above its dissolution temperature for longer times (>10 minutes). Solution grown crystals from water form single crystals where the chains are perpendicular to the basal plane having four monomer units forming a lamellar thickness of 6nm. These observations indicate the presence of tight hairpin-like folds with an amide group incorporated in the fold. The adjacently re-entrant chains within the crystal lead to the formation of hydrogen bonded planes. These observations are in agreement with the earlier reported findings on PA4,6 crystallized from an organic solvent<sup>3</sup> – confirming that the superheated state of water is a good solvent for PA4,6 and this method of dissolution and recrystallization yields PA4,6 single crystals.

Solid state NMR studies performed on the single crystals show two distinct proton mobilities for the amide groups located at the crystal surface and within the hydrogen bonded sheets. The proton mobility of the amide group on the crystal surface is noticeably higher than that of the amide groups within the lattice, confirming the presence of a free proton in the tight folds as envisaged by Atkins *et al.*<sup>3</sup> The free proton present on the crystal surface is likely to adsorb water molecules from the atmosphere making PA4,6 more hygroscopic compared to other nylons that have methylene units in the folds. For crystals grown from a superheated water solution, the <sup>1</sup>H MAS NMR spectra show the presence of water with a significantly reduced mobility and different chemical environment compared to the water present in the acid grown crystals. The NOESY spectra confirm the interaction of these water molecules with the protons of the amide groups in the crystal lattice.

In the FTIR spectroscopy, the presence of water molecules within the lattice influences the hydrogen bonding, resulting in a decrease in the area of the amide bands, and the appearance of two new vibrational bands arising from COO<sup>-</sup> and NH<sub>3</sub><sup>+</sup> vibrations. With the removal of the water molecules upon heating above 180°C, the hydrogen bonding between the carbonyl and NH groups is restored. High resolution TGA combined with DSC, solid state NMR, and FTIR spectroscopy conclusively demonstrate the presence of water molecules which, though present in only a small amount, are likely to be within the crystal lattice in the vicinity of the amide groups.

## Chapter 5

# Crystallization of polyamide 6,6 from superheated water – implications for the $\alpha$ and $\beta$ crystal structures

Here we show that polyamide 6,6 (PA6,6) dissolves in superheated water at 190°C and crystallizes in predominantly the  $\alpha$ -structure, i.e. a progressive shear conformation between the hydrogen bonded sheets. However, a small portion of the PA6,6 crystallizes in the  $\beta$ -structure, an alternately up-and-down sheared conformation, due to the presence of water molecules incorporated in the crystal lattice. These water molecules exit from the lattice at the Brill transition temperature as observed by an exotherm in DSC traces. The presence of the  $\beta$ -structure is seen by weak 110, 100, and 020 reflections in the WAXD data and a small angle diffraction peak at 6nm, in comparison to the expected<sup>4</sup> 5.4nm for pure  $\alpha$ -structured PA6,6. The presence of the  $\beta$ -structure in the water crystallized PA6,6 causes several conformational changes in the methylene units directly surrounding the amide groups.

## 5.1 Introduction

Polyamide 6,6 (PA6,6) is an engineering plastic used in a wide variety of applications such as (reinforcement) fibers, insulation, upholstery, clothing, etc., and is also perhaps the most extensively studied member of the polyamide family. The Brill transition, for example, was first reported for PA6,6 in 1942.<sup>11</sup> Since then, Brill transitions have been reported for many other polyamides.<sup>50</sup> The Brill transition is characterized by a change from a low temperature triclinic/monoclinic crystal structure to a high temperature pseudo-hexagonal phase, which is in turn characterized by the convergence of the two strong interchain and intersheet

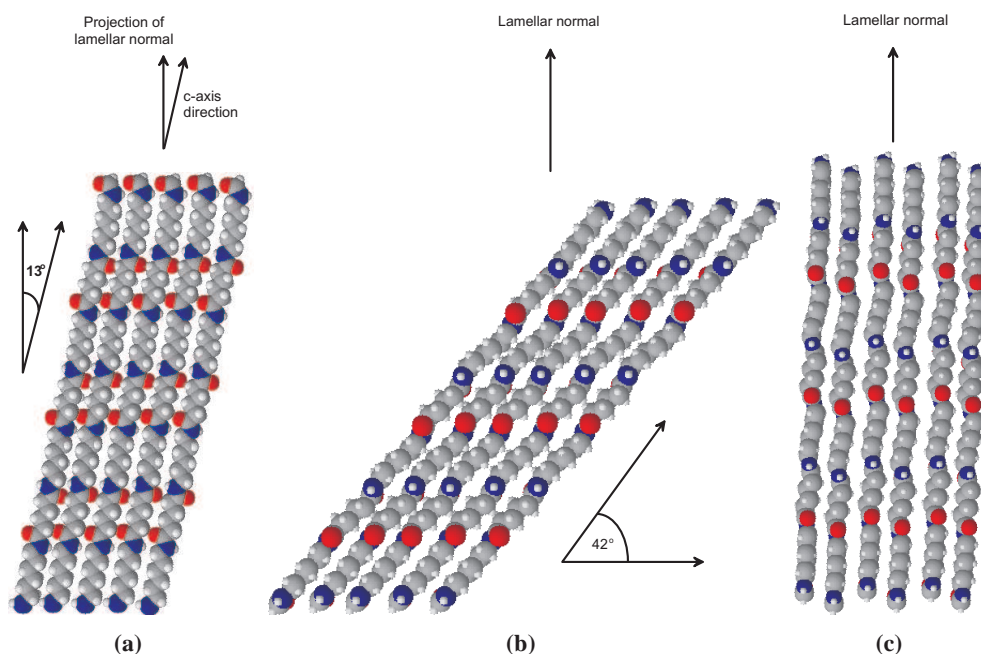


**Figure 5.1:** Projections of polyamide 6,6 structures, adapted from Jones *et al.*<sup>51</sup> Here we adopt the nomenclature used by Bunn and Garner.<sup>13</sup> (a) A single hydrogen bonded sheet with a progressive chain shear of  $13^\circ$ . (b) Viewing parallel to the sheets shown in (a) illustrating the progressive shear between sheets in the  $\alpha$ -structure. The unit cell of the  $\alpha$ -structure is  $a = 0.49\text{nm}$ ,  $b = 0.54\text{nm}$ ,  $c = 1.72\text{nm}$ ,  $\alpha = 48.5^\circ$ ,  $\beta = 77^\circ$ , and  $\gamma = 63.5^\circ$ .<sup>13</sup> (c) Viewing parallel to the sheets shown in (a) illustrating the alternating shear in the direction of the  $c$ -axis typical of the  $\beta$ -structure. The unit cell of the  $\beta$ -structure is  $a = 0.49\text{nm}$ ,  $b = 0.80\text{nm}$ ,  $c = 1.72\text{nm}$ ,  $\alpha = 90^\circ$ ,  $\beta = 77^\circ$ , and  $\gamma = 67^\circ$ .<sup>13</sup> Here hydrogen is white, oxygen is red, nitrogen is blue, and carbon is silver-grey.

reflections to a single reflection in WAXD. The Brill transition is dependent on thermal history and crystallization conditions, and reported Brill transition temperatures for PA6,6 range from 190 to  $260^\circ\text{C}$ .<sup>22,79</sup>

The unit cells for many polyamides are often modelled on, or compared to, the unit cell for PA6,6 first reported by Bunn and Garner<sup>13</sup> in 1947. In order for all the amide units in a chain-folded PA6,6 sheet to form hydrogen bonds, the hydrogen bonded chains must be progressively sheared, with the chain axis tilted at an angle of  $\sim 13^\circ$  to the normal of the chain folded sheet edge as shown in Figure 5.1(a).<sup>51</sup> PA6,6 is known to crystallize in two different structures known as the  $\alpha$ - and  $\beta$ -structures respectively, where the  $\alpha$ -structure consists of progressively sheared hydrogen bonded sheets, and the  $\beta$ -structure consists of alternately up-and-down sheared hydrogen bonded sheets; see Figure 5.1 for more details. In the majority

of solution grown, chain folded lamellae, the hydrogen bonded sheets stack with a pronounced ( $\sim 42^\circ$ ) progressive shear as shown in Figure 5.1(b), i.e. an  $\alpha$ -structure. Also for PA6,6 the most common room temperature structure is a triclinic crystal structure with the unit cell tilted at  $42^\circ$  with respect of the lamellar normal such that the (00 $l$ ) planes are parallel to the lamellar surface.<sup>26,40</sup> The PA6,6 lamellae contain 3.5 chemical repeat units with the chains being adjacently re-entrant and the fold contained in the diacid alkane segment of the repeat unit.<sup>4</sup>

In its folding behavior PA6,6 differs from polyamide 4,6 (PA4,6); although PA4,6 contains 4 repeat units per lamellar thickness and the chains are adjacently re-entrant, the fold is not present in an alkane segment of the chain, but in the amide group. Therefore PA4,6 contains an amide group on the surface of the lamellae<sup>3</sup> whereas PA6,6 contains an alkane unit on the lamellar surface.

The perfect crystal packing of PA4,6 is obtained by solution crystallization.<sup>3</sup> Recently we have used a new solvent for PA4,6, namely superheated water, to study the crystallization behavior.<sup>82,106</sup> It was found that on crystallization from superheated water, PA4,6 packs into 6nm lamellae with intersheet and interchain distances of 0.44nm and 0.37nm. Furthermore it was shown that when in the dissolved state, the amide groups interact with the superheated water molecules, and on crystallization water molecules are incorporated in the PA4,6 crystal lattice in proximity of the amide groups.

The use of superheated water as a solvent for polyamides provides the possibility for an environmentally friendly processing route. For this reason it is important to know and understand how PA6,6, the most commonly used polyamide, reacts to superheated water. Also, the crystal structure, fold mechanism, and chain orientation to the lamellar normal of PA6,6 differs considerably from PA4,6. It is therefore important to investigate how these differences influence the dissolution and crystallization process of PA6,6 in superheated water. This process is investigated using differential scanning calorimetry (DSC), simultaneous small and wide angle X-ray diffraction (SAXS/WAXD), and infrared spectroscopy (FTIR).

## **5.2 Experimental description**

The polymer used in this study is a commercially available PA6,6, produced by BASF under the tradename Ultramid<sup>®</sup> AS2700. A film is prepared by dissolving the polymer in formic acid (5g/l) and subsequently solvent casting the polymer onto a glass plate after which the solvent is allowed to evaporate.<sup>30</sup> Melt crystallized material is obtained by heating the acid crystallized material to the melt and cooling to room temperature at  $10^\circ\text{C}/\text{min}$  using a Linkam TMS94 hotstage.

DSC, FTIR spectroscopy, high resolution WAXD, and simultaneous SAXS/



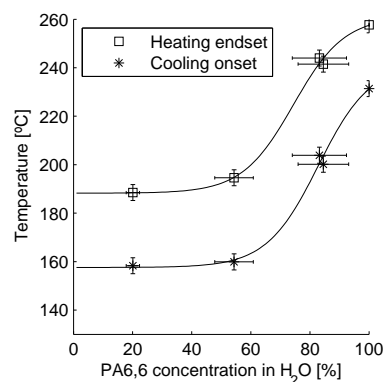


**Figure 5.2:** Influence of polymer concentration on the dissolution of PA6,6 in water. The phase diagram is constructed from the measured end point of the dissolution endotherms and the onset point of the crystallization exotherm, for various concentrations of PA6,6 in water. All lines serve as a guide to the eye.

WAXD together with the WAXD data corrections are performed as discussed in Appendix A.

### 5.3 Phase behavior of PA6,6 in superheated water

Figure 5.2 shows the end point of the DSC endotherm obtained during the second heating run of PA6,6 in the presence of superheated water. From WAXD it is known that this point represents the temperature at which the polyamide has dissolved completely in the superheated water. Figure 5.2 shows both the end of dissolution and the onset of crystallization temperatures as a function of polymer concentration in water. Both the dissolution and crystallization temperatures show an increase with increasing polymer concentration from 190°C for the dissolution temperature and 160°C for the crystallization temperature from ~55wt% polyamide. The general trend set by the dissolution and crystallization temperatures confirms that, just as for PA4,6, superheated water is a solvent for PA6,6.

In an interesting study in which the phase behavior of PA6,6 in both subcritical, i.e. superheated, and supercritical water is investigated, the dissolution of PA6,6 in superheated water was observed at ~237°C for 11% polyamide.<sup>89</sup> Visually the authors were able to confirm that the PA6,6 turned transparent on heating in the presence of water. On dissolution the sample is seen to disperse homogeneously throughout the experimental pressure chamber to fill it completely. On cooling, the solution crystallized to form a suspension of, what the authors called, nylon-like

**Table 5.1:** Melting temperatures and heats of fusion of PA6,6 crystallized from formic acid, water, and the melt.

	Melting temperature		$\Delta H$
	shoulder	peak	
PA6,6 from formic acid	255°C	265°C	106J/g
PA6,6 from water	258°C	267°C	97J/g
PA6,6 from melt	253°C	263°C	76J/g

**Table 5.2:** Dissolution temperatures and heats of fusion in superheated water of PA6,6 crystallized from water and formic acid.

	Dissolution temperature		$\Delta H$
PA6,6 from formic acid	184°C	132J/g	
PA6,6 from water	190°C	81J/g	

material. The authors<sup>89</sup> left the PA6,6 in solution at 264°C for ~12min. From the research performed on the dissolution of PA4,6 in superheated water we know that if left in solution for more than 10 minutes, severe degradation/hydrolysis is to be expected, confirming these author's observations that the remaining material in their pressure chamber was nylon-like, showing properties related to polyamides, but was different from the original sample.

To obtain an estimate of possible hydrolysis in our PA6,6 samples, heats of fusion are investigated. By DSC 106J/g is required to melt an acid crystallized PA6,6 sample whereas 132J/g is required to dissolve the same sample in superheated water, which are both notably higher than the 76J/g required to melt a melt crystallized sample (Tables 5.1 and 5.2). The heat of fusion for dissolving PA6,6 in superheated water is slightly higher than the heat of fusion involved when melting PA6,6. Possibly this is due to the substantially lower dissolution temperature in comparison with the melting temperature. Also, with increasing temperature the hydrogen bonding becomes progressively weaker, though remaining intact up to melting/dissolution. The hydrogen bond strength will therefore be higher at the dissolution temperature than at the melt temperature, therefore leading to a higher heat of fusion for the dissolution process in comparison to the melt process. Upon a second heating run of

dissolving PA6,6 in superheated water only 81J/g is required to dissolve the sample. If this water crystallized sample is dried, i.e. after removing all excess water, 97J/g is required to melt the sample. These results are similar to the enthalpy's reported for melting and dissolution of PA4,6 reported in Chapter 4. Also, these results confirm that the dissolution of PA6,6, similar to PA4,6, proceeds via a physical process as opposed to a chemical hydrolysis/degradation process.

## 5.4 Single crystals grown from superheated water

To perform TEM and electron diffraction studies of water crystallized PA6,6, the polyamide is allowed to crystallize from a dilute solution, forming a suspension which is placed on a carbon coated copper TEM grid coated with gold as an internal diffraction reference. The excess water is allowed to evaporate under ambient conditions overnight. Figure 5.3 shows the TEM and electron diffraction images obtained for water crystallized PA6,6 crystals. The crystals appear lath-like and are  $\sim 4\mu\text{m}$  in length, similar to PA6,6 single crystals grown from 1,4-butanediol.<sup>51</sup> The electron diffraction pattern of the water grown crystals shown in Figure 5.3(b) clearly demonstrates the single crystal nature of these crystals, showing three Bragg reflections at  $0.364 \pm 0.015\text{nm}$ ,  $0.376 \pm 0.018\text{nm}$ , and  $0.436 \pm 0.007\text{nm}$  which are indexed as the 100, 010, and 100 reflections respectively.<sup>3</sup> These crystals show similarities to the water grown PA4,6 crystals shown in Chapter 4.

The sample stage was not rotated to determine the angle between the lamellar normal and the hydrogen bonded sheets, although the incident electron beam is likely parallel to the chain axis and close to  $42^\circ$  to the lamellae normal. It is therefore not possible to estimate the crystal structure,  $\alpha$  or  $\beta$ , when PA6,6 is crystallized from superheated water. However, the obtained diffraction patterns are very similar to the diffraction patterns obtained for PA6,6  $\alpha$ -structures grown from solvents such as 1,4-butanediol.<sup>51</sup> It is therefore likely that on crystallization from superheated water, the PA6,6 crystallizes into the  $\alpha$ -structure, the most common crystal structure for PA6,6.<sup>51,53</sup>

To probe the crystal thickness along the  $c$ -axis of the water grown single crystals together with morphological and crystallographic changes, time resolved SAXS/WAXD is performed during heating/cooling a dried, sedimented PA6,6 single crystal mat. Also high resolution WAXD could provide more insight into the crystallization process of PA6,6 from superheated water.

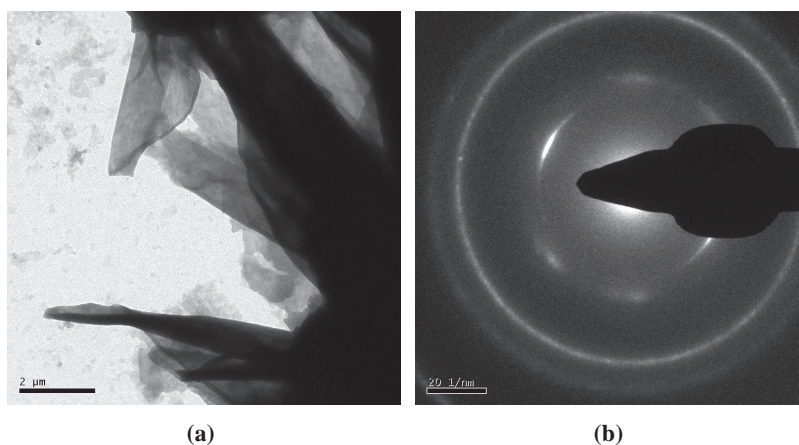


**Figure 5.3:** (a) shows lath-like single crystals obtained on crystallizing PA6,6 from water in a dilute solution. (b) shows an electron diffraction pattern from these crystals containing the 100, 010, and 110 diffraction signals and their corresponding negative pairs. The incident electron beam is parallel to the chain axis and close to  $42^\circ$  to the lamellae normal shown in (a). The outer diffraction rings are from the gold coating used as an internal calibration reference.

## 5.5 High resolution WAXD

High resolution WAXD is performed on PA6,6 on the Materials Science beamline (ID11) at the ESRF. These experiments are essential due to the high resolution achievable on this beamline which enables us to study poorly resolved or weak reflections, not (readily) detectable on the simultaneous SAXS/WAXD data obtained from ID02 shown later in this chapter.

Figure 5.4 shows the WAXD patterns for PA6,6 crystallized from the melt (MC), from superheated water (WC), and after the water crystallized sample has been heated to  $240^\circ\text{C}$  allowing the excess water to evaporate, note that this temperature is below the melt temperature of PA6,6, and cooled to room temperature (WE). Additionally the figure shows the predicted diffraction patterns for both the  $\alpha$ - and  $\beta$ -structures of PA6,6 according to the model given by Bunn and Garner.<sup>13</sup>

The melt crystallized spectrum shows two strong reflections at  $6.5^\circ$  (0.44nm) and  $7.4^\circ$  (0.38nm) known as the 100 interchain/intrasheet and 010 intersheet reflections, respectively. The melt crystallized diffraction pattern corresponds with the calculated  $\alpha$ -structure with the exception of the intersheet reflection. This discrepancy in the assignment of the intersheet reflection can normally be circumvented by annealing the melt crystallized sample at elevated temperatures.<sup>70</sup> The water crystallized pattern shows a well resolved pattern which also closely matches the  $\alpha$ -structure with the exception of weak reflections at  $6.0^\circ$  (0.47nm),  $6.7^\circ$  (0.42nm), and the

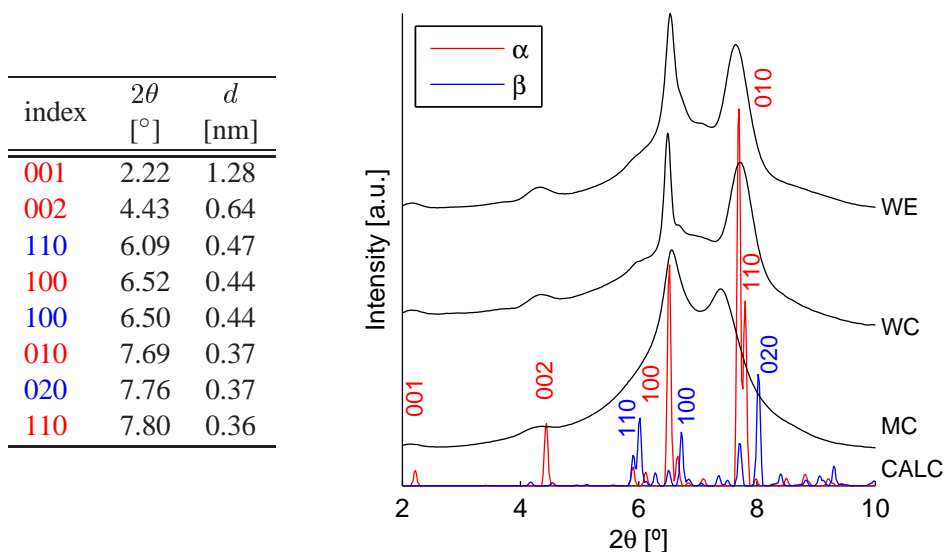


**Figure 5.4:** High resolution WAXD of PA6,6 crystallized from the melt (MC), from superheated water (WC), and after the water crystallized sample is heated to 240°C and cooled down (WE). All images are at 50°C. Additionally the calculated powder diffraction patterns<sup>2</sup> from an atom filled unit cell for the  $\alpha$ - and  $\beta$ -structures of PA6,6 is also shown as determined by Bunn and Garner.<sup>13</sup> The data is plotted as a function of  $2\theta$  for clarity according to Bragg's law, where  $\lambda = 2d \sin \theta$  with wavelength  $\lambda = 0.04956\text{nm}$ .

intersheet reflection at  $7.7^{\circ}$  (0.37nm) being unexpectedly broad. The  $\beta$ -structure of PA6,6 shows relatively strong reflections at  $6.0^{\circ}$  which is the 110 reflection; at  $6.7^{\circ}$  which is the 100 reflection; and at  $8.0^{\circ}$  which is the 020 reflection. The presence of a small amount of  $\beta$ -structured PA6,6 present in the predominantly  $\alpha$ -structured PA6,6 would account for the additional (weak) reflections observed for the water crystallized PA6,6.

The sample is subsequently heated to 240°C, i.e. below the melt temperature of PA6,6 but above the Brill transition temperature and cooled back to 50°C; the resulting diffraction pattern is shown in Figure 5.4 marked WE. After heating the intensity of the reflections associated to the  $\beta$ -structure have decreased, whereas the reflections related to the  $\alpha$ -structure, especially the 002 reflection, increases in intensity. The 001 and 002 reflections arise due to order along the polymer chain.<sup>94</sup> Especially the 002 reflection is strong for PA6,6 which emanates from planes passing through the amide groups. The (002) plane is inclined at a substantial angle of  $42^{\circ}$  to the  $c$ -direction.<sup>3</sup> An increase in the intensity of the 002 reflection could therefore be the result of a reorganization along the polymer chain. The WE sample also shows a weak reflection at  $7.0^{\circ}$  (0.41nm) which is likely a reminiscence of the high temperature pseudo-hexagonal phase which is observed above the Brill transition

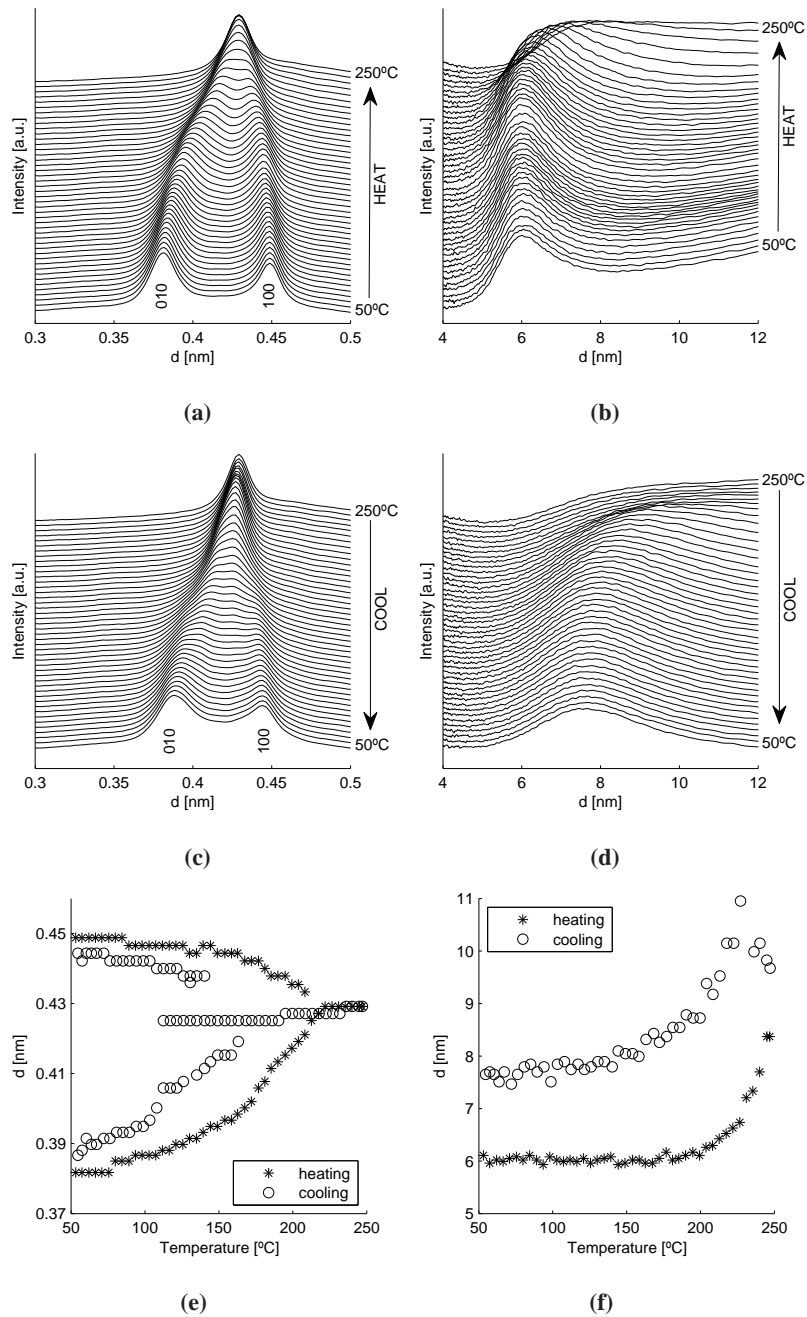
temperature. The presence of the high temperature pseudo-hexagonal phase at room temperature is observed more readily in polyamides that show the presence of both the  $\alpha$ - and  $\beta$ -structures and much less frequent in polyamides showing only the  $\alpha$ -structure.<sup>53</sup> The presence of this high temperature phase in PA6,6 is observed at room temperature when the polymer is quenched rapidly from the melt<sup>88,94</sup> and is generally not observed in PA6,6 single crystals.<sup>53</sup> The presence of the high temperature phase at 50°C could indicate that cooling proceeded too rapidly to allow for a full transition to the low temperature triclinic structure, or it relates to the presence of both the  $\alpha$ - and  $\beta$ -structures observed in the water crystallized PA6,6.

## 5.6 Simultaneous SAXS/WAXD

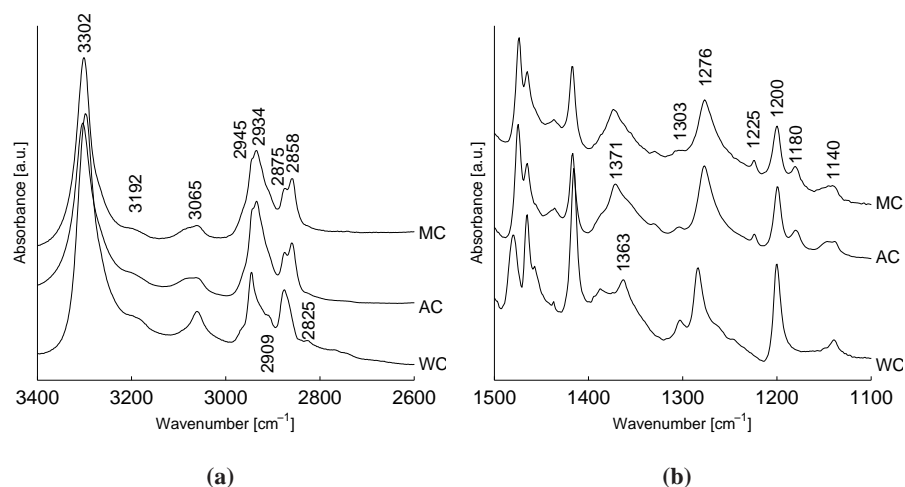
PA6,6 single crystal mats are prepared by filtering a dilute suspension of water crystallized single crystals through a Büchner funnel. This single crystal mat is allowed to dry under ambient conditions before performing simultaneous SAXS/WAXD on the sample.

Figure 5.5 shows X-ray diffraction patterns recorded during the heating/cooling run of a dried sedimented crystal mat between 50 and 250°C at a rate of 10°C/min. Figure 5.5(a) shows the WAXD patterns of the solution grown crystals. The starting values for the interchain and intersheet distances of 0.38nm and 0.45nm respectively are comparable to the crystals grown from other solvents.<sup>3</sup> Note that here the weak reflections observed in Figure 5.4 indicative of the  $\beta$ -structure are not seen. Likely this is due to the lower resolution in the WAXD data on the ID02 beamline in comparison to the ID11 beamline. On heating, the room temperature triclinic structure changes into the high temperature pseudo-hexagonal structure at  $\sim$ 220°C at the Brill transition temperature. This Brill transition temperature compares well with the Brill transition temperature reported for solution grown PA6,6 crystals.<sup>51</sup> The single crystal mat is heated to 250°C, i.e. just below the melt temperature of  $\sim$ 265°C,<sup>51</sup> before cooling to 50°C. On cooling the crystals transform into the triclinic phase at  $\sim$ 160°C. However, between 160 and 110°C remnants of the high temperature pseudo-hexagonal phase are observed. Only after cooling to well below the Brill transition temperature do all of the high temperature phase transform into the low temperature triclinic phase. It is however also possible that reminiscence of the high temperature phase is still present in the sample at 50°C, similar to that seen in Figure 5.4. Should this indeed be the case the information is not visible on the diffraction patterns, likely due to the low resolution of the obtained WAXD data on the beamline.

The simultaneously recorded SAXS data shown in Figure 5.5 shows a single diffraction peak at  $\sim$ 6nm, which on heating starts to increase between 200 and 250°C,



**Figure 5.5:** Simultaneous SAXS/WAXD patterns collected on heating a PA6,6 single crystal mat (PA6,6 was crystallized from water and sedimented to form a mat) from 50°C to 250°C and cooling from 250°C to 50°C; both at 10°C/min.



**Figure 5.6:** FTIR spectra of melt crystallized (MC), water crystallized (WC), and acid crystallized (AC) PA6,6 at 30°C from (a) 3600 to 2600 $\text{cm}^{-1}$  and (b) 1500 to 1100 $\text{cm}^{-1}$ .

finally reaching a maximum of  $\sim 10\text{nm}$ . On cooling between 200 and 110°C the position of the peak decreases to  $\sim 8\text{nm}$ , remaining approximately constant below 110°C.

When PA6,6 crystallizes in the  $\alpha$ -structure, with 3.5 monomer repeats per fold, the SAXS peak should be positioned at  $\sim 5.4\text{nm}$  when grown from 1,4-butanediol solution as reported by Atkins *et al.*<sup>4</sup> Annealing results in better defined, more regular lamellae. Annealing above 230°C can however alter the basic lamellar structure where the crystals tend to thicken to multiples of the original crystals, where 11nm thick crystals usually result.<sup>4</sup> Also, on crystallization from the melt, PA6,6 shows long spacings between 6 and 10nm, depending on the crystallization conditions.<sup>94</sup>

The water crystallized PA6,6 mat initially shows a lamellar thickness of 6nm, which is comparable to the solution crystallized lamellae, yet relatively low in the range of lamellar thicknesses observed for melt crystallized PA6,6. The deviation from the expected 5.4nm for the solution crystallized PA6,6 could arise from a larger variation/distribution in the lamellar thicknesses present in the water crystallized sample or a variation in the angle of tilt of the hydrogen bonded sheets to the lamellar normal. The  $\alpha$ -structure has a tilt of 42°, whereas the  $\beta$ -structure has no tilt, the sheets are perpendicular to the lamellar normal. A mixture of  $\alpha$ - and  $\beta$ -structures, with possible transition regions between the two structures could account for the observed discrepancies.



**Table 5.3:** The main amide bands present in melt/acid crystallized and water crystallized PA6,6. Here vs = very strong, s = strong, m = medium, and w = weak.

Water crystallized	Melt and acid crystallized	Band assignment
3296 vs	3302 vs	NH Stretch <sup>14, 24, 69</sup>
3188 w	3192 w	NH stretch and Amide (I+II) overtone <sup>14, 69</sup>
3061 m	3065 m	NH stretch and Amide II overtone <sup>14, 69</sup>
1635 vs	1636 vs	Amide I (CO stretch) <sup>69</sup>
1541 s	1541 s	Amide II (in-plane NH deformation, with CO and CN stretch) <sup>14, 24, 69</sup>
1363 m	1371 m	Amide III coupled with hydrocarbon skeleton <sup>14, 24</sup> CN stretch and in-plane NH deformation <sup>22</sup>
1284 m	1276 m	Amide III coupled with hydrocarbon skeleton <sup>22, 24</sup>
1200 m	1201 m	Amide III couples with hydrocarbon skeleton “crystalline” band
942 m	934 m	Amide IV (C-CO stretch) <sup>47, 111</sup>
690 m	688 m	Amide V (NH out of plane scissoring) <sup>24</sup>

**Table 5.4:** The main “Brill” bands present in melt/acid crystallized and water crystallized PA6,6. Here m = medium, w = weak, and vw = very weak.

Water crystallized	Melt and Acid crystallized	Band assignment
1389 w	–	CH <sub>2</sub> twisting/wagging <sup>47</sup>
–	1330 vw	CH <sub>2</sub> wagging/twist and Amide III <sup>22, 103</sup>
1303 m	1303 vw	CH <sub>2</sub> twist <sup>46, 47</sup>
–	1225 m	CH <sub>2</sub> twisting/wagging <sup>47</sup>
–	1180 w	CH <sub>2</sub> twisting <sup>47</sup>
–	1066 vw	Skeletal C-C stretch <sup>47</sup>
1140 w	1140 w	Skeletal C-C stretch, <sup>47</sup> gauche conformation <sup>22</sup>
–	906 w	CH <sub>2</sub> rocking <sup>22, 47, 111</sup>

**Table 5.5:** The main methylene stretching and scissoring bands present in melt/acid crystallized and water crystallized PA6,6. Here s = strong, m = medium, w = weak, vw = very weak, and sh = shoulder.

Water crystallized	Melt and Acid crystallized	Band assignment
2945 s	2945 vw	CH <sub>2</sub> $\alpha$ -NH asymmetric stretch <sup>22</sup>
–	2934 s	CH <sub>2</sub> $\beta$ -NH asymmetric stretch <sup>22</sup>
2909 w	2908 sh	CH <sub>2</sub> $\gamma$ -NH and $\beta$ -CO asymmetric stretch <sup>22</sup>
2875 m	2875 m	CH <sub>2</sub> $\alpha$ -NH symmetric stretch <sup>22</sup>
–	2858 s	CH <sub>2</sub> $\beta$ -NH and $\gamma$ -NH symmetric stretch <sup>22</sup>
2825 w	–	CH <sub>2</sub> $\alpha$ -CO symmetric stretch <sup>22</sup>
1480 m	1475 m	CH <sub>2</sub> scissoring next to NH group, trans conformation <sup>22</sup>
1465 m	1465 m	CH <sub>2</sub> scissoring for all methylenes not next to amide group <sup>111</sup>
1416 s	1416 m	CH <sub>2</sub> scissoring next to CO group, trans conformation <sup>22</sup>
–	730 w	CH <sub>2</sub> rocking <sup>24,47,113</sup>

## 5.7 Conformational changes

Figure 5.6 shows the FTIR spectra of PA6,6 crystallized from superheated water, formic acid, and the melt where the spectra have been normalized with respect of the methylene bands between 3000 and 2600cm<sup>-1</sup>. The melt and acid crystallized spectra are very similar, but differ significantly from the water crystallized spectrum. The bands and their assignments are shown in Tables 5.3, 5.4, and 5.5.

The most significant differences between the melt/acid crystallized samples in comparison to the water crystallized sample is in the methylene units. The CH<sub>2</sub> symmetric and asymmetric stretch vibrations, and the CH<sub>2</sub> twisting, rocking, and wagging vibrations all show large differences between the two samples. The CH<sub>2</sub> twisting, wagging, and rocking vibrations at 1180, 1066, 1041, 906, and 731cm<sup>-1</sup> are absent in the water crystallized sample. Together with these methylene vibrations, the Amide III vibration, which is sensitive to changes in the conformation of the main chain, moves from 1276 to 1284cm<sup>-1</sup>. There are also similarities between the samples; the methylene bands at 1465 and 1416cm<sup>-1</sup>. The band at 1465cm<sup>-1</sup> is attributed to the main chain methylene units which apparently are unaltered between

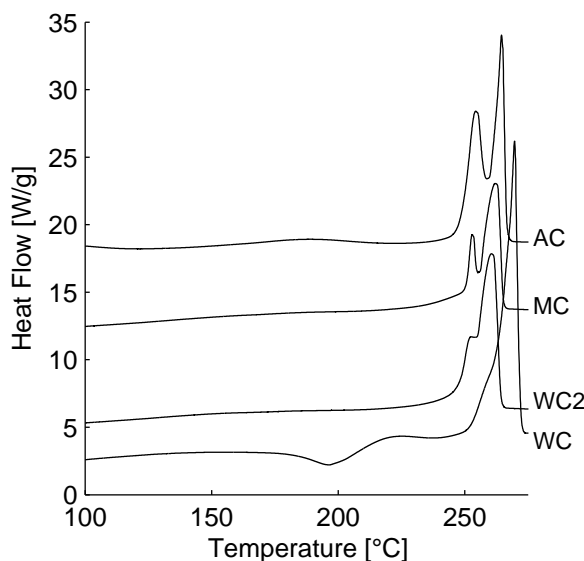


**Figure 5.7:** DSC results obtained for PA6,6 crystallized from water (WC), melt (MC), and acid (AC). Additionally, the second heating run, i.e. after melting, of the water crystallized sample is also shown (WC2).

the samples. This implies that the differences between the samples originates at the amide group, and not the main polymer chain. On heating the water crystallized sample above 200°C, its spectra become very similar to that of the melt/acid crystallized samples.

## 5.8 DSC on dried water crystallized PA6,6 crystals

As mentioned previously in this chapter, on crystallization from superheated water, PA6,6 crystallizes to form a crystal suspension, which is subsequently allowed to dry ambiently. DSC results of these dried crystals are shown in Figure 5.7 together with the results for PA6,6 crystallized from formic acid and from the melt.

The most striking observation is the presence of an exotherm at 197°C for the water crystallized sample. This exotherm is not observed for the acid or melt crystallized samples. When the water crystallized sample is heated a second time to the melt, trace WC2 in Figure 5.7, this exotherm is no longer observed. The presence of the exotherm at 197°C correlates well with the Brill transition temperature of 210°C seen in Figure 5.5(a). These observations are similar to the observations for PA4,6 as shown in Figure 4.17.

## 5.9 Influence of superheated water on the PA6,6 $\alpha$ - and $\beta$ -structures

The presence of two crystal structures, i.e.  $\alpha$ - and  $\beta$ -structured PA6,6, in the water crystallized sample could cause the differences observed in the methylene units between the melt/acid and water crystallized samples and explain the differences between the samples seen in the WAXD and SAXS data. The formation of a  $\beta$ -structure in PA6,6 single crystals is not common; usually only the  $\alpha$ -structure is observed in chain-folded PA6,6 lamellar crystals.<sup>51</sup> The  $\alpha$ -structure consists of progressively sheared hydrogen bonded sheets, although the degree of intersheet shear varies between different polyamides. The alternately sheared hydrogen bonded sheets typical of the  $\beta$ -structure are commonly found in other polyamides such as PA6,8.<sup>50</sup> The formation of the  $\alpha$ - or  $\beta$ -structure depends on the particular polyamide under consideration, and to some extent on the crystallization conditions.<sup>50</sup>

From the work presented in Chapter 4 we know that the behavior seen in the DSC traces for the water crystallized PA6,6 could indicate the presence of water molecules in the crystal lattice which exit from the proximity of the amide groups on heating above the Brill transition. Although only one crystal structure is observed for PA4,6, the intercalation of water molecules in the crystal lattice in the vicinity of the amide groups and the subsequent behavior on heating the samples in the DSC is similar to that observed for PA6,6. It is likely that a similar event occurs for PA6,6; on crystallization from superheated water, water molecules are incorporated in the PA6,6 crystal lattice in close proximity of the amide groups causing the hydrogen bonded planes to slip, leading to the formation of the  $\beta$ -structure. A possible co-existence of the  $\alpha$ - and  $\beta$ -structures is shown schematically in Figure 5.8. This representation is based on the model proposed by Bunn and Garner<sup>13</sup> for the co-existence of the two phases. It is known that the amount of water molecules intercalated into the polyamide structure is very small;<sup>106</sup> this might explain why the  $\beta$ -structure is only weakly observed in the X-ray data.

In Chapter 7 we will show a similar behavior for PA2,14 where the presence of two crystal structures is also observed on crystallization from superheated water.

## 5.10 Conclusions

The dissolution of PA6,6 in superheated water occurs at 190°C and on crystallization from a dilute water solution, single crystals are formed which appear to have mostly the  $\alpha$ -structure. However, a small, but not negligible portion of the polyamide crystallizes in the  $\beta$ -structure as observed by high resolution WAXD.

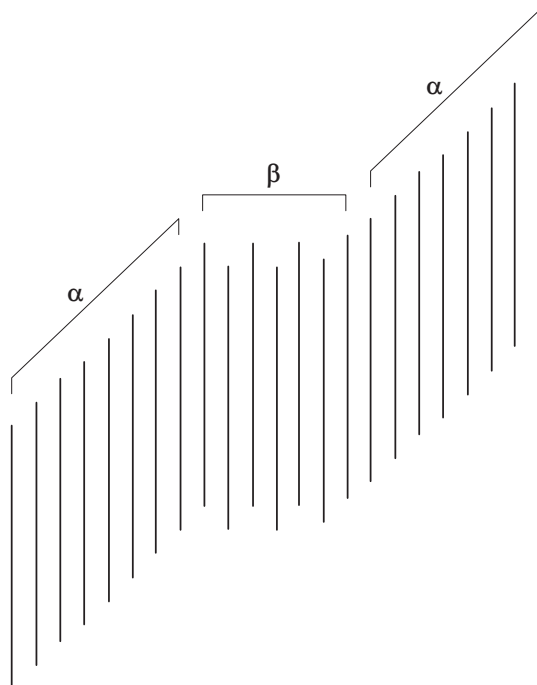


**Figure 5.8:** Representation of a possible co-existence of the  $\alpha$ - and  $\beta$ -structures in water crystallized PA6,6 after the model proposed by Bunn and Garner.<sup>13</sup> The lines represent hydrogen bonded sheets seen edgewise. Likely the water molecules cause the hydrogen bonded sheets to slip, altering the predominantly  $\alpha$ -structure observed in PA6,6 to the  $\beta$ -structure.

The co-existence of two structures causes a slightly higher lamellar thickness of 6nm in comparison to the expected 5.4nm for solution grown PA6,6 crystals.<sup>4</sup> Bunn and Garner<sup>13</sup> already envisaged the co-existence of the  $\alpha$ - and  $\beta$ -structures with an intermediate transition region between the two structures. It seems plausible that on crystallization from superheated water the PA6,6 crystallizes in both the  $\alpha$ - and  $\beta$ -structures where the water molecules most likely promote the formation of the  $\beta$ -structure. The water molecules incorporated in the crystal lattice in the proximity of the amide groups cause the hydrogen bonded sheets to slip, probably facilitating the formation of the  $\beta$ -structure.

On heating the water crystallized PA6,6 which shows both the  $\alpha$ - and  $\beta$ -structures above the Brill transition temperature, the water molecules at the position of the amide groups escape from the lattice. This causes an exotherm at the expected Brill transition temperature in DSC traces. Above the Brill transition temperature the polyamide chains are more mobile, allowing for lamellar doubling to occur to values similar to those reported in literature.<sup>4,94</sup>

## Chapter 6

# Dissolution and crystallization of other even–even polyamides in superheated water

With the help of DSC we demonstrate that superheated water is a solvent for several even-even polyamides. For the polyamides investigated, the diacid chain length does not influence the temperature ( $186 \pm 3^\circ\text{C}$ ) at which dissolution of 30wt% polyamide in water occurs. The dissolution temperature of the polyamide in water is determined by the length of the diamine unit. On heating dried, water crystallized polyamide single crystal mats to the melt an exothermic event below the melting temperature is observed. This holds true for many of the polyamides investigated. From previous work<sup>106</sup> it is known that this exothermic peak arises from water molecules that are encapsulated in the crystal lattice on crystallization from superheated water. The water molecules exit from the lattice when heating the mats above the Brill transition temperature. It can therefore be proposed that the even-even polyamides investigated here also show the intercalation of water molecules in the crystal lattice in the vicinity of the amide groups.

## 6.1 Introduction

Polyamides, commonly known as nylons, are a class of materials with a high chemical resistance to many materials such as hydrocarbons, oils, and cleaning solutions. Hence the reason why polyamides have found such a wide application range. This chemical resistance is in many instances a desirable property; however for solution processing it becomes an undesirable property. There are only a limited number of solvents available for solution processing polyamides; the most common

are organic acids, phenols, diols, fluor-compounds, and other oxidizing agents.<sup>8</sup> All of these solvents are essentially ecologically unfriendly.

As shown in Chapter 4, superheated water is a solvent for polyamide 4,6 (PA4,6). Water has the potential to be an environmentally friendly alternative to acids and phenols in the solution processing of polyamides. For such a possibility to be feasible water has to be a solvent for a wide range of commercially available polyamides with different chain lengths, such as polyamide 6,6 (PA6,6), polyamide 6 (PA6), polyamide 6,10 (PA6,10), and polyamide 6,12 (PA6,12).

In this chapter the commercially available even-even polyamides PA4,6, PA6,6, PA6,10, and PA6,12 are investigated. A comparative study is performed using differential scanning calorimetry (DSC) and infrared spectroscopy (FTIR). To better understand the influence of methylene chain length on the dissolution behavior of polyamides in water, these polyamides are also compared to the synthesized polyamide 12,6 (PA12,6) and polyamide 2,14 (PA2,14).

## 6.2 Experimental description

The polyamides used here are the commercially available PA6,6 Ultramid<sup>®</sup> AS2700 from BASF, PA4,6 Stanyl<sup>®</sup> from DSM, PA6,10 and PA6,12 are purchased from Aldrich. The synthesis and characterization of PA12,6<sup>100,101</sup> and PA2,14<sup>98</sup> are described elsewhere. A film is prepared by dissolving the polymers in formic acid (5g/l) and solvent casting the polymers onto a glass plate after which the solvent is allowed to evaporate.<sup>30</sup> Melt crystallized material is obtained by heating acid crystallized films to the melt and cooling to room temperature at 10°C/min using a Linkam TMS94 hotstage. DSC is performed on the polyamide films as discussed in Appendix A.6.

## 6.3 Dissolution of even-even polyamides in superheated water

Figure 6.1(a) shows the temperature of the end of dissolution endotherm of PA6,6, PA6,10, and PA6,12 in superheated water as a function of the polyamide concentration. All three polyamides show an increase in dissolution temperature with decreasing water concentration. For PA6,6 there is no influence of concentration on the dissolution temperature below ~50wt% polyamide in water, whereas for PA6,10 and PA6,12 this trend is seen for concentrations below ~70wt%. The cause of this difference in the polymer concentration at which the dissolution plateau occurs is a

result of differences in molecular weight. Here PA6,6 has a higher molecular weight than PA6,10 and PA6,12.

Figure 6.1(b) shows the influence of diacid chain length on the melt and dissolution temperatures for PA6,y, where y = 6, 10, 12. Here the dissolution temperature is taken at ~30wt% polyamide concentration, i.e. where polymer concentration no longer has an influence on the dissolution temperature. The melt temperatures show a decrease with increasing diacid methylene chain segment length. This is in line with earlier published results<sup>27,50</sup> and is related to a decreasing hydrogen bond density with increasing diacid chain length. The dissolution temperature however remains approximately constant at  $186 \pm 3^\circ\text{C}$ , albeit for only three data points. This implies that for the polyamides shown in Figure 6.1, the dissolution temperature is independent of the diacid chain length. It might be possible however that for polyamides with long alkane segments, such as polyamide 6,24 and polyamide 6,34,<sup>27</sup> that the dissolution temperature could prove to be lower than  $186^\circ\text{C}$  as the overall hydrogen bond density decreases with increasing diacid chain length. This will be shown to be the case in Chapter 7. However, based on our observation for the shown diacid chain length, we will assume no (or only very minor) influence of this length on the dissolution temperature.

To determine the possible influence of the diamine chain length on the dissolution process, the PAx,6 family, where x = 4,6,12, is investigated. Figure 6.2 shows the influence of varying the diamine segment length in the polyamide main chain. Figure 6.2(a) shows the phase diagram for PA4,6, PA6,6, and PA12,6 in superheated water. From ~60wt% polymer in water, concentration no longer has an influence on the dissolution temperature. Figure 6.2(b) shows the dissolution temperature at 30wt% polyamide in superheated water as a function of the diamine chain length. Here a clear decrease in the dissolution and melt temperatures is seen. This could imply that the number of methylene groups in the diamine part of the polyamide chain is the governing factor in determining the dissolution temperature.

In Chapter 2 it is shown that the Brill transition is related to disorder in the main chain methylene units, and is determined by the motions of the CH<sub>2</sub> groups next to the amide groups. However, there is a larger influence coming from the CH<sub>2</sub> unit next to the NH group than from the CH<sub>2</sub> unit next to the CO group. Therefore it is reasonable to conclude that the dissolution of a polyamide is determined by the length of the diamine unit in the polyamide chain and not by the length of the diacid unit.



**Table 6.1:** The table summarizes DSC results obtained on melting various polyamides. The Brill transition temperature is also given for these polyamides. These values are taken from literature.<sup>50,105</sup> In all events the maximum temperature of the endo or exotherm is given. For certain polyamides two endotherms or an endotherm together with an exotherm are observed on melting; for these polyamides both peak maxima are given. The heat of fusion is for the total endotherm.

Polyamide	Crystallization	Exotherm		Endotherm			$T_B$
		$T$	$\Delta H$	$T_m$	$T_m$	$\Delta H$	
PA2,14	water (1H)	164°C	22J/g	–	241°C	82J/g	165°C
	water (2H)	–	–	–	238°C	82J/g	
	formic acid	–	–	–	240°C	45J/g	
	melt	–	–	–	236°C	80J/g	
PA4,6	water (1H)	220°C	22J/g	–	290°C	106J/g	245°C
	water (2H)	–	–	–	287°C	84J/g	
	formic acid	–	–	–	289°C	106J/g	
	melt	–	–	–	286°C	84J/g	
PA6,6	water (1H)	197°C	25J/g	258°C	267°C	97J/g	230°C
	water (2H)	–	–	253°C	261°C	76J/g	
	formic acid	–	–	255°C	265°C	106J/g	
	melt	–	–	253°C	263°C	76J/g	
PA6,10	water (1H)	208°C	19J/g	–	227°C	90J/g	220°C
	water (2H)	–	–	–	220°C	57J/g	
	formic acid	–	–	–	225°C	97J/g	
	melt	–	–	–	223°C	57J/g	
PA6,12	water (1H)	–	–	203°C	215°C	93J/g	215°C
	water (2H)	–	–	200°C	215°C	53J/g	
	formic acid	–	–	203°C	215°C	103J/g	
	melt	–	–	198°C	214°C	59J/g	
PA12,6	water (1H)	–	–	–	195°C	30J/g <sup>b</sup>	183°C
	water (2H)	–	–	–	207°C	26J/g	
	formic acid	–	–	223°C	226°C	39J/g	
	melt	–	–	209°C <sup>a</sup>	222°C	33J/g	

<sup>a</sup> exotherm

<sup>b</sup> very broad endotherm

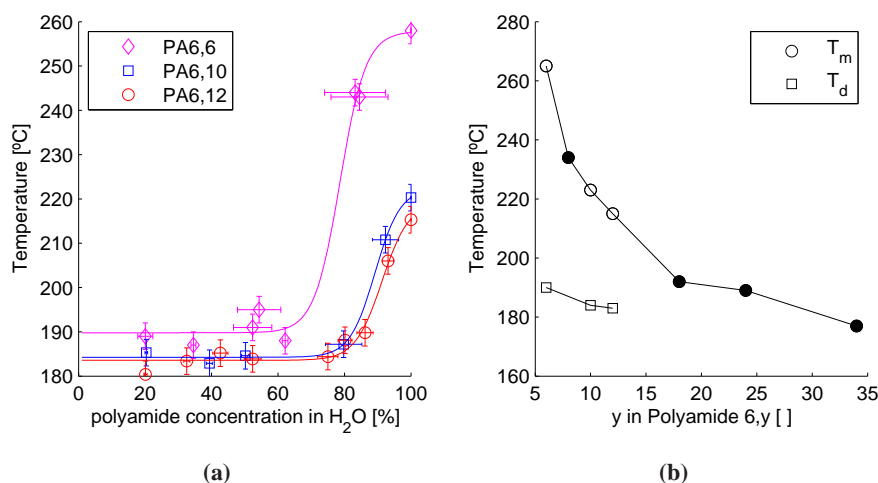


**Figure 6.1:** (a) Phase behavior of polyamide 6,6 (PA6,6), polyamide 6,10 (PA6,10), and polyamide 6,12 (PA6,12) in superheated water. Here the end of the melt/dissolution endotherm is shown. This is the temperature at which the polyamide has completely melted/dissolved. All lines serve as a guide to the eye. (b) Comparison between the melt ( $T_m$ ) and dissolution ( $T_d$ ) temperatures at 30wt% in water for the polyamide 6,y (PA6,y) family. Here  $\circ$  is taken from this work,  $\bullet$  is taken from literature.<sup>27,50</sup>

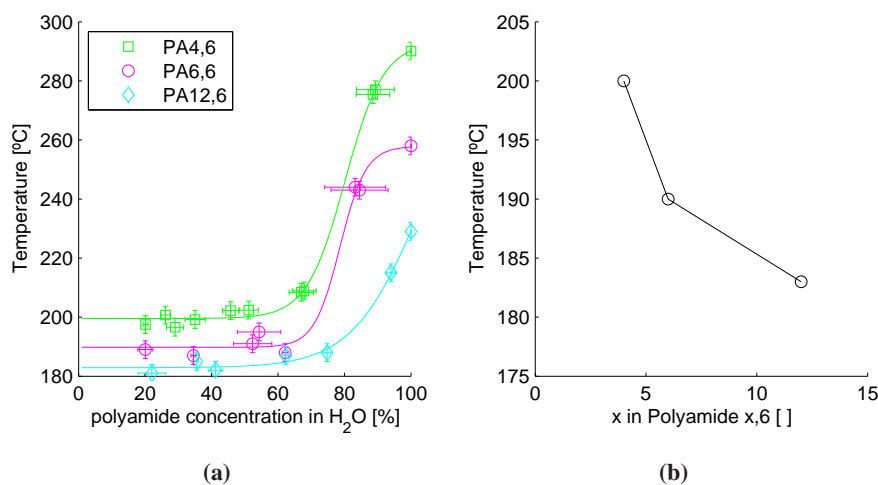


**Figure 6.2:** (a) Phase behavior of polyamide 4,6 (PA4,6), polyamide 6,6 (PA6,6), and polyamide 12,6 (PA12,6) in superheated water. Here the end of the melt/dissolution endotherm is shown which is the temperature at which the polyamide has completely melted/dissolved. (b) Dissolution temperature at 30wt% polyamide in superheated water for the polyamide x,6 (PAx,6) family. All lines serve as a guide to the eye.

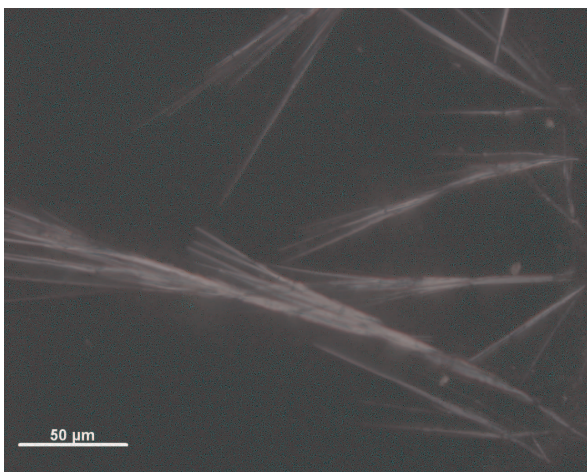


**Figure 6.3:** Optical micrograph of PA6,12 crystals grown from water.

## 6.4 Crystallization of even-even polyamides from superheated water

In the previous section it is shown that superheated water is a good solvent for various even-even polyamides. On cooling the water solution, the polyamide crystallizes from the solution, forming a suspension of single crystals in water. The excess water is allowed to evaporate under ambient conditions. Optical microscopy and DSC is performed on the thus obtained crystal mats.

Figure 6.3 shows an optical micrograph of water grown PA6,12 crystals. The micrograph shows many large needle-like crystals up to  $100\mu\text{m}$  in length. Similar needle-like crystals are obtained for PA12,6, PA2,14 and PA6,10 on crystallization from superheated water.

Table 6.1 gives a summary of the DSC results obtained when heating different polyamides crystallized from superheated water, formic acid, and the melt to the melt. From the results the presence of an exotherm for the water crystallized polyamides is immediately apparent for PA2,14, PA4,6, PA6,6, and PA6,10. Although the position of this exotherm varies for the different polyamides, the heat of fusion involved is similar, all are in the order of  $20\text{J/g}$ . The position of the exotherm closely matches the (expected) Brill transition temperature for the various polyamides. For PA6,12 and PA12,6 no such exotherm is observed. Likely this is because the Brill transition is too close (or even coincides) with the melt temperature.

## **6.5 Conclusions**

Superheated water is a solvent for the investigated even-even polyamides. The dissolution temperature is determined by the length of the diamine unit and not by the length of the diacid unit of the polyamide chain. This is related to the methylene group next to the NH unit having a larger influence on the dissolution temperature than the methylene group next to the CO unit.

Furthermore, many of the dried water crystallized even-even polyamides investigated show an exothermic event in the vicinity of the Brill transition prior to melting. The work presented in Chapter 4 shows that this exothermic event is due to water molecules which are trapped in the polyamide crystal lattice exiting from positions close to the amide group when heating the water crystallized polyamide above the (expected) Brill transition temperature. Indeed, for the water crystallized polyamides that do not show such an exotherm prior to melting, the Brill transition coincides, or closely matches, with the melt temperature.

## Chapter 7

# The influence of superheated water on hydrogen bonding in piperazine based (co)polyamides

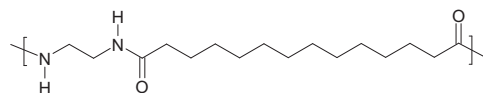
Here we demonstrate that superheated water is a solvent for polyamide 2,14 and piperazine based copolyamides up to a piperazine content of 62mol%. The incorporation of piperazine allows for a variation of the hydrogen bond density without altering the crystal structure, i.e. the piperazine units co-crystallize with the PA2,14 units.<sup>39</sup> It is shown that the crystallization of PA2,14 from superheated water greatly influences the crystal structure. Water molecules incorporated in the PA2,14 crystal lattice cause a slip on the hydrogen bonded planes; resulting in a co-existence of a triclinic and a monoclinic crystal structure. On heating above the Brill transition, the water molecules exit from the lattice, restoring the triclinic crystal structure. Incorporation of piperazine into the PA2,14 chain results in a decrease in the hydrogen bond density. With increasing piperazine content, the dissolution temperature decreases. It is only possible to grow single crystals from superheated water up to a piperazine content of 62mol%. For these single crystals, the incorporation of water molecules in the vicinity of the amide group is seen by the presence of  $\text{COO}^-$  stretch vibrations using FTIR spectroscopy. These vibrations disappear on heating above the Brill transition temperature and the water molecules exit from the amide groups. For copolyamides with more than 62mol% piperazine no Brill transition is observed,<sup>105</sup> no single crystals can be grown from water, and no water molecules are observed in the vicinity of the amide groups. The high piperazine content (co)polyamides have less hydrogen bond donors, and are therefore less likely to have any interactions with the water molecules. This work demonstrates the relation between the

Brill transition, the dissolution of polyamide in superheated water, and its influence on the hydrogen bonds and the amide groups.

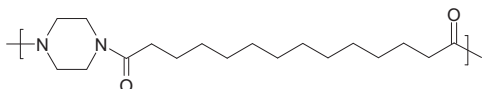
## 7.1 Introduction

The thermal properties in polyamides are largely due to the hydrogen bonds present between recurring amide groups. By varying the density of these hydrogen bonds it is possible to greatly influence the polyamide's physical properties;<sup>27</sup> less hydrogen bonds generally imply a lower melting temperature. A readily available route to change the hydrogen bond density is to change the length of the aliphatic portions in the linear polyamide chains, which results in a change in the spatial separation between the amide groups, and hence an overall change in the hydrogen bond density.<sup>12</sup> An alternative is to replace the amide group with a different chemical unit that reduces the possibility of hydrogen bond formation, but has similar structural features as the amide group. Piperazine is an example of such a chemical unit. When varying piperazine concentrations are incorporated in a polyamide 2,14 (PA2,14) backbone, a set of copolymers as shown schematically in Figure 7.1 are obtained. Piperazine residues incorporated in the polyamide chain do not contain any amide hydrogens and are therefore only hydrogen bond acceptors and not hydrogen bond donors.<sup>39,98,105</sup> The PA2,14 units can act as hydrogen bond donors and acceptors. By introducing piperazine into the chain, the overall hydrogen bond density decreases.

Copolyamides of polyamide 2,14 (PA2,14) and polyamide piperazine,14 (PApip,14)<sup>39,98</sup> are synthesized from 1,12-dodecanedicarboxylic acid and variable amounts of 1,2-ethylenediamine and piperazine. A range of copolyamides (PA2,14-co-pip,14) with a piperazine content ranging from 30 to 90mol% are prepared together with the homopolymers PA2,14 and PApip,14. The copolymers exhibit a decrease in melting and crystallization temperature with increasing piperazine content.<sup>98</sup> Although the introduction of a rigid cyclic monomer usually leads to an increase in melting temperature with respect to the homopolymer due to an increased rigidity of the polymer chain, and, consequently, in a decrease of the gain in entropy upon melting,<sup>98</sup> the reduced possibility of the piperazine units to form hydrogen bonds overrules this effect. Additionally up to a piperazine content of 62mol%, the PA2,14 and PApip,14 units co-crystallize into a common crystal lattice, which differs only slightly from the PA2,14 crystal lattice.<sup>39</sup> For a piperazine content of 90mol% and higher, the crystal structure is distorted from that of PApip,14. For an intermediate piperazine content of 70mol% and 82mol%, a co-existence of the PA2,14 and PApip,14 crystal structures is observed.<sup>39</sup> It is further concluded that the piperazine rings incorporated into the copolyamides are planar to the hydrogen bonded sheets, the sheets being shear to one another.



(a) PA2,14



(b) PApip,14

**Figure 7.1:** Chemical structure of (a) 1,2-ethylenediamine-based and (b) piperazine-based repeat units.

The effect of temperature on the (co)polyamides is investigated in Chapter 2. Upon heating many polyamides show a Brill transition,<sup>11,50</sup> which entails a solid state crystalline transition from the low temperature triclinic phase to the high temperature pseudo-hexagonal phase, i.e. in WAXD, the 100 reflection related to the interchain distance and the 010 reflection related to the intersheet distance merge into a single reflection. The series of (co)polyamides are investigated, and it is found that the Brill transition is independent of the piperazine content,<sup>105</sup> despite changes in the melt and dissolution temperatures. It is shown that the Brill transition temperature is not related to the hydrogen bond density, but directly related to and primarily caused by conformational changes occurring in the polyamide main chain, in particular in the alkane segments.

In Chapter 4 it is shown using WAXD that polyamide 4,6 (PA4,6) can be dissolved in superheated water at  $\sim 200^\circ\text{C}$ . This is well below the melting point of  $\sim 295^\circ\text{C}$  for PA4,6.<sup>8</sup> Considering this information, it is interesting to learn how the dissolution of a hydrogen bonded polymer in water is affected by the hydrogen bond density. Additionally, the influence of the hydrogen bond density on the (co)polyamides' interaction with superheated water is significant. The series of novel piperazine based (co)polyamides present a unique opportunity to study the effect of reduced hydrogen bond formation on the dissolution process of polyamides in superheated water.

The present chapter aims to give more insight into the effect of incorporating a secondary diamide that reduces hydrogen bond formation on the dissolution process in superheated water and the subsequent crystal structure. Initially, high pressure differential scanning calorimetry (DSC) is performed for a range of (co)polyamide

concentrations in water in order to investigate the dissolution process. The dissolution process can also be followed by wide angle X-ray diffraction. Single crystals grown from an aqueous solution are investigated by transmission electron microscopy (TEM). To determine the influence of water molecules on hydrogen bonding and other conformation changes, Fourier transform infrared (FTIR) spectroscopy studies are performed.

## **7.2 Experimental description**

The homopolymers PA<sub>2,14</sub> and PApip<sub>14</sub> as well as copolymers PA<sub>2,14-co-pip,14</sub> are synthesized via a polycondensation reaction of 1,12-dodecanedicarbonyl dichloride and varying amounts of 1,2-ethylenediamine and piperazine as described elsewhere.<sup>98</sup> The piperazine based copolyamides used in this study have a piperazine molar fraction of 0.30, 0.46, 0.54, 0.62, 0.82, and 0.90. These copolymers are referred to as coPA 0.30 through to coPA 0.90, respectively.

DSC is performed on the as-synthesized (co)polyamide and water as described in Appendix A.6. Simultaneous SAXS/WAXD is performed on the as-synthesized (co)polyamides as discussed in Appendix A.2.2 using the in-house designed pressure cell shown in Appendix A.1. The WAXD data is corrected as described in Appendix A.2.3. TEM and FTIR spectroscopy is performed on the water crystallized (co)polyamides as discussed in Appendix A.3 and A.4.

## **7.3 Dissolution behavior of piperazine based (co)polyamides**

DSC is used to follow the phase behavior of PA<sub>2,14</sub> and its piperazine based copolymers in water, where the latter acts as a solvent when in the superheated state.<sup>82,106,108</sup> Figure 7.2 shows the results obtained from DSC measurements on the (co)polyamides in the presence of superheated water. Here the end temperature of the endotherms as a function of polymer content in water are plotted. The temperature represents the temperature at which the polymer is completely dissolved in superheated water as confirmed by WAXD.

Figure 7.2(a) shows the phase behavior of several piperazine based copolymers and the homopolymers PA<sub>2,14</sub> and PApip<sub>14</sub> in water as a function of polymer concentration in water. All lines serve as a guide to the eye. The general observation is that the dissolution temperature increases with increasing polymer content. In a heating run, with increasing temperature, conformational changes in the main



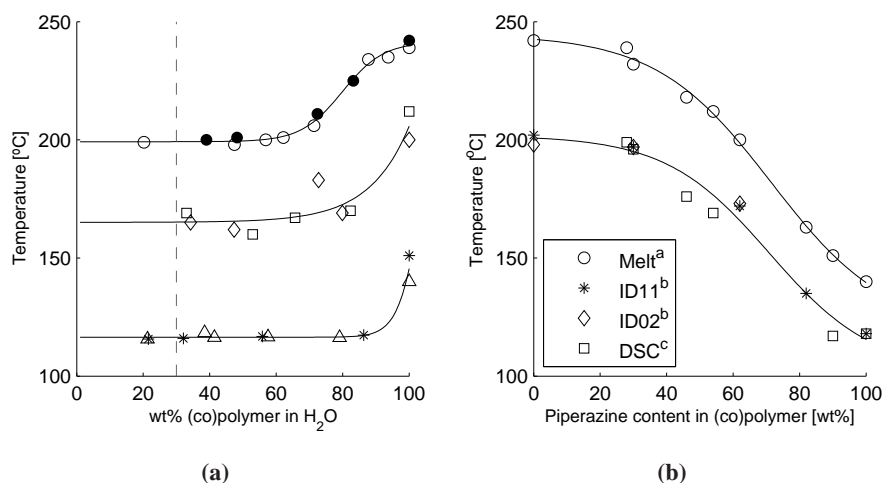


**Figure 7.2:** Influence of polymer concentration on the dissolution temperature of the piperazine based (co)polyamides in water. (a) shows the phase diagram that evolved from the measured temperatures of the end of the DSC dissolution endotherms for various concentrations of (co)polyamide in water. Here ● = PA2,14; ○ = coPA 0.30; □ = coPA 0.54; ◇ = coPA 0.62; \* = coPA 0.90; and △ = PApip,14. (b) shows the melt and dissolution temperatures as a function of piperazine content. Here a - melt data taken from Vanhaecht *et al.*;<sup>98</sup> b - dissolution temperature X-ray diffraction data for 30wt% polyamide in water; and c - plateau dissolution temperature DSC data. All lines serve as a guide to the eye. Heating rate applied during the X-ray diffraction and DSC experiments is 10°C/min.

chain occur. With the incoming of gauche conformers in the main chain, the chain starts to apply an increasing strain on the hydrogen bonds. The gauche conformers are localized in the alkane chain segments along the main chain and finally reach the amide group.<sup>105</sup> Due to the high mobility of these gauche conformers, the superheated water molecules, which are highly mobile due to the superheated state,<sup>25,56</sup> have the opportunity to enter the crystal lattice and break the hydrogen bonds between the amide groups.

In Figure 7.2(a) a guideline is shown at 30wt% concentration; a point within the region where concentration no longer influences the dissolution temperature. Three different temperatures can be distinguished; PA2,14 and coPA 0.30 have a dissolution temperature of ~200°C, coPA 0.54 and coPA 0.62 have a dissolution temperature of ~165°C, and coPA 0.90 and PApip,14 have a dissolution temperature of ~118°C. This is in accordance with the three distinct crystal types reported for the copolymers;<sup>39</sup> i.e. a PA2,14 type crystal lattice, a PApip,14 type crystal lattice, and an intermediate structure which shows features of both the PA2,14 and PApip,14 structures respectively. The (co)polyamide's dissolution temperature is therefore related to the amount of piperazine present in the polymer and thus maybe directly

related to the hydrogen bond density.

The influence of piperazine content on the dissolution process is shown more clearly in Figure 7.2(b). The figure denotes the dissolution temperature at 30wt% (co)polyamide in water as a function of piperazine content. The melt temperatures<sup>98</sup> of the (co)polymers are also plotted for comparison. All lines serve as a guide to the eye. The data are obtained from DSC experiments and *in situ* WAXD and SAXS/WAXD experiments of the dissolution process performed on the beamlines ID11 and ID02. The melt temperature decreases with increasing piperazine content. This is because the hydrogen bond density decreases with an increase in piperazine content. The incorporation of the secondary piperazine diamine results in a decreased possibility of hydrogen bond formation because the piperazine residues are only hydrogen bond acceptors, and therefore a decrease in enthalpy occurs due to weaker interchain interactions. The incorporation of piperazine residues however also results in an increase in entropy due to an increase in chain rigidity. The reduced possibility of hydrogen bond formation of the piperazine residues dominates the chain rigidity aspect. The reduced melt temperature with increasing piperazine content is the cumulative effect of both opposing phenomena.<sup>39,98,105</sup> The difference in melt temperatures is also mimicked by the dissolution temperature. Due to the weakening hydrogen bond strength in the (co)polyamides with increasing piperazine content, less gauche conformers are needed along the polymer main chain to allow for the superheated water to disrupt the crystal lattice. The (co)polyamides rich in piperazine are therefore expected to exhibit a lower dissolution temperature than the (co)polyamides rich in 1,2-ethylenediamine.

The data presented in Figure 7.2 conclusively demonstrates that water in the superheated state is a solvent for the piperazine based (co)polyamides. The data presented here further strengthens the notion that the dissolution of aliphatic polyamides in superheated water is a universal phenomenon applicable to many polyamides, whether synthetic or biological in nature.

## 7.4 Influence of superheated water on crystallography of PA2,14

Figures 7.3(a) and 7.3(b) show the WAXD pattern of PA2,14 crystallized from the melt (MC) and from water (WC). The melt crystallized sample shows a single sharp reflection at  $1.49^\circ$ , 001 reflection, and two broader reflections at  $6.83^\circ$ , 100 reflection, and  $7.17^\circ$ , 010 reflection. The WAXD pattern for the melt crystallized PA2,14 compares well with other results.<sup>39,68,105</sup> However, the WAXD pattern obtained for PA2,14 crystallized from water is remarkably different from the melt crystallized diffraction pattern. The water crystallized sample shows several additional sharp

and broad reflections, see Figures 7.3(a) and 7.3(b), perhaps indicating a different crystalline structure in comparison to the melt crystallized sample. Thus the unit cell of PA2,14 needs to be considered.

The triclinic unit cell<sup>55,68</sup> for PA2,14 is  $a = 0.49 \pm 0.01\text{nm}$ ,  $b = 0.51 \pm 0.01\text{nm}$ ,  $c = 2.23 \pm 0.01\text{nm}$ ,  $\alpha = 60 \pm 2^\circ$ ,  $\beta = 77 \pm 1^\circ$ ,  $\gamma = 59 \pm 1^\circ$ . The predicted/calculated WAXD pattern for the above mentioned unit cell is determined using PowderCell 2.4<sup>62</sup> and is also shown in Figure 7.3(b); for more information see Appendix B. The positions of the calculated triclinic diffraction pattern compares well with the experimental diffraction pattern of the melt crystallized sample. However, as mentioned previously, the water crystallized sample shows a different diffraction pattern from the melt crystallized sample. Several of the reflections in the water crystallized diffraction pattern are either not present or shifted in the calculated triclinic diffraction pattern. Studying the 001 reflection for the water crystallized PA2,14 originating from the  $c$ -axis of the unit cell more closely, see Figure 7.3(a), it is apparent that next to the predicted/expected peak at 1.91nm there is also an additional peak at 2.12nm. Both of these peaks must be correlated to the  $c$ -axis, which is 2.23nm. This indicates the possible presence of a different PA2,14 crystal structure.

A second, monoclinic unit cell with parameters  $a = 0.46 \pm 0.01\text{nm}$ ,  $b = 0.41 \pm 0.01\text{nm}$ ,  $c = 2.31 \pm 0.01\text{nm}$ ,  $\beta = 113 \pm 1^\circ$  is also shown in Figures 7.3(a) and 7.3(b). The reflections which are poorly matched with the triclinic unit cell are fitted reasonably well by the monoclinic unit cell.

It is apparent from the calculated diffraction patterns for both the triclinic and the monoclinic unit cells that the reflections arising from the (010) planes and all planes making a small angle with the (010) plane, that the calculated intensities are much larger than the observed intensities, while the opposite is true for planes perpendicular to the (010) plane, i.e. the (100) planes. We were unable to reduce these discrepancies in the atomic parameters. Two possible explanations exist for this discrepancy, and indeed both could play a role in producing the observed effect.<sup>13</sup> One is that the thermal vibrations of the molecules are restricted due to the hydrogen bonds present in the sheets resulting in lower vibrations in the (010) plane. Therefore the intensity of the reflections from the (010) planes will be reduced in comparison to those from other planes. A second explanation is a possible distortion of the crystals in the direction normal to the  $b$ -axis due to the stacked hydrogen bonded sheet which make up the crystals with van der Waals forces between the sheets. The sheets are flexible in directions perpendicular to the sheets, but less flexible (and therefore less distorted) within the sheets owing to the hydrogen bonding. The effect on the intensity would be similar to that of thermal vibrations. It is likely that both processes play a role in influencing the relative intensities.

Nonetheless, the WAXD pattern for the water crystallized PA2,14 suggests

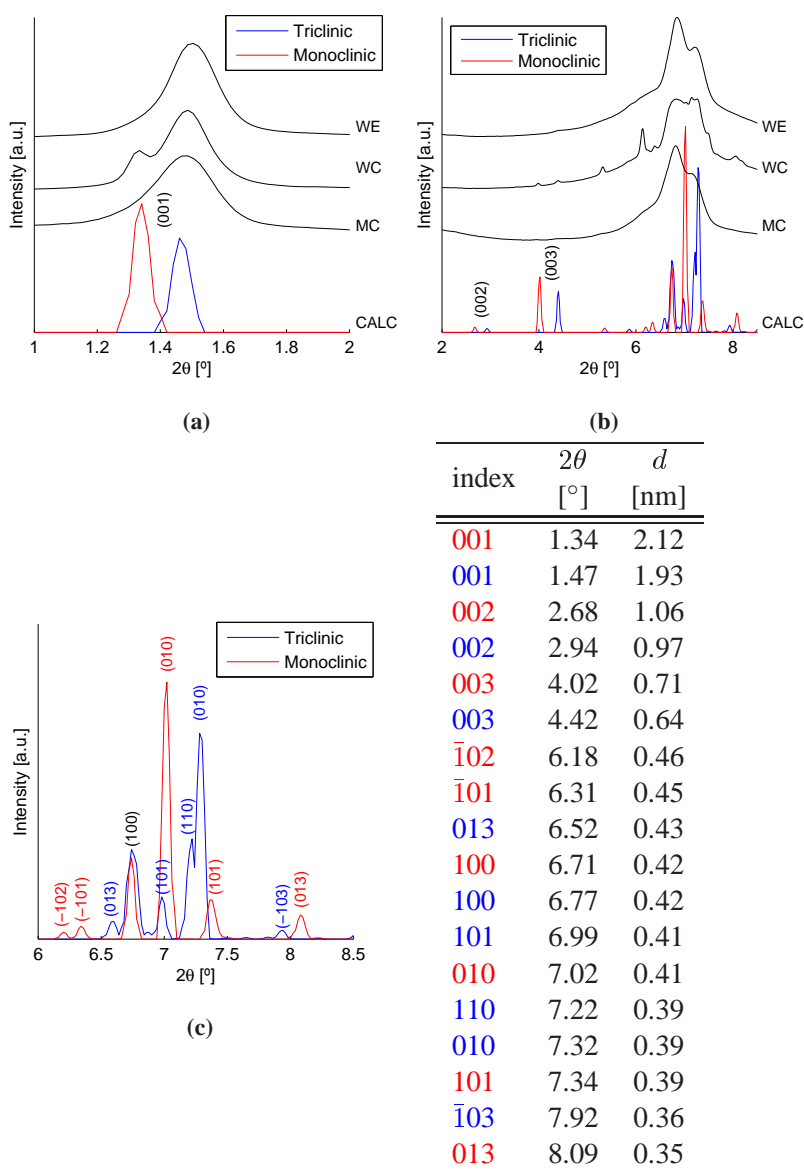


**Figure 7.3:** WAXD data of PA2,14. The graphs show the diffraction patterns of the melt crystallized sample (MC), water crystallized sample (WC), and after heating the water crystallized sample to 210°C (WE). All results shown are at 50°C. The calculated WAXD pattern is based on a theoretical calculation of the computed unit cell. The triclinic unit cell<sup>55,68</sup> is  $a = 0.49 \pm 0.01\text{nm}$ ,  $b = 0.51 \pm 0.01\text{nm}$ ,  $c = 2.23 \pm 0.01\text{nm}$ ,  $\alpha = 60 \pm 2^\circ$ ,  $\beta = 77 \pm 1^\circ$ ,  $\gamma = 59 \pm 1^\circ$ . The monoclinic unit cell is  $a = 0.46 \pm 0.01\text{nm}$ ,  $b = 0.41 \pm 0.01\text{nm}$ ,  $c = 2.31 \pm 0.01\text{nm}$ ,  $\beta = 113 \pm 1^\circ$ . (c) shows the triclinic and monoclinic peak indexing in more detail. Here the blue indices are triclinic, the red indices are monoclinic, and the black indices are both for the triclinic and monoclinic structures. The data is plotted as a function of  $2\theta$  for clarity and is related to  $d$ -spacing according to Bragg's law  $\lambda = 2d \sin \theta$ , plotted for wavelength  $\lambda = 0.04959\text{nm}$ .

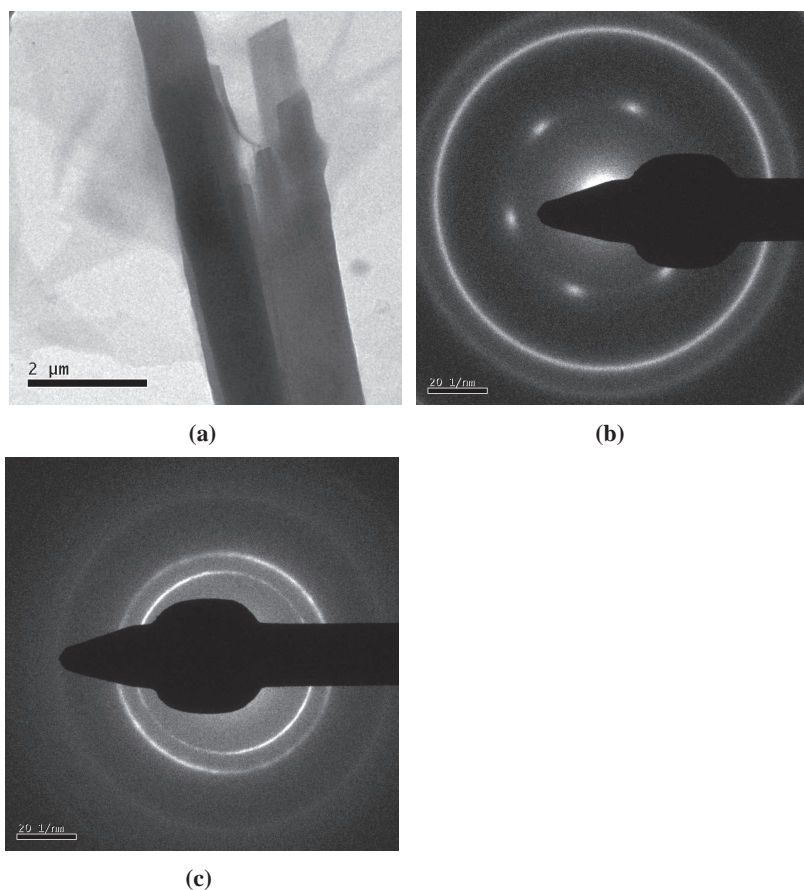


**Figure 7.4:** TEM and electron diffraction images of PA2,14 crystallized from superheated water. (a) shows lath-like and needle-like structures. (b) is an electron diffraction image of the lath-like structures. (c) is an electron diffraction image of the needle-like structures. The outer rings shown in (b) and (c) originate from the gold used as a calibration reference.

the presence of both triclinic and monoclinic crystals. In Figure 7.4 the possible co-existence of two crystals is investigated using TEM and electron diffraction images for PA2,14 single crystals grown from water. Figure 7.4(a) shows the single crystals obtained from PA2,14 where two distinct types of crystals are observed; lath-like and needle-like crystals. The needle-like crystals are large structures ( $\sim 1\text{mm}$ ) easily visible under the optical microscope. The lath-like crystals are much smaller in dimension. Figures 7.4(b) and 7.4(c) show the electron diffraction patterns obtained from the water grown PA2,14 single crystals. Two, distinctly different diffraction patterns are observed; a pattern consisting of two (large) arcs oriented approximately orthogonal to each other (Figure 7.4(c)) spaced at 0.44nm and 0.37nm, and a pattern

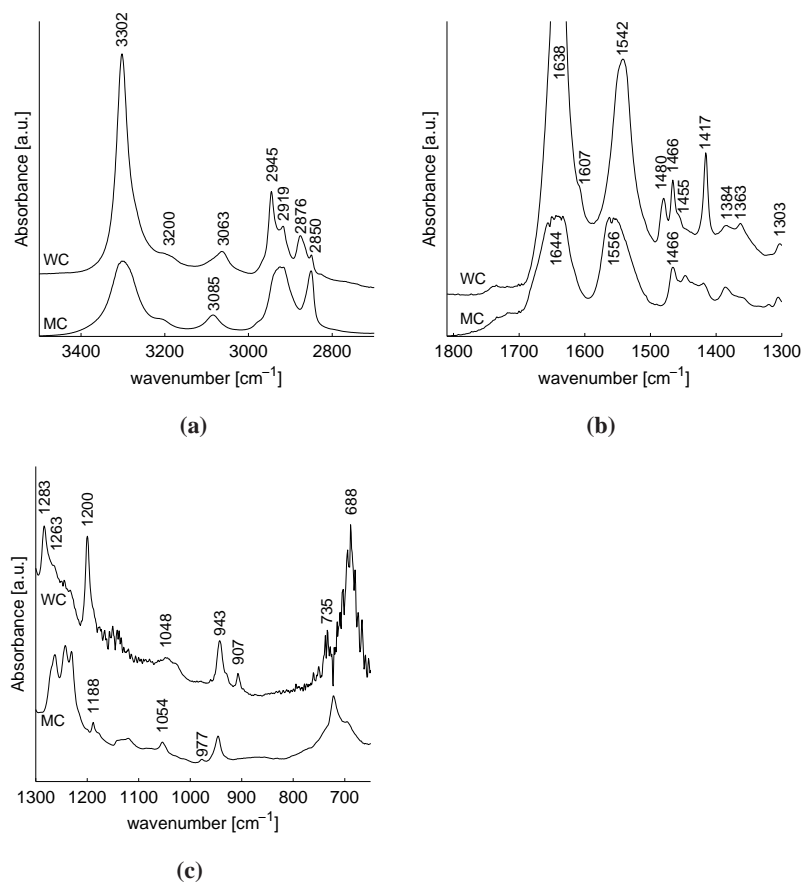
displaying a six point symmetry (Figure 7.4(b)) with spacings of 0.42nm, 0.44nm, and 0.42nm. The difference between these two patterns is striking, again suggesting the presence of two crystal structures.

Figure 7.3(b) also shows the WAXD pattern obtained after heating the water crystallized PA2,14 to 210°C and subsequently cooling to 50°C (WE). Note that the PA2,14 is not melted. The diffraction pattern now resembles the diffraction pattern of the melt crystallized sample. The additional reflections noted in the water crystallized sample all disappear simultaneously at ~200°C and do not reappear on cooling.

## **7.5 Conformational changes in water crystallized PA2,14**

Figure 7.5 shows the FTIR spectra at 30°C obtained when crystallizing PA2,14 from superheated water and the melt. The melt crystallized spectra are taken from the results presented in Chapter 2. The data is normalized to the area under the methylene bands between 2800 and 3000cm<sup>-1</sup>.

Figure 7.5(a) shows the spectral range between 3500 and 2700cm<sup>-1</sup> and is summarized in Tables 7.1 and 7.2. Figure 7.5(a) shows several remarkable differences between the melt and water crystallized samples. Firstly, although the position of the NH stretch vibration at 3302cm<sup>-1</sup> is identical between the two samples, the shape and area of the two are different. The NH stretch vibration of the melt crystallized sample is much broader than the water crystallized sample which shows a much sharper, narrower peak. This shows that the hydrogen bonds between the two samples are significantly different. Additionally, the Amide I and II overtone bands show a large shift in position: 3063cm<sup>-1</sup> in the water crystallized sample and 3085cm<sup>-1</sup> in the melt crystallized sample. The fingerprint region of the melt and water crystallized spectra between 1800 and 650cm<sup>-1</sup> are shown in Figures 7.5(b) and 7.5(c) together with their assignment in Tables 7.1, 7.2, and 7.3. The most significant differences between the two samples are the amide bands, certain methylene scissoring bands, and the so-called “Brill” bands. The figures show the Amide I and II bands moving to lower wavenumbers on crystallization from superheated water. This is an indication for more hydrogen bond formation.<sup>84</sup> When more hydrogen bonds are formed by the CO groups in the polyamide, the Amide I vibration shifts to lower wavenumbers. This is consistent with the sharp NH stretch vibration at 3302cm<sup>-1</sup> observed for the water crystallized sample. The presence of more hydrogen bonds in the water crystallized sample suggests that superheated water is a good solvent for the PA2,14 and facilitates crystallization into a perfect crystal packing. Next to the Amide I and II vibrations, the Amide III vibrations also show significant changes between the two samples. Amide III vibrations are sensitive to changes in the main chain methylene units.



**Figure 7.5:** FTIR spectra of water crystallized (WC) and melt crystallized (MC) PA2,14 at 30°C. (a) shows the spectra from 3450 to 2700 $\text{cm}^{-1}$ , (b) from 1800 to 1300 $\text{cm}^{-1}$ , and (c) from 1300 to 650 $\text{cm}^{-1}$ .

In Figure 7.5(a) the symmetric and asymmetric methylene stretch vibrations show the most remarkable difference. The melt crystallized sample shows the symmetric and asymmetric vibrations at 2850 and 2919 $\text{cm}^{-1}$  respectively. The water crystallized sample shows two additional vibrations at 2876 and 2945 $\text{cm}^{-1}$ . These two bands are also coupled to symmetric (2876 $\text{cm}^{-1}$ ) and asymmetric (2945 $\text{cm}^{-1}$ )  $\text{CH}_2$  vibrations. Methylene stretch vibrations, like in small cyclic alkanes, are known to shift to higher wavenumbers when strained.<sup>69</sup> Almost all of the “Brill” bands summarized in Table 7.3 also show a variation between the two samples. The most important are the appearance of two bands at 1607 and 1455 $\text{cm}^{-1}$  in the water crystallized sample. These are asymmetric and symmetric  $\text{COO}^-$  vibrations<sup>69</sup> which may occur if the water molecules, incorporated in the crystal lattice, associate to the

**Table 7.1:** The main amide bands present in melt crystallized and water crystallized PA2,14. Here vs = very strong, s = strong, m = medium, w = weak, and sh = shoulder.

Water crystallized	Melt crystallized	Band assignment
3302 vs	3302 s	NH Stretch <sup>14, 24, 69</sup>
3200 w	3200 w	NH stretch and Amide (I+II) overtone <sup>14, 69</sup>
3063 m	3085 m	NH stretch and Amide II overtone <sup>14, 69</sup>
1638 vs	1644 s	Amide I (CO stretch) <sup>69</sup>
1542 s	1556 s	Amide II (in-plane NH deformation, with CO and CN stretch) <sup>14, 24, 69</sup>
1283 m		Amide III <sup>24</sup>
1263 sh	1263 m	Amide III coupled with hydrocarbon skeleton <sup>14, 24</sup>
1200 m	1188 w	Amide III coupled with hydrocarbon skeleton <sup>14, 24</sup> crystalline band <sup>22</sup>
943 m	943 m	Amide IV (C-CO stretch) <sup>47, 111</sup>
688 m	690 w	Amide V (NH out of plane scissoring) <sup>24</sup>

**Table 7.2:** The main methylene stretching and scissoring bands present in melt crystallized and water crystallized PA2,14. Here vs = very strong, s = strong, m = medium, w = weak, and sh = shoulder.

Water crystallized	Melt crystallized	Band assignment
2945 s	–	CH <sub>2</sub> asymmetric stretch <sup>22</sup>
2919 s	2919 s	CH <sub>2</sub> asymmetric stretch <sup>22</sup>
2876 s	–	CH <sub>2</sub> symmetric stretch <sup>22</sup>
2850 m	2850 s	CH <sub>2</sub> symmetric stretch <sup>22</sup>
1480 s	–	CH <sub>2</sub> scissoring next to NH group, trans conformation <sup>22</sup>
1466 s	1466 m	CH <sub>2</sub> scissoring for all methylenes not next to amide group <sup>111</sup>
	1447 m	
1416 vs	1419 m	CH <sub>2</sub> scissoring next to CO group, trans conformation <sup>22</sup>



**Table 7.3:** The main “Brill” bands present in melt crystallized and water crystallized PA2,14. Here vs = very strong, s = strong, m = medium, w = weak, and sh = shoulder.

Water crystallized	Melt crystallized	Band assignment
1607 sh	–	COO <sup>-</sup> asymmetric <sup>69</sup>
1455 sh	–	COO <sup>-</sup> symmetric <sup>69</sup>
1384 m	1386	CH <sub>2</sub> wagging and twist <sup>103</sup> fold band <sup>22</sup>
–	1320 w	CH <sub>2</sub> wagging or twist <sup>22,103</sup>
1303 m	1305	CH <sub>2</sub> twist <sup>46,47</sup>
–	1243 m	Skeletal C-C stretch <sup>47</sup>
–	1230 m	Skeletal C-C stretch <sup>47</sup>
1048 w	1054 w	Skeletal C-C stretch <sup>47,67,103</sup>
907 m	977 w	CH <sub>2</sub> rocking <sup>22,47,111</sup>
735 w	721 m	CH <sub>2</sub> rocking <sup>24,113</sup>

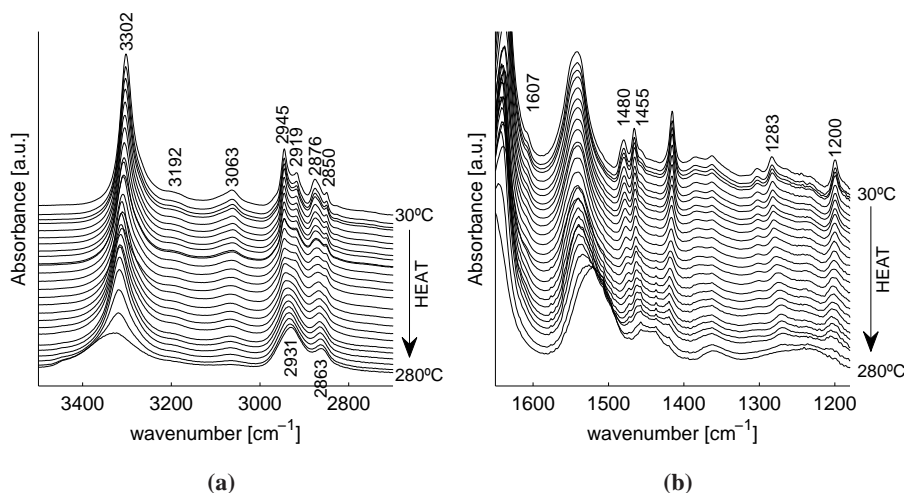


**Figure 7.6:** FTIR spectra obtained on heating PA2,14 crystallized from superheated water from 30°C to the melt at 10°C/min.

	Exotherm		Endotherm	
	T	$\Delta H$	T	$\Delta H$
1H	164°C	22J/g	241°C	82J/g
2H	–	–	238°C	82J/g

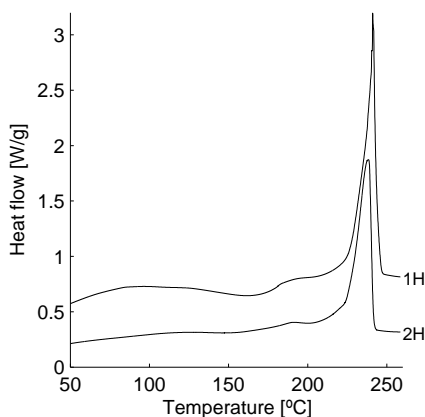


**Figure 7.7:** The figure shows the first (1H) and second (2H) heating runs of water crystallized PA2,14. The table gives the peak maxima/minima and heats of fusion observed for the endo and exotherms respectively.

amide group to form a  $\text{COO}^-$  group.<sup>34,106</sup>

On heating, all of the “new” or “altered” bands in the water crystallized sample disappear or move to a different position at 190°C, the Brill transition temperature for PA2,14.<sup>105</sup> The asymmetric and symmetric  $\text{CH}_2$  stretch bands at 2945 and 2876 $\text{cm}^{-1}$  shift and merge with the bands at 2919 and 2850 $\text{cm}^{-1}$ , see Figure 7.6(a), and the  $\text{COO}^-$  asymmetric and symmetric vibrations at 1607 and 1455 $\text{cm}^{-1}$  also disappear, see Figure 7.6(b).

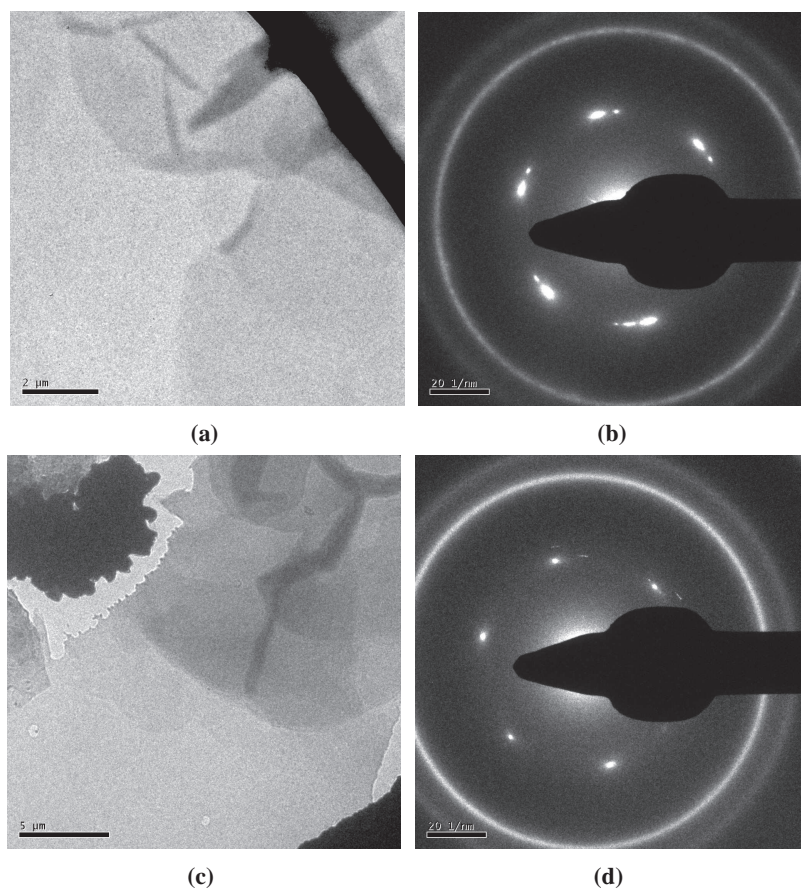
## 7.6 Melting behavior of water crystallized PA2,14

Figure 7.7 shows the DSC traces obtained when heating a dried, water crystallized PA2,14 sample to the melt. In the first heating run, a broad exotherm is observed at 164°C with a heat of fusion of 22J/g which is not observed in the second heating run. The melt endotherm for both heating runs occurs at a similar temperature ( $\sim 240^\circ\text{C}$ ) and a heat of fusion of 82J/g. The melt endotherm corresponds well with other reported values,<sup>39,98,105</sup> whereas the exotherm observed during the first heating run is unusual. A similar event was observed for water crystallized PA4,6 presented in Chapter 4. We address this event in the following section.

## 7.7 Influence of superheated water on PA2,14

From previous studies on PA4,6<sup>82,106</sup> it is known that when PA4,6 crystallizes from superheated water it is in a monoclinic structure with water molecules incorporated in the crystal lattice in close proximity of the amide groups. The presence of asymmetric and symmetric  $\text{COO}^-$  vibrations confirm the presence of water molecules in the PA2,14 crystal lattice in proximity of the amide groups. It is to be noted that the two methylene groups in the diamine segment of the PA2,14 are highly rigid and unable to deform as longer methylene sequences in other polyamide families can. The diamine alkane segment is also too short to allow chain folding to occur in this part of the chain.<sup>55</sup> Therefore, when water molecules are incorporated in the PA2,14 crystal lattice in proximity of the amide groups, the methylene sequence is too short and therefore too rigid to allow for even the slightest deformation of the main chain. Hence the water molecules force the hydrogen bonded planes to slip. The slip in the hydrogen bonded planes causes an alteration in how the planes align, giving rise to the monoclinic crystal structure. In addition the scissoring band of the  $\text{CH}_2$  unit next to the NH group is present at  $1480\text{cm}^{-1}$  in the water crystallized sample and absent in the melt crystallized sample. The scissoring band of the  $\text{CH}_2$  next to the CO group is virtually unchanged between the two samples at  $\sim 1417\text{cm}^{-1}$ . This confirms that conformational changes in the methylene chain segments between the melt and water crystallized samples are indeed in the diamine units. The presence of features from the melt crystallized sample in the spectra and diffraction patterns obtained from the water crystallized sample confirms the existence of two crystal conformations in the water crystallized PA2,14.

The effect of strain and slip in the hydrogen bonded planes also implies that (a portion of the) methylene segments in the water crystallized PA2,14 are distorted. On heating the water crystallized sample above the Brill transition the “additionally” present methylene bands disappear. This indicates that the water molecules in the vicinity of the amide groups are released at the Brill transition. The removal of these water molecules from the crystal lattice at a temperature well above the bulk boiling point of water is also observed in DSC where an exothermic event is observed at the expected Brill transition of PA2,14. The Brill transition is caused by gauche conformers in the main chain,<sup>105</sup> increasing the chain mobility and allowing enough freedom for the water molecules to escape. The incoming of gauche conformers is seen in the decrease of the band at  $1480\text{cm}^{-1}$  in the water crystallized sample.



**Figure 7.8:** TEM and electron diffraction of coPA 0.30 ((a),(b)) and coPA 0.62 ((c),(d)) crystallized from superheated water.

## 7.8 Piperazine copolyamide water grown single crystals

The DSC data presented in Section 7.3 suggest that superheated water is a solvent for all the piperazine based copolymers under investigation. However, it is only possible to grow single crystals up to a piperazine content of 62mol%. Above 62mol% the copolyamide does not form a crystal suspension from the water solution. Instead, the copolyamide forms a crystalline, bulky solid. Therefore TEM and electron diffraction images are available for only the coPA 0.30 and coPA 0.62 crystals.

The TEM images of coPA 0.30 appears similar to the homopolymer PA2,14, showing both needle and lath-like crystals as shown in Figure 7.8(a). However, there appears to be only one type of electron diffraction pattern for both these crystals; a six point symmetrical pattern. The single crystals of coPA 0.62 show only the lath-like

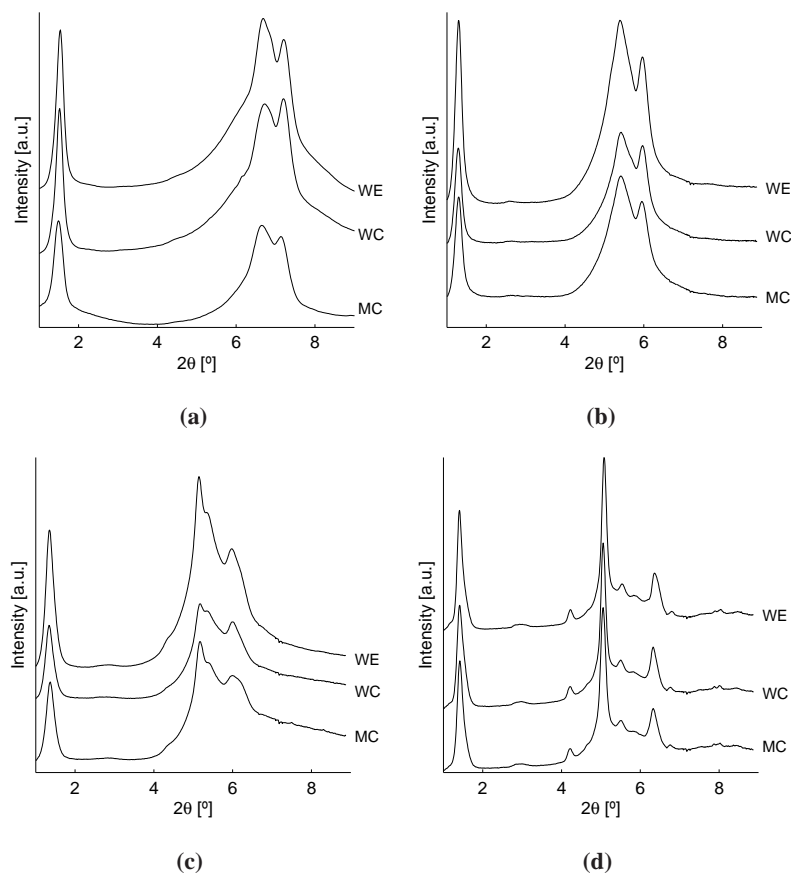


**Figure 7.9:** WAXD data of (a) coPA 0.30, (b) coPA 0.62, (c) coPA 0.82, and (d) PApip,14. The graphs show the diffraction patterns of the melt crystallized sample (MC), water crystallized sample (WC), and after heating the water crystallized sample to temperatures just below the melting temperature (WE). All results shown are at 50°C. Here the data is plotted as a function of scattering angle  $2\theta$  for clarity, where  $\lambda = 2d \sin \theta$  with  $\lambda = 0.04959\text{nm}$ .

morphology and also have a six point electron diffraction pattern, (Figure 7.8(d)).

The electron diffraction patterns conclusively show that single crystals are formed up to a piperazine content of 62mol%. For higher piperazine content, it is not possible to grow such single crystals indicating that the (co)polyamides with a high piperazine content do not truly dissolve in the superheated water, but merely melt in the presence of water. This notion is further strengthened by the small difference between the melt and dissolution temperature of only 20°C observed for PApip,14 as compared to the 45°C observed for PA2,14 in Figure 7.2(b).

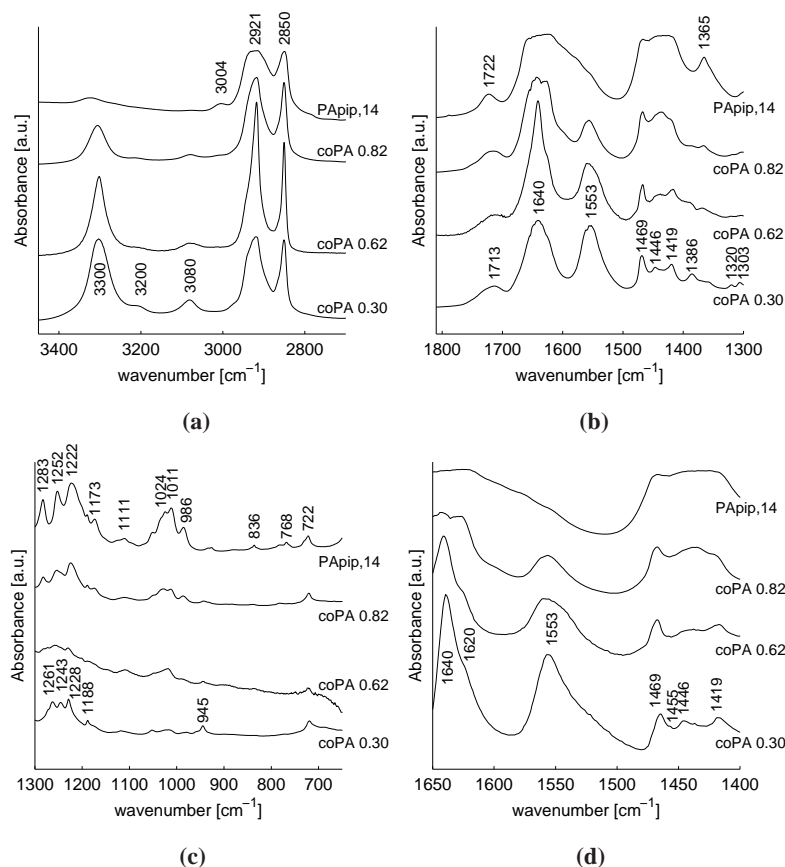
## **7.9 Influence of superheated water on crystallography of piperazine copolyamides**

Figure 7.9 shows WAXD data of coPA 0.30, coPA 0.62, coPA 0.82, and PApip,14 crystallized from the melt (MC), crystallized from water (WC), and after heating the water crystallized samples to a temperature below the melt and cooling to room temperature (WE). For clarity only the final diffraction patterns at 50°C are shown. The data show similar observations for all these (co)polyamides; the WAXD and SAXS data (SAXS data not shown) for the melt crystallized, water crystallized, and water crystallized samples that have been heated are similar. This suggests that the incorporation of piperazine in PA2,14 prevents the crystallization into two crystal structures, i.e. a triclinic and a monoclinic structure, when crystallizing from water. For the copolyamides shown here it is likely that once in the dissolved state, the hydrogen bonds interact with the water molecules. Because piperazine is only a hydrogen bond acceptor and not a hydrogen bond donor, the number of interactions between the amide groups in the polymer chain and the water molecules in the superheated state greatly reduces with the introduction of piperazine. On crystallization, less water molecules can be incorporated in the crystal lattice and no slip of the hydrogen bonded planes occur. Additionally, the increased rigidity of the main chain by the introduction of piperazine residues also prevents the slippage of the hydrogen bonded planes. It is likely that a much lower piperazine content of e.g. 5mol% could show the monoclinic structure on crystallization from superheated water.

## **7.10 Conformational changes in water crystallized piperazine copolyamides**

In a similar procedure to the water crystallized PA2,14, the piperazine based copolyamides are also studied using FTIR spectroscopy. CoPA 0.30 and coPA 0.62 form a crystal suspension on cooling from the dissolved state which is placed on a ZnSe disk and allowed to dry under ambient conditions. CoPA 0.82 and PApip,14 do not form such a suspension; instead a solid residue is formed. For these two samples a piece of the residue is cut off and analyzed in a similar fashion to coPA 0.30 and coPA 0.62.

Figure 7.10 shows the FTIR spectra obtained for the piperazine (co)polyamides crystallized from water. The observed vibrations are in line with those seen for PA2,14 as assigned in Tables 7.1, 7.2, and 7.3. Additionally there are bands present at 3004, 1365, 1283, 1226, 1252, 1173, 1024, 1011, 986, 836, 768cm<sup>-1</sup>. These bands



**Figure 7.10:** FTIR spectra obtained for water crystallized coPA 0.30, coPA 0.62, coPA 0.82, and PApip,14 at 30°C. (d) is an enlargement of the region 1650 to 1400cm<sup>-1</sup> shown in (b).

are all correlated to the piperazine unit incorporated in the polyamide chain<sup>105</sup> and all originate from methylene bending, wagging, twisting, and stretching motions. With an increase in piperazine concentration, these peaks increase in intensity. Furthermore, the vibrational bands associated with hydrogen bonding, i.e. the NH stretch vibration at 3300cm<sup>-1</sup> and the Amide I vibration at 1640cm<sup>-1</sup>, show a strong decrease and broaden significantly with increasing piperazine content.

Figure 7.10(d) shows an enlargement of the spectra in the region 1650 to 1400cm<sup>-1</sup>. Of significance here is the presence of the shoulder at 1455cm<sup>-1</sup> in coPA 0.30 and coPA 0.62 which is absent in coPA 0.82 and PApip,14. This band is related to symmetric COO<sup>-</sup> vibrations. The presence of this band together with the asymmetric COO<sup>-</sup> vibration at 1620cm<sup>-1</sup> (see Figure 7.10(b)) shows the presence of water molecules in the vicinity of the amide groups, similarly to that seen in

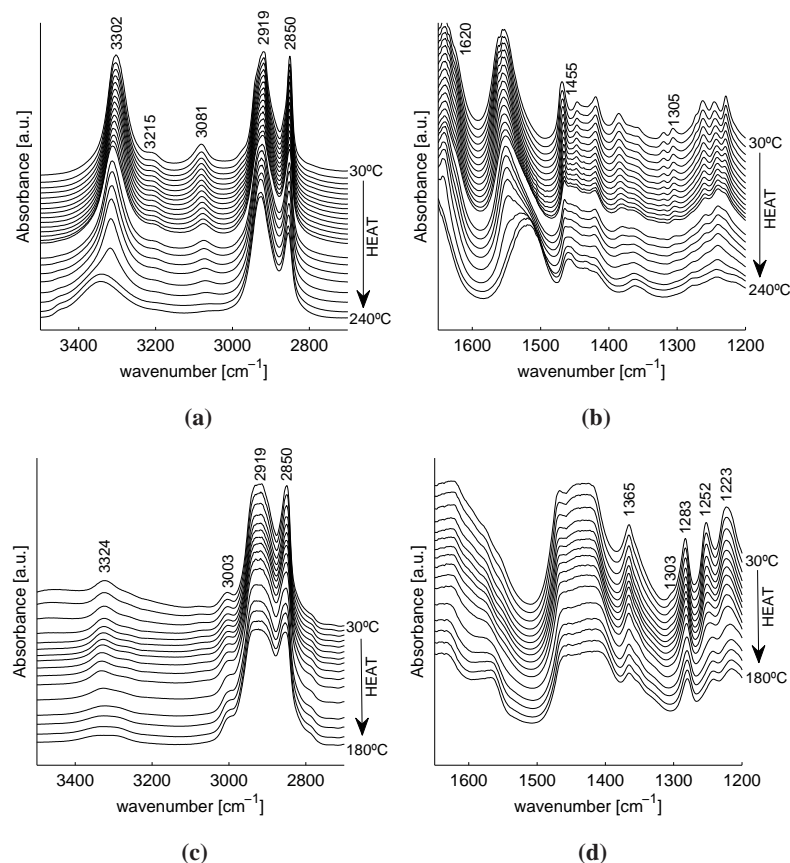


**Figure 7.11:** FTIR spectra obtained on heating coPA 0.30 ((a),(b)) and PApip,14 ((c),(d)) crystallized from superheated water from 30°C to the melt. CoPA 0.62 shows a behavior similar to coPA 0.30 and coPA 0.82 shows a behavior similar to PApip,14.

PA<sub>2,14</sub> in the previous sections. These bands are not present in coPA 0.82 and PApip,14. This strongly suggests that the water molecules are only present in the lower piperazine based copolymers. From previous work<sup>105</sup> it is known that up to a piperazine content of 62mol% the copolyamides show a Brill transition (see also Figure 2.3). This strongly suggests that the Brill transition forms an integral part during the water inclusion in the polyamide crystal lattice.

Figure 7.11 shows the behavior on heating coPA 0.30 and PApip,14 from 30°C to the melt. On heating, the COO<sup>-</sup> symmetric and asymmetric bands at 1620 and 1455cm<sup>-1</sup> disappear near the Brill transition temperature. PApip,14 shows similar behavior to the melt crystallized sample shown in Chapter 2. This strongly suggests that PApip,14 does not dissolve in superheated water, but melts in the presence of water. CoPA 0.62 shows a similar behavior to coPA 0.30 and CoPA 0.82 to PApip,14.



## 7.11 Conclusions

The work presented in this chapter combines the knowledge obtained in Chapters 2 and 4 where we show that the Brill transition is not dependent on hydrogen bond density and that superheated water is a solvent for PA4,6. In this chapter we show that superheated water is a solvent for polyamide 2,14. The PA2,14 dissolves in superheated water at  $\sim 200^\circ\text{C}$ . On cooling PA2,14 crystallizes in two crystal structures: a triclinic and a monoclinic structure. Water molecules incorporated in the crystal lattice cause slip in the hydrogen bonded sheets, directly affecting how the sheets align. FTIR spectra show upon crystallization from a water solution that water molecules are incorporated in a portion of the PA2,14 single crystals. The incorporated water molecules cause strain in the diamine part of the methylene chains, resulting in additional  $\text{CH}_2$  stretch vibrations at  $2945\text{cm}^{-1}$  and  $2876\text{cm}^{-1}$ . Also, the presence of symmetric and asymmetric  $\text{COO}^-$  stretch vibrations strongly suggests that water molecules are indeed present in the vicinity of the amide groups. On heating above the Brill transition temperature, the  $\text{COO}^-$  and  $\text{CH}_2$  stretch vibrations disappear at the Brill transition temperature, resulting in a spectrum similar to the spectrum of a melt crystallized sample. On heating the water crystallized PA2,14, the incoming gauche conformers allow for enough translational motion along the main chain for water molecules to escape from the amide group at the Brill transition. Heating the water crystallized sample above the Brill transition and not melting the sample results in a diffraction pattern similar to the triclinic diffraction pattern.

With the introduction of piperazine into the main chain the dissolution of the copolyamide is only possible up to a piperazine content of 62mol%. From previous work<sup>105</sup> on these piperazine copolyamides it is known that the Brill transition is only observed up to a piperazine content of 62mol%. This suggests that the dissolution of a polyamide in superheated water is directly related to the Brill transition. For coPA 0.82 and PApip,14, which do not show a Brill transition, no single crystals could be grown. Instead the (co)polyamide show a melt point depression of  $20^\circ\text{C}$  in the presence of water, and on cooling a crystalline solid residue is obtained. Similar to PA2,14, coPA 0.30 and coPA 0.62 show the presence of  $\text{COO}^-$  stretch vibrations. These bands are absent in coPA 0.82 and PApip,14. However, these vibrations are considerably weaker in the copolyamides in comparison to PA2,14. Also in the copolyamides the  $\text{COO}^-$  vibrations disappear at the Brill transition temperature of  $\sim 190^\circ\text{C}$ .

## Chapter 8

# Technological assessment and outlook

In this thesis, chemistry is used to manipulate the chemical and physical properties of polyamides by influencing the hydrogen bond density. The use of chemistry enables us to understand the mechanisms involved in the Brill transition. We found that the Brill transition is related to conformational changes occurring in the methylene groups in the polyamide main chain on heating. The use of copolymers and chemistry in processing applications is not new; controlling physical properties with chemistry is a common industrial practice.

The chemistry employed to tailor and process polyamides can involve harsh chemicals and solvents. Usually polyamides are melt processed, but in certain applications such as film preparations and recycling, organic solvents and acids are used. The work presented in this thesis shows that superheated water is a solvent for many commercially available polyamides. The knowledge gained from studying the Brill transition and the chain motions present in polyamides provides the mechanisms required for understanding the influence of water on polyamides. Although the use of superheated water as a solvent inadvertently involves using elevated temperatures, the use of water, which truly is a “green” solvent, opens the door for environmentally friendly processing. The (petro)chemical industry greatly desires an environmentally friendly image. Water as a processing solvent instead of potentially harmful substances is a key element in obtaining such an image.

The use of superheated water in industrial applications could involve foam extrusion applications, spray coating applications, and recycling. The spinning of fibers from a water solution at elevated temperatures and pressures is currently unachievable. However, the success and application of processing polyamides with superheated water is described in a patent<sup>59,60</sup> in which an extruder is used to manufacture polyamide foams. The extruder setup uses a high polymer concentration with usually more than 80wt% polymer. The same technology, in more dilute concentrations, could also be used in a spraying setup to make polyamide (insulating) coatings. Superheated water could also provide an easy route to recycling polyamides from composite materials such as glass fiber reinforced polyamides. The superheated

water dissolves the polyamide, leaving the glass fibers intact, enabling these two components to be separated.

The ultimate goal is to control the crystallization process to manufacture highly oriented, extended chain polyamide fibers. These high performance fibers would mimic materials such as silk in their properties, combining high strength with high toughness. Unfortunately the making of such fibers has always remained elusive.<sup>77</sup> The processing of polyamides using superheated water as presented in this thesis could provide a route to making such fibers. The dissolution process for the polyamides described in this thesis all take place at high temperatures, usually in the order of 200°C. To ease processing and fiber spinning applications it is desirable to have the polyamide in a water solution at room temperature and atmospheric pressure. This cannot be obtained by using water alone. In the work of Harings *et al.*<sup>33-35</sup> the addition of salts to the superheated water could, once the polyamide has been dissolved, prevent hydrogen bonds from reforming on cooling, and thus prevent crystallization. These ions should be easily removable from the polyamide fibers by merely washing with water, reinstating the hydrogen bonding.

This thesis contains fundamental research into the dissolution process involved when a polyamide dissolves in superheated water. However, to obtain a complete understanding of this process, a study on the dissolution of model compounds in superheated water is desirable. The use of oligoamides could provide the required insights in the dissolution and crystallization mechanisms. The principles behind the dissolution of polyamides in superheated water should apply to all hydrogen bonded materials. Therefore synthetic materials such as thermoplastic polyurethanes, polyaniline, and polyester-amides and natural materials such as keratin, wool, and other proteins should be (and are) investigated.<sup>34, 109</sup>

Recent work on understanding the biomimetic spinning of silks has led to the hope that the spinning of artificial fibers using natural materials or polymers could become a reality.<sup>80</sup> Using superheated water it is possible to dissolve keratin in water; unfortunately this leads to a breakup of the keratin into oligopeptides.<sup>109</sup> Should it be possible to reduce and control this molecular weight change it could be possible to use water as a solvent in the biomimetic spinning of silk. On the other hand, the hydrolysis that occurs in keratin is highly promising because it provides oligopeptide building blocks which can and should be used as a natural feedstock for biobased polymers.

The work presented in this thesis provides a greater understanding of the Brill transition and the dissolution process of polyamides in superheated water.

## Appendix A

# Experimental techniques and conditions

### A.1 In-house designed pressure cell for superheated water

An in-house designed and built pressure cell is used to perform experiments on polymer samples in the presence of superheated water. A schematic representation of the device is given in Figure A.1(left) with an actual depiction on the right. The device consists of a copper mantle which is heated by a 1mm diameter SEI coil with a 50cm heating section and a 20cm cold end purchased from Thermocoax which is soldered onto the copper mantle. A glass capillary (2.3mm outer diameter with 0.05mm wall) containing a polymer sample and water is placed inside a 2.3mm opening inside the copper mantle. A steel lid is placed over the top of the capillary and bolted down onto the copper mantle. In order to seal the capillary so that the water cannot escape when heating above 100°C, an o-ring is used. The o-ring seals both the glass capillary and the steel lid to the copper mantle. In order to perform *in situ* X-ray diffraction experiments, a 1mm diameter entrance hole is made for an incoming X-ray beam. The outgoing, diffracted, beam passes through a tapered hole, which has a total angle of 75°. A Pt100 temperature sensor is placed as close as possible to the measuring position, i.e. where the incoming X-ray beam intersects with the glass capillary. The Pt100 sensor and the heating coil are connected to a Linkam TMS94 controller, which is used to operate the device. As a safety precaution, a 1/2" disk type thermostat (not shown in Figure A.1) with a maximum temperature of 245°C is connected between the heating coil and the Linkam controller to prevent the system from overheating. Overheating would result in weakening of the soldering of the heating coil onto the copper mantle. As a result, the maximum operating temperature of this device is 240°C. The whole device is mounted onto an aluminum base plate by means of an A-frame. The device can be cooled by an external airflow. This device is used both for *in situ* diffraction experiments as well as sample preparation.

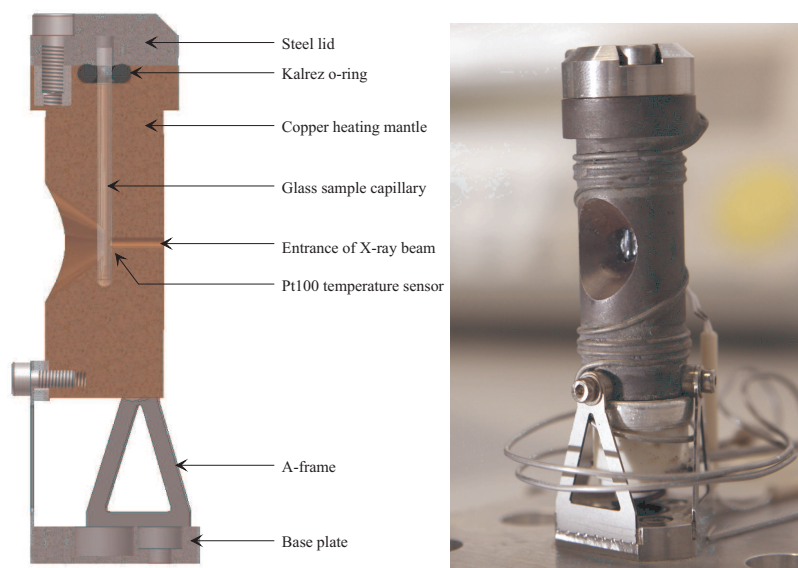


**Figure A.1:** A schematic representation of the experimental setup used to perform the *in situ* X-ray experiments discussed in this thesis. A glass capillary is housed in a copper heating mantle and sealed with an o-ring and a steel lid. The device is controlled with a Linkam TMS94 controller. An opening allows for the entry and exit of the (diffracted) X-ray beam.

## A.2 X-ray diffraction (XRD)

Due to the nature of the experiments performed in this thesis, conventional X-ray sources such as copper or molybdenum targets do not suffice. Hence synchrotron radiation is used to perform the X-ray diffraction experiments. Synchrotron radiation is characterized by high brightness and high intensity, many orders of magnitude higher than the X-rays produced by conventional lab sources.<sup>29,42</sup> Additionally the sharper wavelength of the incident beam used in Synchrotron radiation results in less line broadening compared to conventional sources. The high intensity of synchrotron radiation makes it possible to perform time-resolved experiments with a great level of accuracy.<sup>42</sup> All synchrotron experiments are performed at the European Synchrotron Radiation Facility (ESRF) situated in Genoble, France.

### A.2.1 High resolution wide-angle X-ray diffraction WAXD

High resolution WAXD experiments are performed on the Materials Science beamline (ID11).<sup>63</sup> Typically an X-ray beam with an energy of 25keV (wavelength  $\lambda = 0.04956\text{nm}$ ) and beamsizes of  $300\mu\text{m}$  is used. Dry powder samples or powder samples in the presence of water are heated using a Linkam hotstage or the in-house



**Figure A.2:** A schematic representation of the experimental setup on the High Brilliance beamline ID02.<sup>96</sup>

built pressure cell described above; both controlled by a Linkam TMS94 controller. A hole in both the silver hotstage and the pressure cell allow for the X-ray beam to be transmitted through the sample. Typical experimental conditions are a heating rate of 10°C/min from room temperature to the melt/dissolution temperature. Two-dimensional X-ray diffraction patterns are collected using a Bruker CCD detector with a sample to detector distance of ~40cm. Typically a diffraction pattern is collected every 10 to 12 seconds with an exposure time in the order of 6 seconds. A silicon standard is used to calibrate the sample-to-detector distance and all diffraction patterns are corrected for spatial distortions and integrated to give intensity against diffraction angle.

### A.2.2 Simultaneous small and wide-angle X-ray diffraction (SAXS/WAXD)

Simultaneous small and wide-angle X-ray diffraction experiments are performed on the High Brilliance beamline (ID02)<sup>96</sup> as shown in Figure A.2. Here an X-ray beam with an energy of 12keV ( $\lambda = 0.09951\text{nm}$ ) and  $300\mu\text{m}$  beam size is used. The WAXD detector is placed at an angle relative to the sample position resulting in a limited, and also fixed, scattering range being available for data collection. An intricate geometric data correction procedure corrects for the sample position because the sample is not in the center of the WAXD detector. As a result of the positioning of the WAXD detector the resolution available for the WAXD data is less than for example the WAXD data from ID11. Time resolved, simultaneous SAXS/WAXD measurements are performed on samples using a Linkam hotstage and controller or the homebuilt pressure cell described above. Typically a heating rate of 10°C/min is used from 50°C to the melt. X-ray patterns are collected every 12 to 30 seconds with an exposure time in the order of 1 second. A Princeton WAXD detector and a Frelon 1K SAXS detector are used to collect the diffraction patterns. The SAXS detector

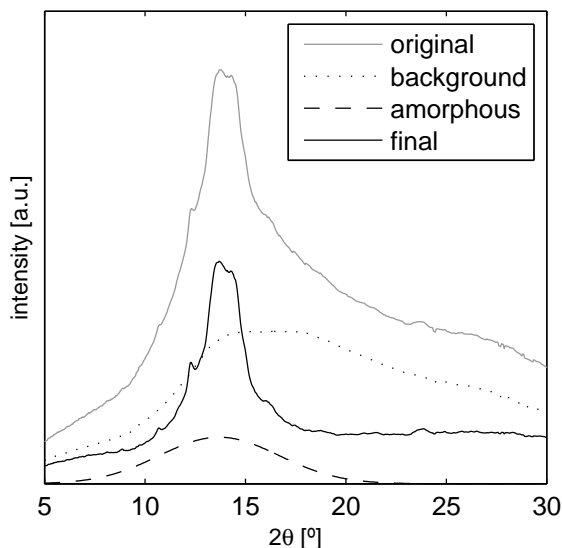


**Figure A.3:** A schematic of how the data subtraction for the WAXD has been performed. The background diffraction pattern originating from the water, glass, and air scatter was determined experimentally. The background diffraction pattern is subtraction from the total diffraction pattern. The amorphous part of the polymer is modeled with a Gaussian distribution and also subtracted from the diffraction pattern, resulting in a final diffraction pattern that only contains the crystalline reflections.

is placed at a distance of 2-5m from the sample and the WAXD detector at  $\sim 25$ cm. Para-bromo-benzoic acid (PBBA) is used to calibrate the WAXD sample-to-detector distance and Lupolen is used to calibrate the SAXS sample-to-detector distance. All diffraction patterns are corrected for absolute intensity and integrated to give intensity against the scattering vector  $q$ . The magnitude of the scattering vector is converted to  $d$ -spacing using the relation  $d = 2\pi/q$ . The SAXS results are Lorentz corrected, i.e. the intensity data is multiplied by  $q^2$ .

### A.2.3 WAXD background correction

It is important to separate the crystalline peaks from the amorphous component and the background scatter obtained during the WAXD experiments. The halo in the WAXD data originating from the amorphous component of the polymer, the water encapsulated in the capillary, and the glass capillary itself are subtracted, leaving only the crystalline part of the diffraction pattern which originates from the polymer as shown in Figure A.3. The amorphous halo originating from the water and glass are determined experimentally. The temperature of the polymer-water-glass diffraction

pattern is matched to the temperature of the water-glass diffraction pattern to within 1°C. So as to account for absorption in the sample, the correct proportion of the background scattering pattern is subtracted from the original diffraction pattern. A Gaussian distribution is used to model the halo resulting from the amorphous component of the polymer. The shape and area of the Gaussian distribution are kept constant over the course of the experiment, i.e. the same Gaussian distribution is subtracted for all diffraction patterns of the same polymer. Hence it is still possible to resolve any changes in crystallinity or the amorphous halo arising in the course of the experiment. The position of the Gaussian distribution is however allowed to vary so as to account for thermal expansion. The Gaussian distribution is subtracted from the spectra from which the water-glass background has already been subtracted resulting in the final spectra used to study the effect of (superheated) water on the polyamides used in this thesis. Figure A.3 shows a diffraction pattern, together with the subtracted water-glass pattern and the subtracted Gaussian distribution to give the final diffraction pattern. The final diffraction pattern is no longer superimposed on an amorphous halo.

### **A.3 Transmission electron microscopy (TEM) and electron diffraction (ED)**

In the current work all samples, prepared as a crystal suspension in water, are placed on a carbon-coated copper TEM grid coated with gold. The gold serves as an internal calibrant for the electron diffraction patterns. The TEM distances are calibrated using standard grating replicas. The suspension is allowed to dry under ambient conditions. Low dose diffraction images are collected on a Fei Technai 20 transmission electron microscope operating at 200kV.

### **A.4 Fourier transform infrared spectroscopy (FTIR)**

For the infrared experiments performed in this work, all samples are placed on a zinc selenium disk and heated or cooled at 10°C/min using a Linkam TMS94 hotstage and controller. FTIR spectra, all averages of 128 scans, are collected using a Bio-Rad FTS6000 spectrometer with a resolution of 2cm<sup>-1</sup>. During heating/cooling spectra are collected in steps of 10°C. During data collection, the temperature is kept constant. The resulting spectra are scaled to the area under the methylene bands between 3000 and 2800cm<sup>-1</sup>.



## A.5 Gel permeation chromatography (GPC)

In this thesis GPC analysis is used to test for hydrolysis and/or degradation. Polyamide crystals crystallized from a 15wt% water solution are prepared using a glass capillary and the in-house designed pressure cell. The method deviates from the standard protocol described in Section 4.2.2 used to produce the single crystals because a faster heating rate of 50°C/min is used and the sample is quenched to room temperature at ~300°C/min using a strong air flow around the device. The polyamide is left in solution at 200°C for different lengths of time ranging from 0.1 to 1440 minutes before quenching. The crystallized samples are removed from the glass capillaries and the excess water evaporated by placing the samples in a vacuum oven at 50°C for 2 hours. The molecular weight of the dried water grown crystals is determined by GPC to test for hydrolysis and/or degradation. The polymer samples are dissolved in 1,1,1,3,3,3-HexaFluoro-2-propanol (HFIP) (Biosolve) at a concentration of 3mg/ml. Calibration of the detectors has been done by the injection of PMMA standards of known concentration and molecular weight.

## A.6 Differential scanning calorimetry (DSC)

DSC measurements are performed on dry polymer samples and samples in the presence of water. When samples are measured in the presence of water varying amounts of polymer and water are placed in large volume capsules (LVC) and cycled twice between 30°C and 220°C at 10°C/min under nitrogen using a Perkin Elmer Pyris 1 DSC. The amount of polymer and water is carefully weighed into the capsules, sealed, and reweighed after sealing so as to verify the amount of water in the capsule. After the two heating cycles, the capsules are weighed again to establish if any leakage occurred. When dry polymer samples are analyzed, the samples are placed in hermetic aluminium pans and cycles twice under nitrogen using a TA Instruments Q1000 DSC between 25°C and the polymer's melting temperature. In all events the second heating cycle is used for data analysis.

## **A.7 Solid state nuclear magnetic resonance (NMR) spectroscopy**

Dried polymer crystals obtained from the melt, water, and formic acid are investigated with solid state NMR spectroscopy. Large volume samples (in the order of milligrams) are prepared by sealing a larger amount of sample with water in a vessel (vol. ~10ml) and following the previously described heating/cooling cycle (Section 4.2.2). As a comparison, spectra of acid and melt crystallized samples are also recorded. Solid state NMR experiments are performed at 700 MHz  $^1\text{H}$  Larmor frequency using a Bruker Advance NMR console situated at the Max Planck Institute for Polymer Science, Mainz, Germany. The samples are placed in zirconia rotors with 2.5mm outer diameter and spun at the magic angle at 30,000 cycles/sec (30kHz) in a commercial solid state MAS probe.  $^1\text{H}$  MAS measurements are performed at 27°C, 67°C, and 117°C, collecting 16 transients for all spectra.

## **A.8 Thermogravimetric analysis and high resolution TGA**

Polymer samples are analyzed using a TA Instruments Q500 TGA. The analysis are performed using the Hi-Res<sup>TM</sup> procedure available in the TGA software. High resolution TGA involves a dynamic variation of the heating rate as a function of weight change in the sample, thus improving the resolution of the individual weight loss events.<sup>66,85</sup> The increased resolution obtained with the HiRes procedure is essential for the experiments performed here due to the limited magnitude of the weight loss events. The samples are heated from 30 to 500°C with a maximum heating rate of 10°C/min and a resolution of 5.

## Appendix B

# Indexing water grown PA2,14 crystals

The X-ray diffraction peaks arising from the water grown crystals discussed in Chapter 7 are indexed using CELREF V3<sup>2</sup> which is a program designed to refine cell parameters from powder diffraction patterns. The polyamide 2,14 (PA2,14) monoclinic unit cell described in Chapter 7 is indexed and refined from an initial monoclinic unit cell based on polyamide 4,6 taken from Atkins *et al.*<sup>3</sup> where the *c*-axis is adjusted to allow for the larger PA2,14 chain length.

Predictions for the monoclinic and triclinic diffraction patterns are made using PowderCell for Windows Version 2.4<sup>62</sup> which allows for the simultaneous representation of the unit cell and the calculated powder pattern. PowderCell predicts a powder diffraction pattern based on the placement of atoms according to their relative atomic coordinates, the space group, and unit cell dimensions. The resulting powder pattern can be directly compared to experimental data.

The atomic positions for PA2,14 are adapted from the positions given by Bunn and Garner<sup>13</sup> for polyamide 6,10 and Holmes *et al.*<sup>41</sup> for polyamide 6. All chain angles are assumed to be equal to 112°, and the values for the bond lengths are shown in Figure B.1. The relative atomic coordinates for PA2,14 are

Atom	<i>x</i>	<i>y</i>	<i>z</i>
CH <sub>2</sub> (1)	0.174600	-0.046	0.05688
N	0.006847	0.037	0.11150
C	0.166600	-0.046	0.16360
O	0.415600	-0.022	0.16360
CH <sub>2</sub> (2)	-0.007988	0.046	0.22050
CH <sub>2</sub> (3)	0.166600	-0.046	0.27730
CH <sub>2</sub> (4)	-0.007988	0.046	0.33420
CH <sub>2</sub> (5)	0.166600	-0.046	0.39110
CH <sub>2</sub> (6)	-0.007988	0.046	0.44800
CH <sub>2</sub> (7)	0.166600	-0.046	0.50490

where the carbon, nitrogen, and oxygen atoms are as show in Figure B.2.

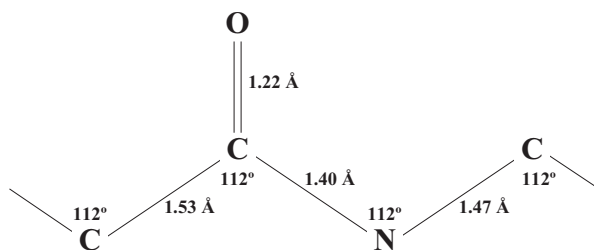


**Figure B.1:** Chain parameters used to determine the atomic positions.<sup>20,41</sup>

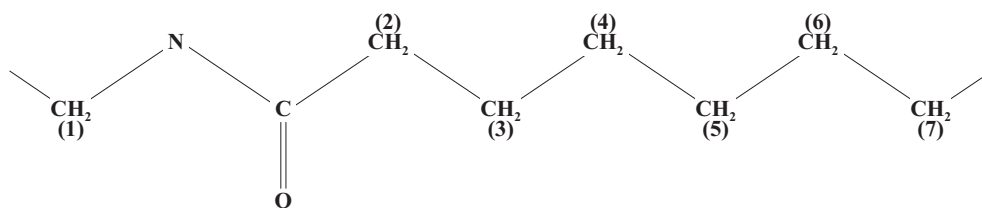


**Figure B.2:** Atom positions and numbers of PA2,14.

# Bibliography

- [1] L.E. Alexander, X-ray diffraction methods in polymer science, John Wiley and Sons, Inc., New York, 1969.
- [2] U.D. Altermatt and I.D. Brown, A real-space computer-based symmetry algebra, *Acta Cryst.* **1987**, *A43*, 125–130.
- [3] E.D.T. Atkins, M. Hill, S.K. Hong, A. Keller, and S. Organ, Lamellar structure and morphology of nylon 46 crystals. A new chain folding mechanism for nylons, *Macromolecules* **1992**, *25*, 917–924.
- [4] E.D.T. Atkins, A. Keller, and D.M. Sadler, Structure analysis of chain-folded lamellar polyamide crystals from x-ray diffraction, *J. Polym. Sci.: Part A-2* **1972**, *10*, 863–875.
- [5] P.W. Atkins, Physical Chemistry, 6th ed., Oxford University Press, Oxford, 1998.
- [6] A. Basile, M.M. Jimenez-Carmona, and A.A. Clifford, Extraction of rosemary by superheated water, *J. Agricultural and Food Chemistry* **1998**, *46*, 5205–5209.
- [7] J. Bella, B. Brodsky, and H.M. Berman, Hydration structure of a collagen peptide, *Structure* **1995**, *3*, 893–906.
- [8] N. M. Bikales (ed.), Encyclopedia of Polymer Science and Technology, vol. 10, Interscience Publishers, New York, 1969.
- [9] T. Bluhm, Y. Deslanders, R.H. Marchessault, and P.R. Sundararajan, New insights into the crystal structure hydration of polysaccharides, *ACS Symposium Series* **1980**, *127*, 253–272.
- [10] M. Borsboom, W. Bras, I. Cerjak, D. Detollenaere, D. G. van Loon, P. Goedtkindt, M. Konijnenburg, P. Lassing, Y. K. Levine, B. Munneke, M. Oversluizen, R. van Tol, and E. Vlieg, The Dutch-Belgian beamline at the ESRF, *J. Synchrotron Radiation* **1998**, *5*, 518–520.

- [11] R. Brill, Behavior of polyamides on heating, *J. Prakt. Chem.* **1942**, 161, 49–64.
- [12] J. Brydson, *Plastics Materials*, 7th ed., Butterworth-Heinemann, Oxford, UK, 1999.
- [13] C.W. Bunn and E.V. Garner, The crystal structures of two polyamides ('nylons'), *Proc. Roy. Soc.* **1947**, A189, 39–68.
- [14] C.G. Cannon, Infrared spectra and molecular configurations of polyamides, *Spectrochimica Acta* **1960**, 16, 302–319.
- [15] C.G. Cannon, F.P. Chappel, and J.I. Tidmarsh, Temperature dependence of birefringence of nylon 66 and the structure of spherulites, *J. Textile Inst.* **1963**, 54, 210–221.
- [16] W.H. Carothers, Linear condensation "superpolymers" suitable for production of pliable, strong, elastic fibers, *Patent US 2071250* **1937**.
- [17] G. Challa, Water in polymeren II, *Plastica* **1969**, 22, 250–253.
- [18] A.A. Clifford, Separations using superheated water, *Green separation processes* **2005**, 323–339.
- [19] T. Clifford, *Fundamentals of supercritical fluids*, Oxford University Press, Oxford, 1999.
- [20] G. Cojazzi, A. Fichera, V. Malta, and R. Zannetti, The crystal structure of polycapryllactam (nylon 8) and of polycapriclactam (nylon 10), *Makromolekulare Chemie* **1978**, 509–518.
- [21] M.L. Colclough and R. Baker, Polymorphism in nylon 66, *J. Materials Science* **1978**, 13, 2531–2540.
- [22] S.J. Cooper, M. Coogan, N. Everall, and I. Priestnall, A polarised  $\mu$ -FTIR study on a model system for nylon 6 6: implications for the nylon Brill structure, *Polymer* **2001**, 42, 10119–10132.
- [23] X. Cui, W. Li, and D. Yan, A study of the crystalline transitions of polyamides X 18, *Polymer International* **2004**, 53, 2031–2037.
- [24] X. Cui and D. Yan, Crystalline transition of polyamide-10,20 investigated by *in situ* Fourier transform infrared spectroscopy, *J. Polym. Sci.: Part B Polym. Phys.* **2004**, 42, 4017–4022.

- [25] K.A. Dill, T.M. Truskett, V. Vlachy, and B. Hribar-Lee, Modeling water, the hydrophobic effect, and ion solvation, *Annu. Rev. Biophys. Biomol. Struct.* **2005**, *34*, 173–199.
- [26] P. Dreyfuss and A. Keller, Chain folding in polyamides: a study on nylons 66, 610, and 612 as crystallized from solution, *J. Macromol. Sci. - Phys.* **1970**, *B4*, 811–836.
- [27] M. Ehrenstein, S. Dellsperger, C. Kocher, N. Stutzmann, C. Weder, and P. Smith, New polyamides with long alkane segments: nylon 6.24 and 6.34, *Polymer* **2000**, *41*, 3531–3539.
- [28] M.H. Eikani, F. Golmohammad, and S. Rowshanzamir, Subcritical water extraction of essential oils from coriander seeds (*Coriandrum sativum* L.), *J. Food Eng.* **2007**, *80*, 735–740.
- [29] European Synchrotron Radiation Facility (ESRF), A light for science, ESRF, Grenoble, 2005.
- [30] R.J. Gaymans, T.E.C. van Utteren, J.W.A. van den Berg, and J. Schuyer, Preparation and some properties of nylon 46, *J. Polym. Sci.: Polym. Chem. Ed.* **1977**, *15*, 537–545.
- [31] J. Gosline, M. Lillie, E. Carrington, P. Guerette, C. Ortlepp, and K. Savage, Elastic proteins: biological roles and mechanical properties, *Phil. Trans. R. Soc. Lond. B* **2002**, *357*, 121–132.
- [32] L. Haar, J.S. Gallagher, and G.S. Kell, NBS/NRC Steam tables, Hemisphere Publishing Corp., New York, 1984.
- [33] J.A.W. Harings, Y.S. Deshmukh, E. Vinken, and S. Rastogi, Polyamide with reduced crystallinity, *Patent pending* **2008**.
- [34] J.A.W. Harings, O. van Asselen, R. Graf, R. Broos, and S. Rastogi, The role of superheated water on shielding and mediating hydrogen bonding in N,N-1,2-ethanediyl-bis(6-hydroxy-hexanamide) crystallization, *Cryst. Growth Des.* **2008**, submitted.
- [35] J.A.W. Harings, O. van Asselen, R. Graf, R. Broos, and S. Rastogi, The role of superheated water on the crystallization of N,N-1,2-ethanediyl-bis(6-hydroxy-hexanamide): implications on crystallography and phase transitions, *Cryst. Growth Des.* **2008**, *8*, 2469–2477.
- [36] R.L. Harlow, The structure of water as organized in an rgd peptide crystal at -80°C, *JACS* **1993**, *115*, 9838–9839.

- [37] M.J. Hill and E.D.T. Atkins, Morphology and structure of nylon 68 single crystals, *Macromolecules* **1995**, *28*, 604–609.
- [38] J. Hirschinger, H. Miura, K.H. Gardner, and A.D. English, Segmental dynamics in the crystalline phase of nylon 66: solid-state  $^2\text{H}$  NMR, *Macromolecules* **1990**, *23*, 2153–2169.
- [39] S. Hoffmann, B. Vanhaecht, J. Devroede, W. Bras, C.E. Koning, and S. Rastogi, Cocrystallization in piperazine-based polyamide copolymers: Small- and Wide-angle X-ray diffraction studies at 30°C, *Macromolecules* **2005**, *38*, 1797–1803.
- [40] V.F. Holland, Morphology and electron diffraction of nylon 66 single crystals, *Makromolekulare Chemie* **1964**, *71*, 204–206.
- [41] D.R. Holmes, C.W. Bunn, and D.J. Smith, The crystal structure of polycaproatamide: nylon 6, *J. Polym. Science* **1955**, *17*, 159–177.
- [42] B.S. Hsiao, A.D. Kennedy, R.A. Leach, B. Chu, and P. Harney, Studies of structure and morphology development during the heat-draw process of nylon 66 fiber by synchrotron X-ray diffraction and scattering techniques, *J. Appl. Cryst.* **1997**, *30*, 1084–1095.
- [43] X. Hu, D. Kaplan, and P. Cebe, Effect of water on the thermal properties of silk fibroin, *Thermochimica Acta* **2007**, *461*, 137–144.
- [44] E. Iizuka, The physico-chemical properties of silk fibers and the fiber spinning process, *Experimentia* **1983**, *39*, 449–454.
- [45] T. Itoh, T. Yamagata, Y. Hasegawa, M. Hashimoto, and T. Konishi, Energetically stable conformations of nylon 66 and nylon 6 molecules in crystals, *Jpn. J. Appl. Phys.* **1996**, *35*, 4474–4475.
- [46] J. Jakeš and S. Krimm, Normal coordinate analyses of molecules with the amide group, *Spectrochimica Acta* **1971**, *27A*, 35–63.
- [47] J. Jakeš and S. Krimm, A valence force field for the amide group, *Spectrochimica Acta* **1971**, *27A*, 19–34.
- [48] G.A. Jeffrey, An introduction to hydrogen bonding, Oxford University Press, New York, 1997.
- [49] G.A. Jeffrey and W. Saenger, Hydrogen bonding in biological structures, Germany, 1994.



- [50] N.A. Jones, E.D.T. Atkins, and M.J. Hill, Comparison of structures and behavior on heating of solution-grown, chain-folded lamellar crystals of 31 even-even nylons, *Macromolecules* **2000**, *33*, 2642–2650.
- [51] N.A. Jones, E.D.T. Atkins, and M.J. Hill, Investigation of solution-grown, chain-folded lamellar crystals of the even-even nylons 6 6, 8 6, 8 8, 10 6, 10 8, 10 10, 12 6, 12 8, 12 10, and 12 12, *J. Polym. Sci.: Part B Polym. Phys.* **2000**, *38*, 1209–1221.
- [52] N.A. Jones, E.D.T. Atkins, M.J. Hill, S.J. Cooper, and L. Franco, Chain-folded lamellar crystals of aliphatic polyamides. Comparisons between nylons 4 4, 6 4, 8 4, 10 4, and 12 4, *Macromolecules* **1996**, *29*, 6011–6018.
- [53] N.A. Jones, E.D.T. Atkins, M.J. Hill, S.J. Cooper, and L. Franco, Chain-folded lamellar crystals of aliphatic polyamides. Investigation of nylons 4 8, 4 10, 4 12, 6 10, 6 12, 6 18 and 8 12, *Polymer* **1997**, *38*, 2689–2699.
- [54] N.A. Jones, E.D.T. Atkins, M.J. Hill, S.J. Cooper, and L. Franco, Polyamides with a choice of structure and crystal surface chemistry. Studies of chain-folded lamellae of nylons 8 10 and 10 12 and comparison with the other 2N 2(N+1) nylons 4 6 and 6 8, *Macromolecules* **1997**, *30*, 3569–3578.
- [55] N.A. Jones, S.J. Cooper, E.D.T. Atkins, M.J. Hill, and L. Franco, Temperature-induced changes in chain-folded lamellar crystals of aliphatic polyamides. Investigation of nylons 2 6, 2 8, 2 10, and 2 12, *J. Polym. Sci.: Part B Polym. Phys.* **1997**, *35*, 675–688.
- [56] D. Kilburn, S. Townrow, V. Meunier, R. Richardson, A. Alam, and J. Ubbink, Organization and mobility of water in amorphous and crystalline trehalose, *Nature Materials* **2006**, *5*, 632–635.
- [57] C. Kittel, Introduction to solid state physics, 7th ed., John Wiley and Sons, Inc., New York, 1996.
- [58] E.A. Klop and M. Lammers, XRD study of the new rigid-rod polymer fibre PIPD, *Polymer* **1998**, *39*, 5987–5998.
- [59] R.A. Korbee, Method for the preparation of thermosetting compositions that can be shaped by application of heat and pressure, *Patent WO98/02485* **1998**.
- [60] R.A. Korbee and A.A. van Geenen, Process for the preparation of a polyamide nanocomposite composition, *Patent WO99/29767* **1999**.
- [61] R.A. Korbee and A.A. van Geenen, Process for the preparation of a polyamide nanocomposite composition, *Patent US6350805* **2002**.

- [62] W. Kraus and G. Nolze, POWDER CELL – a program for the representation and manipulation of crystal structures and calculation of the resulting X-ray powder patterns, *J. Appl. Cryst.* **1996**, *29*, 301–303.
- [63] A. Kvikic, Materials science research at the European Synchrotron Radiation Facility, *Nucl. Instrum. Methods Phys. Res. B.* **2003**, *199*, 531–535.
- [64] P.J. Lemstra, Processing for ultimate properties, *NATO Science Series II: Mathematics, Physics and Chemistry* **2004**, *175*, 201–217.
- [65] S. León, C. Alemán, M. Bermúdez, and S. Muñoz Guerra, Structure of nylon 46 lamellar crystals: An investigation including adjacent chain folding, *Macromolecules* **2000**, *33*, 8756–8763.
- [66] T. Lever, I. Groves, and N. Hawkins, Strengthening resolve, *Laboratory Practice* **1991**, *40*, 19–25.
- [67] W. Li, Y. Huang, G. Zhang, and D. Yan, Investigation on Brill transition of nylons 6/16, 4/16 and 2/16 by variable-temperature WAXD and FTIR, *Polymer International* **2003**, *52*, 1905–1908.
- [68] Y. Li, G. Zhang, D. Yan, and E. Zhou, Morphology and structure of nylon-2,14 single crystals from dilute solution, *J. Polym. Sci.: Part B Polym. Phys.* **2002**, *40*, 1913–1918.
- [69] D. Lin-Vien, N.B. Colthup, W.G. Fateley, and J.G. Grasselli, The handbook of Infrared and Raman characteristic frequencies of organic molecules, Academic Press, San Diego, 1991.
- [70] J.H. Magill, M. Girolamo, and A. Keller, Crystallization and morphology of nylon-6,6 crystals: 1. Solution crystallization and solution annealing behaviour, *Polymer* **1981**, *22*, 43–55.
- [71] Y. Maréchal, Observing the water molecule in macromolecules and aqueous media using infrared spectrometry, *J. Mol. Struct.* **2003**, *648*, 27–47.
- [72] Y. Maréchal, Observing the water molecule in macromolecules using infrared spectrometry: structure of the hydrogen bond network and hydration mechanism, *J. Mol. Struct.* **2004**, *700*, 217–223.
- [73] McMurry, Organic Chemistry, 4th ed., Brooks/Cole Publishing Company, United States of America, 1996.
- [74] L. Meng, Y. Zhang, Y. Huang, M. Shibata, and R. Yosomiya, Studies on the decomposition behavior of nylon-66 in supercritical water, *Polymer Degradation and Stability* **2004**, *83*, 389–393.

- [75] D.E. Newton, Encyclopedia of water, Greenwood press, Westport, 2003.
- [76] R. Parathasarathy, S. Chaturvedi, and K. Go, Design of crystalline helices of short oligopeptides as a possible model for nucleation of  $\alpha$ -helix: Role of water molecules in stabilizing helices, *Proc. Natl. Acad. Sci.* **1990**, *87*, 871–875.
- [77] A.R. Postema, P. Smith, and A.D. English, Ultra-drawing of polyamides: the hydrogen bond barrier, *Polymer Communications* **1990**, *31*, 444–447.
- [78] C. Ramesh, New crystalline transitions in nylons 4,6, 6,10, and 6,12 using high temperature X-ray diffraction studies, *Macromolecules* **1999**, *32*, 3721–3726.
- [79] C. Ramesh, A. Keller, and S.J.E.A. Eltink, Studies on the crystallization and melting of nylon-6,6: 1. The dependence of the Brill transition on the crystallization temperature, *Polymer* **1994**, *35*, 2483–2487.
- [80] S. Rammensee, U. Slotta, T. Scheibel, and A.R. Bausch, Assembly mechanism of recombinant spider silk proteins, *PNAS* **2008**, *105*, 6590–6595.
- [81] S. Rastogi, A.B. Spoelstra, J.G.P. Goossens, and P.J. Lemstra, Chain mobility in polymer systems: on the borderline between solid and melt. 1. Lamellar doubling during annealing of polyethylene, *Macromolecules* **1997**, *30*, 7880–7889.
- [82] S. Rastogi, A.E. Terry, and E. Vinken, Dissolution of hydrogen-bonded polymers in water: a study of nylon-4,6, *Macromolecules* **2004**, *37*, 8825–8828.
- [83] L.P. Razumovskii, V.S. Markin, and G.Y. Zaikov, Solubility and diffusion coefficient of water in aliphatic polyamides, *Pol. Sci. USSR* **1985**, *27*, 341–346.
- [84] G. Rotter and H. Ishida, FTIR separation of nylon-6 chain conformations: Clarification of the mesomorphous and gamma-crystalline phases, *J. Polym. Sci.: Part B Polym. Phys.* **1992**, *30*, 489–495.
- [85] I. Salin and J.C. Seferis, Kinetic analysis of high resolution TGA variable heating rate data, *Polymer Preprints* **1992**, *22*, 372–373.
- [86] H. Savage, Water structure in vitamin B<sub>12</sub> coenzyme crystals. I. Analysis of the neutron and x-ray solvent densities, *Biophys.* **1986**, *50*, 947–965.
- [87] H. Savage, Water structure in vitamin B<sub>12</sub> coenzyme crystals. II. Structural characteristics of the solvent networks, *Biophys.* **1986**, *50*, 967–980.

- [88] R. Sengupta, V.K. Tikku, A.K. Somani, T.K. Chaki, and A.K. Bhowmick, Electron beam irradiated polyamide-6,6 films – I: characterization by wide angle X-ray scattering and infrared spectroscopy, *Radiation Physics and Chemistry* **2005**, *72*, 625–633.
- [89] R.L. Smith, Z. Fang, H. Inomata, and K. Arai, Phase behavior and reaction of nylon 6/6 in water at high temperatures and pressures, *J. Appl. Polym. Sci.* **2000**, *76*, 1062–1073.
- [90] T.W. Graham Solomons, *Organic Chemistry*, 6th ed., John Wiley and Sons, Inc., New York, 1996.
- [91] T. Srikrishnan and R. Parthasarathy, ‘Sandwiched’ water molecule between pyrimidine bases and intra-molecular C–H...O hydrogen bonding in 5-nitro-1-( $\beta$ -D-ribosyluronic acid)-uracil monohydrate, *Nature* **1976**, *264*, 379–380.
- [92] H.W. Starkweather, The sorption of water by nylons, *J. Appl. Polym. Sci.* **1959**, *2*, 129–133.
- [93] H.W. Starkweather, Water in nylon, *ACS Symposium Series* **1980**, *127*, 433–440.
- [94] H.W. Starkweather, J.F. Whitney, and D.R. Johnson, Crystalline order in nylon 66, *J. Polym. Sci.: Part A Polym. Chem.* **1963**, *1*, 715–723.
- [95] K. Tashiro and Y. Yoshioka, Conformational disorder in the Brill transition of uniaxially-oriented nylon 10/10 sample investigated through the temperature-dependent measurement of X-ray fiber diagram, *Polymer* **2004**, *45*, 6349–6355.
- [96] V. Urban, P. Panine, C. Ponchut, and T. Narayanan, Two-dimensional camera for millisecond range time-resolved small- and wide-angle X-ray scattering, *J. Appl. Cryst.* **2003**, *36*, 809–811.
- [97] J.C.M. van Hest and D.A. Tirrell, Protein-based materials, toward a new level of structural control, *Chem. Commun.* **2001**, *19*, 1897–1904.
- [98] B. Vanhaecht, J. Devroede, R. Willem, M. Biesemans, W. Goonewardena, S. Rastogi, S. Hoffmann, P.G. Klein, and C.E. Koning, Cocrystallization phenomena in piperazine-based copolyamides as examined by differential scanning calorimetry, wide-angle X-ray diffraction, and solid-state NMR, *J. Polym. Sci.: Part A Polym. Chem.* **2003**, *41*, 2082–2094.

- [99] B. Vanhaecht, B. Goderis, P.C.M.M. Magusin, B. Mezari, I. Dolbnya, and C.E. Koning, Stereochemistry driven distribution of 1,4-diaminocyclohexane residues over the crystalline and amorphous phase in copolyamides 4.14/1,4-DACH.14. A solid-state NMR and temperature-dependent WAXD study, *Macromolecules* **2005**, *38*, 6048–6055.
- [100] B. Vanhaecht, B. Rimez, R. Willem, M. Biesemans, and C.E. Koning, Influence of stereochemistry on the thermal properties of partially cycloaliphatic polyamides, *J. Polym. Sci.: Part A Polym. Chem.* **2002**, *40*, 1962–1971.
- [101] B. Vanhaecht, M.N. Teerenstra, D.R. Suwier, R. Willem, M. Biesemans, and C.E. Koning, Controlled stereochemistry of polyamides derived from *cis/trans*-1,4-cyclohexanedicarboxylic acid, *J. Polym. Sci.: Part A Polym. Chem.* **2001**, *39*, 833–840.
- [102] B. Vanhaecht, R. Willem, M. Biesemans, B. oderis, M. Basiura, P.C.M.M. Magusin, I. Dolbnya, and C.E. Koning, A WAXD and solid-state NMR study on cocrystallization in partially cycloaliphatic polyamide 12.6-based copolymers, *Macromolecules* **2004**, *37*, 421–428.
- [103] N. Vasanthan, N.S. Murthy, and B.G. Bray, Investigation of Brill transition in nylon 6 and nylon 6,6 by infrared spectroscopy, *Macromolecules* **1998**, *31*, 8433–8435.
- [104] J.F.V. Vincent, Structural biomaterials, Princeton University Press, Princeton, 1990.
- [105] E. Vinken, A.E. Terry, S. Hoffmann, B. Vanhaecht, C.E. Koning, and S. Rastogi, The influence of hydrogen bonding on the conformational changes, the Brill transition, and lamellae thickening in piperazine based (co)polyamides, *Macromolecules* **2006**, *39*, 2546–2552.
- [106] E. Vinken, A.E. Terry, O. van Asselen, A.B. Spoelstra, R. Graf, and S. Rastogi, Role of superheated water in dissolution and perturbation of hydrogen bonding in the crystalline lattice of polyamide 4,6, *Langmuir* **2008**, *24*, 6313–6326.
- [107] F. Vollrath and D.P. Knight, Liquid crystalline spinning of spider silk, *Nature* **2001**, *410*, 541–548.
- [108] M.G.M. Wevers, T.F.J. Pijpers, and V.B.F. Mathot, The way to measure quantitatively full dissolution and crystallization of polyamides in water up to 200°C and above by DSC, *Thermochimica Acta* **2007**, *453*, 67–71.

- [109] J. Yin, S. Rastogi, A.E. Terry, and C. Popesco, Self-organization of oligopeptides obtained on dissolution of feather keratins in superheated water, *Biomacromolecules* **2007**, *8*, 800–806.
- [110] Y. Yoshioka and K. Tashiro, Structural change in the Brill transition of nylon m/n (1) nylon 10/10 and its model compounds, *Polymer* **2003**, *44*, 7007-7019.
- [111] Y. Yoshioka and K. Tashiro, Structural changes in phase transitions of nylon compounds. 1. Transition behavior of model compounds of R–NHCO–R' type, *J. Phys. Chem.* **2003**, *107*, 11835–11842.
- [112] Y. Yoshioka, K. Tashiro, and C. Ramesh, New interpretation of progression bands observed in infrared spectra of nylon-m/n, *J. Polym. Sci.: Part B Polym. Phys.* **2003**, *41*, 1294–1307.
- [113] Y. Yoshioka, K. Tashiro, and C. Ramesh, Structural change in the Brill transition of nylon m/n (2) conformational disordering as viewed from the temperature-dependent infrared spectral measurements, *Polymer* **2003**, *44*, 6407–6417.
- [114] Z. Yu, G. Hu, J. Varlet, A. Darsari, and Y. Mai, Water-assisted melt compounding of nylon-6/pristine montmorillonite nanocomposites, *J. Polym. Sci.: Part B Polym. Phys.* **2005**, *43*, 1100–1112.

# Samenvatting

*Polyamides: Waterstofbruggen, de Brill transitie, en superverhit water*

Alifatische polyamide, beter bekend als nylon, was de werelds eerste synthetische vezel en heeft een brede toepassingsveld gevonden in banden, vloerbekleding, kousen, stoffering, en hechtstoffen. Alle polyamides hebben een herhalende amide ( $-\text{CONH}-$ ) groep in het moleculere structuur aanwezig met waterstofbruggen tussen deze amide groepen. In vergelijking met andere polymeren zoals polyethyleen hebben polyamides een hoog smelt temperatuur. Polyamides zijn extensief bestudeerd door verschillende onderzoeksgroepen, echter is er nog altijd veel te leren en te bereiken aangaande deze materialen.

Het eerste belangrijke resultaat dat is bereikt met dit proefschrift is een nieuw en verbeterd inzicht in de Brill transitie die waargenomen wordt in veel polyamides. De Brill transitie is een vaste stof kristallijne transitie die waargenomen wordt bij het verhitten van polyamides. De Brill transitie temperatuur is de temperatuur waarbij de karakteristieke intersheet en interchain reflecties waargenomen in röntgen diffractie (WAXD) samenvallen tot een enkele reflectie welke behouden blijft totdat de polyamide smelt. De aard van de Brill transitie en de onderliggende mechanismen zijn een onderwerp van discussie sinds de transitie voor het eerst werd waargenomen in 1942. De resultaten in dit proefschrift creëren een beter begrip van de onderliggende mechanismen en de invloed van waterstofbruggen op de Brill transitie; een belangrijke factor voor de eigenschappen van veel polyamides.

Het lijkt aannemelijk dat de Brill transitie beïnvloed wordt door waterstofbruggen, of beter gezegd, door een verzwakking van waterstofbruggen. We kunnen de relatie tussen de Brill transitie en waterstofbruggen bestuderen door een unieke verzameling op piperazine gebaseerde copolyamides te gebruiken, welke speciaal vervaardigd zijn om de invloed van waterstofbruggen op verschillende (fysische) eigenschappen te onderzoeken. We tonen aan dat de Brill transitie onafhankelijk is van de piperazine concentratie, en dus ook onafhankelijk van de waterstofbrugdichtheid. De Brill transitie wordt veroorzaakt door conformationele veranderingen in de polyamide keten, die de methyleen eenheden laten draaien, terwijl de waterstofbruggen behouden blijven. Wanneer de methyleen eenheden naast

de amide groepen voldoende kunnen draaien wordt de Brill transitie waargenomen. De Brill transitie is daarom geen eerste noch tweede orde transitie, maar een vaste stof kristallijne transitie aangedreven door krukas bewegingen in de polyamide hoofdketen.

De resultaten in dit proefschrift over de Brill transitie dragen bij aan een significante toename in het begrijpen van deze transitie. Het gebruik van speciaal vervaardigde en ontworpen copolyamides in combinatie met vele, kwalitatief hoogwaardige analytische technieken vormen de sleutel tot het bereikte succes. Het werk in dit proefschrift combineert de kennis en expertise van twee verschillende, maar elkaar aanvullende kennisgebieden in polymeer onderzoek.

Het inzicht verkregen door het onderzoek naar de Brill transitie en de bewegingen van de ketens die aanwezig zijn in polyamides, bieden de mogelijkheid om de invloed van water op polyamides in het algemeen te begrijpen, en meer specifiek de invloed van superverhit water, i.e. water boven 100°C. Het tweede belangrijke resultaat dat beschreven wordt in dit proefschrift betreft het oplossen van polyamides in water. We tonen aan dat superverhit water een oplosmiddel is voor verschillende (commerciële) polyamides, waaronder polyamide 4,6 en polyamide 6,6. De conformationele veranderingen in de polyamide tijdens de Brill transitie vormen de sleutel in het oplosproces, daar ze zeer mobiele watermoleculen in de superverhitte toestand toestaan het kristalrooster te penetreren en de waterstofbindingen tussen de amide groepen te verbreken. Bij kristallisatie uit de waterige oplossing, wat gebeurt door de oplossing af te koelen, hechten water moleculen zich aan de amide groep in het kristalrooster, en daardoor worden de amide-amide waterstofbindingen verzwakt. Door het gedroogde, water gekristalliseerde polyamide te verhitten tot boven de Brill transitie, worden de watermoleculen bevrijd uit het kristalrooster en worden de waterstofbruggen hersteld. De verwijdering van de watermoleculen bij de Brill transitie gaat gepaard met een exothermische gebeurtenis in differential scanning calorimetry (DSC) experimenten uitgevoerd op gedroogde, gesedimenteerde water gekristalliseerde polyamide kristallen. De invloed van water op het kristalrooster wordt zeer duidelijk waargenomen in polyamide 2,14, waar de watermoleculen ingesloten in het kristalrooster een slip veroorzaken in de waterstofbrug gebonden vlakken. Deze slip resulteert in een coëxistentie van een triclinische en monoclinische kristalstructuur die waargenomen wordt in WAXD. Bij verhitting boven de Brill transitie temperatuur verlaten de watermoleculen het kristalrooster en toont de polyamide alleen nog de triclinische structuur.

De resultaten die in dit proefschrift gepresenteerd worden, in het bijzonder de resultaten met betrekking tot het gebruik van superverhit water als oplosmiddel voor polyamide, maaken de weg vrij voor een milieuvriendelijk en duurzaam productieproces. Een proces waar water wordt gebruikt om polyamides te verwerken, in plaats van organische oplosmiddelen en zuren. Voor het gebruik van



(superverhit) water in productie toepassingen zoals film casting en recycling, is het van essentieel belang dat de polyamide kristallisatie vanuit superverhit water een gecontroleerd proces is. Momenteel is dit niet het geval; tijdens het koelen van de polyamide/water oplossing kristalliseert de polyamide snel en ongecontroleerd wanneer voldoende onderkoeling wordt bereikt. Deze snelle kristallisatie belemmert bijvoorbeeld de groei van grote, enkel kristallen. De volgende stap die moet worden ondernomen is een gecontroleerde kristallisatie, bijvoorbeeld door zouten toe te voegen aan de oplossing,<sup>33</sup> waardoor kristallisatie bij kamertemperatuur gemanipuleerd wordt. Afhankelijk van de keuze van ionen en de vereiste voor bepaalde toepassingen kan de kristallisatie op de juiste wijze beïnvloed, dan wel onderdrukt worden. De mogelijkheden om met behulp van op water gebaseerde technieken en op milieuvriendelijke wijze polyamides te vervaardigen is een veelbelovend en innovatief vooruitzicht voor de toekomst.

# List of Publications

## Publications from this thesis

E. Vinken, A.E. Terry, O. van Asselen, A.B. Spoelstra, R. Graf, and S. Rastogi, Role of superheated water in dissolution and perturbation of hydrogen bonding in the crystalline lattice of polyamide 4,6, *Langmuir* **2008**, *24*, 6313–6326.

J. Harings, Y.S. Deshmukh, E. Vinken, and S. Rastogi, Polyamide with reduced crystallinity, *Patent pending* **2008**.

S. Rastogi, E. Vinken, J. Harings, J. Yin, and A. Terry, Dissolution of hydrogen bonded polymers in water, from synthetic to biopolymers, *Technical Proceedings of the NSTI Nanotechnology Conference and Trade Show* **2006**, *2*, 762–765.

E. Vinken, A.E. Terry, S. Hoffmann, B. Vanhaecht, C.E. Koning, and S. Rastogi, The influence of hydrogen bonding on the conformational changes, the Brill transition, and lamellae thickening in (co)polyamides, *Macromolecules* **2006**, *39*, 2546–2552.

S. Rastogi, A.E. Terry, and E. Vinken, Dissolution of Hydrogen Bonded Polymers in Water: a study on Nylon 4,6, *Macromolecules* **2004**, *37*, 8825–8828.

E. Vinken, A.E. Terry, A.B. Spoelstra, and S. Rastogi, Role of superheated water in dissolution of polyamide 6,6 and other even-even polyamides, *In preparation* **2008**.

E. Vinken, A.E. Terry, A.B. Spoelstra, and S. Rastogi, Influence of superheated water on hydrogen bonding in piperazine based copolyamides, *In preparation* **2008**.

E. Vinken, A.E. Terry, C.E. Koning, and S. Rastogi, The influence of stereochemistry on the conformational changes and the Brill transition in 1,4-diaminocyclohexane based (co)polyamides, *In preparation* **2008**.

## Other publications

A. M. Nardes, M. Kemerink, M.M. de Kok, E. Vinken, and R. A. J. Janssen, Conductivity and environmental stability of PEDOT:PSS thin films mixed with sorbitol, *Organic Electronics* **2008**, in press.

J. Reijenga and E. Vinken, Self-reflection on Professional Competences in Chemical Engineering Education, *Proceedings of the 20th International Conference on Chemical Education* **2008**, in press.

H.J.M. Belderock, J.A. van Oijen, M.J. Prins, E. Vinken, L.P.H. de Goey, T. Brunner, and I. Obernberger, Kinetic modeling of the pyrolysis of biomass, *Submitted to J. Analytical and Applied Pyrolysis* **2008**.

F.B. Waanders, E. Vinken, A. Mans, and A.F. Mulaba-Bafubiandi, Iron minerals in coal, weathered coal and coal ash – SEM and Mössbauer results, *Hyperfine Interactions* **2003**, 148/149, 21–29.

# Dankwoord

Een proefschrift schrijven is niet iets dat je even uit de mouw schudt. Iedereen die het ooit gedaan heeft weet dat het hard werken is. Soms wil je de hele boel er gewoon bij neergooien en zie je het echt even niet meer zitten; maar

*Ik vermag alle dingen door Christus, Die mij kracht geeft.*

Staten Vertaling (1977) – Filippenzen 4:13

Ik kan het zelf niet beter zeggen dan dat Paulus dat doet. Het is niet op eigen kracht dat ik dit proefschrift heb kunnen schrijven maar door Hem die mij in alles bijstaat.

Er waren ook veel mensen die mij hebben bijgestaan. Als eerste denk ik aan mijn echtgenoot Willem. Zonder zijn liefde en ondersteuning was ik er zeker mee gestopt. Mijn ouders horen ook in dit rijtje thuis. Mammie, Pappie, heel erg bedankt voor de ondersteuning, ook al wisten jullie niet altijd waar het precies over ging, jullie waren altijd bereid te luisteren.

Iemand die wel precies wist waar het allemaal over ging en van wie ik ontzettend veel heb mogen leren is Sanjay Rastogi, mijn dagelijkse begeleider. Sanjay, thank you for having faith in me and for the enthusiasm with which you approached my PhD. I have learned a great deal from you and I truly hope that we will keep in touch. Een half jaar nadat ik was begonnen met mijn promotie onderzoek heb ik Ann Terry leren kennen. Ann is in de loop van mijn onderzoek een steeds belangrijkere rol gaan spelen. Ann, thank you so much for believing in me; thank you for all your help, both on a professional and a personal level. I hope we will remain friends long after my PhD is finished. Tegen het eind van mijn promotie is mijn tweede promotor, Piet Lemstra, op de voorgrond getreden. Piet, bedankt voor voor je feedback bij het lezen van mijn proefschrift.

Tijdens mijn promotie onderzoek ben ik verschillende keren naar de ESRF in Grenoble geweest voor röntgendiffractie experimenten. Het was altijd heel hard werken en weinig slapen; werkdagen van 24 uur waren meer regel dan uitzondering. Ik vond het echter altijd heel fijn om te gaan, en deze “uitstapjes” zal ik dan ook echt gaan missen. Aan al de mensen met wie ik naar Grenoble ben geweest, en dan denk ik met name aan Jules, Luigi, Joost, Guido, Ann, en Sanjay; bedankt voor de gezellige sfeer en het lekker eten bij de Tex Mex! And Luigi: “that” SMS was a pleasure! Er

moest natuurlijk ook gewerkt worden en daarom wil ik de beamline scientists van ID02, Peter Boesecke, en ID11, Gavin Vaughan en Silvia Capelli, bedanken voor hun technische ondersteuning tijdens de experimenten. In het bijzonder wil ik Andy Goetz noemen; hij heeft het iedere keer weer mogelijk gemaakt om met de Linkam onze experimenten te kunnen doen. Andy, thanks for all your help with your magic “blue box”.

Ik ben een aantal keer naar het Max Planck instituut voor polymeer onderzoek in Mainz geweest om NMR experimenten te doen. I would like to thank Robert Graf and Yefeng Yao for the help they provided in measuring my samples. Thank you very much for finding the time in your busy schedules for helping me in performing my experiments.

Bij de TU zijn er ook verschillende mensen geweest die mij hebben geholpen met mijn metingen. Ik wil graag Wieb Kingma (SPC) bedanken voor de GPC metingen. Binnen de vakgroep SKT waar ik mijn promotie onderzoek heb mogen doen is er een aantal mensen dat er voor mij uitspringt. Anne Spoelstra heeft heel veel tijd en energie gestopt in het maken van TEM en electron diffractie opnames van mijn samples. Anne, bedankt voor al de moeite die je voor mij hebt gedaan. Ook wil ik graag Otto van Asselen bedanken voor zijn hulp en expertise die hij heeft verleend bij het begrijpen en interpreteren van mijn infrarood data; Otto, heel erg bedankt. Als laatste wil ik Jules Harings noemen. Jules, bedankt voor de vele inhoudelijke discussies die wij hebben gehad. Jouw opmerkingen en inzichten zijn zeer waardevol geweest.

Er zijn ook mensen die mij hebben geholpen met metingen en experimenten welke, om uiteenlopende redenen, niet in mijn proefschrift terecht zijn gekomen. Desondanks hebben deze mensen veel moeite voor mij gedaan. Ik wil dan ook graag Brahim Mezari en Pieter Magusin (SKA) bedanken voor NMR experimenten, Hans Kranenburg (SMN) voor nanoindenting, Martijn Kemerink van Natuurkunde (MMN) voor AFM metingen, en Dmytro Byelof van Amolf voor SAXS/WAXD metingen.

Aan mijn twee kamergenoten Bob en Marjolein, alsook Anne, Pauline, Jules, Roy, en Chunxia; bedankt voor het gezelschap van de afgelopen vier jaar. Aan de rest van de (oud) collega's van SKT, bedankt voor de gezellige lunches, het vlaai eten en koffie drinken.

Mocht ik in deze lange lijst van mensen die mij hebben bijgestaan en geholpen toch nog onverhoopt iemand vergeten zijn, aanvaard dan aub mijn oprechte verontschuldigheden, en dan alsnog bedankt!

# Curriculum vitae

Esther Vinken was born on the 22<sup>nd</sup> of October 1978 in the little town of Oirsbeek in the south of The Netherlands. She lived here until she was four years old at which point she immigrated with her family to South Africa.

In South Africa she completed her primary school education at Lumiere Primêre Skool in 1991 and graduated from Sasolburg High School in 1996. After school she enrolled at the Potchefstroom University for Christian Higher Education where she received a Bachelors degree in Chemical Engineering and Mineral Processing in 2000 and a Masters degree in Applied Mathematics in 2004. In August 2001 she moved to the Netherlands to follow the post-masters program Mathematic for Industry at the Eindhoven University of Technology which she completed in 2003. In January 2004 she started her Ph.D., also at the Eindhoven University of Technology, which lead to the work presented in this thesis.